University of Alberta
Department of Civil Engineering

Structural Engineering Report No. 92

An Investigation of Concrete Masonry Wall and Concrete Slab Interaction

by

R.M. Pacholok

J. Warwaruk

and

J. Longworth

October, 1980

THE UNIVERSITY OF ALBERTA

AN INVESTIGATION OF CONCRETE MASONRY WALL AND CONCRETE SLAB INTERACTION

by

R.M. Pacholok[1], J. Warwaruk[2], and J. Longworth[3]

October 1980

Department of Civil Engineering

Edmonton, Alberta

[1] Former Graduate Student, Dept. of Civil Engineering, University of Alberta, Edmonton, Canada.
[2] Professor of Civil Engineering, University of Alberta, Edmonton, Canada, T6G 2G7.
[3] Professor of Civil Engineering, University of Alberta, Edmonton, Canada, T6G 2G7.

Acknowledgements

This investigation was made possible through funds from the Natural Sciences and Engineering Research Council of Canada and the Alberta Masonry Institute. Testing facilities were provided by the Department of Civil Engineering at the University of Alberta. The concrete blocks and the ready-mix concrete used in the fabrication of the test specimens were donated by Edcon Block Products and Consolidated Concrete Products.

This report was originally prepared as a Master of Science thesis under the joint supervision of Profs. J. Longworth and J. Warwaruk at the University of Alberta.

ABSTRACT

Masonry building codes such as CSA Standard S304-1977[1] present simple and easy to use methods for the design of masonry bearing walls once the end moments and end loads on the wall are know. However, these codes do not present any method or guidelines to assist the designer in determining the wall end loadings that result from the interaction between a vertical masonry wall and a horizontal floor slab. The designer must use his engineering judgment and expertise in selecting the end moments and loads.

The purpose of this study is to test various full-scale masonry wall-floor slab specimens in an attempt to better understand joint behavior and performance as it relates to moment resistance.

Sixteen full-scale masonry wall-floor slab specimens were tested in the I.F. Morrison Structural Engineering Laboratory at the University of Alberta. The variables investigated in this study included:

1. The level of axial load on the wall.
2. The amount of vertical reinforcement in the wall.
3. The mortar strength.
4. The degree of slab penetration into the wall cross-section.
5. The block size, i.e. wall thickness.

TABLE OF CONTENTS

CHAPTER PAGE

LIST OF TABLES

LIST OF FIGURES

LIST OF PHOTOGRAPHIC PLATES

NOTATION

Dimensions and Section Properties

A_g	Gross cross-sectional area of masonry wall
A_s	Area of steel reinforcement
A_v	Cross-sectional area of vertical steel reinforcement
e	Eccentricity
h	Height of wall
I	Moment of inertia
I_e	Effective moment of inertia of a cracked wall about the centroid
I_{eL}	Effective moment of inertia of the lower wall
I_{eu}	Effective moment of inertia of the upper wall
I_{emin}	Minimum effective moment of inertia
I_o	Uncracked moment of inertia of the wall
t	Thickness of wall

Material Properties

E	Modulus of elasticity
E_c	Modulus of elasticity of concrete
E_m	Modulus of elasticity of masonry
E_s	Modulus of elasticity of steel

Forces and Moments

M	Bending moment
M_L	Moment on lower wall
M_{max}	Maximum applied moment on wall
M_{pl}	Moment at which joint begins to rotate plastically
M_{slab}	Applied moment from slab

M_u	Moment on upper wall
M_{ult}	Calculated ultimate moment
M_{wall}	Moment on wall
P	Applied load
P_b	Applied load at balanced failure
P_L	Load on lower wall
P_{max}	Maximum applied wall load
P_u	Load on upper wall
P_{wall}	Applied load on wall
P-Delta	Moment caused by axial load and deflection of the wall
T	Tie back force

Stresses and Strains

f'_c	Ultimate compressive strength of concrete
f'_m	Ultimate compressive strength of masonry
fs_{ult}	Ultimate tensile strength of steel
f_y	Yield stress of reinforceing steel
σ_1	Maximum stress at outer fibre
σ_2	Minimum stress at outer fibre
σ_{edge}	Maximum stress at edge of wall
$\sigma_{ult\ axial}$	Ultimate compressive strength of masonry loaded axially

Deflections

ΔB	Horizontal deflection of wall at transducer B
$\Delta \mathfrak{L}$	Horizontal deflection of wall-slab joint
ΔI	Horizontal deflection of wall at transducer I

Miscellaneous

w/c	Water to cement ratio
α	Ratio of plastification moment to ultimate moment M_{pl}/M_{ult}
θ	Difference between the rotation of a horizontal member and a vertical member
θ_{ult}	Ultimate plastic joint rotation
ϕ_h	Rotation of a horizontal member
ϕ_v	Rotation of a vertical member
ϕ_{vL}	Rotation of the lower wall end
ϕ_{vu}	Rotation of the upper wall end

CHAPTER I

INTRODUCTION

1.1 General Remarks

Until the twentieth century, masonry was the principal building material. But the development of structural steel and reinforced concrete enabled structures to be built on a more economical and massive basis. The surge in the use of steel and reinforced concrete as building materials, was due to large amounts of theoretical and experimental research. From this research the capabilities of these new materials were accurately defined. The rules-of-thumb used for masonry, which resulted in extreme overdesigning, and hence excessive costs, could not compete with the newly developed building codes for steel and concrete which would give the most economical and efficient designs possible.

Within the last two decades extensive research has been devoted toward structural masonry. New masonry building codes are now being developed which allow a designer to fully utilize the structural capabilities of masonry. Forty storey buildings can now be constructed using masonry with costs that compare with, or are even less than those for steel or reinforced concrete.

Although large amounts of research have been devoted to masonry, the majority of these studies have focussed on the behavior of masonry walls under combined axial load and moment, with very little research being done on the interaction of the wall-slab connection. The result of this unbalance in research is that a number of design procedures have been developed to enable an easy yet efficient masonry bearing

wall design for a given set of axial load and end moments, but no suitable methods of design has been developed that accurately determines the value of the axial load and end moments that are placed on the wall by the wall-floor connection. While some wall-floor joint tests have been conducted and documented by various authors, the results of these tests are inconclusive and the empirical relationships presented are in a form much too complex for a designer to use. Thus, a designer must use his own judgment in determining the loads and moments that the wall-floor joint will actually place on the masonry wall. The designer's lack of understanding of the interaction of the masonry structure will lead to very conservative design assumptions resulting in the structure being less economical than it should be. The designer may even choose the more researched materials such as steel and reinforced concrete to use in place of the masonry.

This study is the continuation of a research project started at the University of Alberta in 1978 to study the interaction of masonry walls with concrete floor slabs. It is hoped that the theoretical findings and experimental data presented in this study will complement other current research programs and assist in the formulation of design rules comparable with those for structural steel and reinforced concrete.

1.2 Object and Scope

The main objectives of this study are:

a. To examine existing theories for evaluating wall-slab joint performance.

b. To examine the relationship between axial load and joint performance of wall-slab combinations as it relates to moment resistance.

c. To examine the relationship between mortar strength and joint performance.

d. To examine the effect of vertical wall reinforcement on the joint performance.

e. To examine the relationship between wall thickness and joint performance.

f. To examine the relationship between the degree of slab penetration into the wall cross-section and joint performance.

g. To observe behavior, cracking and failure types of various wall-slab combinations.

h. To determine whether masonry wall-floor slab junctions can be analyzed by existing rigid frame analysis procedures.

i. To lay foundations for further study of related masonry aspects.

CHAPTER II

REVIEW OF PREVIOUS WORK AND PRESENT DESIGN PRACTICE

2.1 Introduction

A brief review of the previous research and present design practice for masonry wall-concrete floor slab connections is presented in this chapter.

At the juncture of a horizontal load carrying member (the floor or roof) and a vertical load carrying member (the bearing wall), a bending moment will occur due to the clamping action on the floor slab by the bearing wall, and the bonding of the slab to the wall. This moment is developed due to the unequal floor loading on each side of an interior wall, or loading from only one side on an exterior wall. This moment (or equivalent eccentricity), of prime importance in the determination of wall capacity, is subject to considerable discussion by engineers. Limited research investigation has been carried out on the behavior and characteristics of the masonry wall-slab connection. Thus little progress has been made in understanding and predicting the performance of the wall-slab joint.

The working stress design method is used in North America for the design of load bearing masonry walls. The moments on the wall ends are converted to equivalent eccentricities of the axial load. The allowable axial load for a wall of zero height is calculated, and then this allowable axial load is reduced to account for slenderness, eccentricity of load and end moments. The

slenderness and eccentricity coefficients are given by empirical formulations in codes such as the CSA Standard S304[1]. The design procedure is very simple and straightforward once the equivalent eccentricity is known, but few guidelines are available for the determination of the eccentricity of the load. The designer must use his own judgment in selecting the magnitude of the eccentricity to be used.

2.2 Review of Previous Work

2.2.1 Wall-Floor Slab Behavior

Little research has been carried out on the interaction of masonry wall-floor slab joints, with only a few research programs having been conducted over the past two decades. Although the information obtained has given some insight into the behavior of the joint, it is too inconclusive for the formulation of design procedures.

The first documented tests on joint behavior were performed by Sahlin[2] in 1959 when he began testing frame structures of brick masonry walls and concrete floor slabs. Tests were performed with different wall compression loads to simulate different storeys in a real structure. Sahlin attempted to determine the amount of restraint that the wall put on the floor slab due to the clamping action of the wall and the stiffness or resistance of rotation of the wall. Sahlin was able to calculate the effective eccentricity on the wall by dividing the negative moment of the slab at the wall face by the axial load on the wall.

In a later paper Sahlin[3] stated that the rotations of the joint were the key to understanding the wall-slab joint behavior. He defined the joint rotation, θ, as the difference between the rotation of the

slab, ϕ_h, and the rotation of the wall end at the slab, ϕ_v.

$$\theta = \phi_h - \phi_v$$

Sahlin also defined a 'plastification moment', M_{pl}. Up until the plastification moment, the wall rotation followed the slab rotation.

$$\theta = 0 \quad \text{i.e. } \phi_v = \phi_h \text{ for } M < M_{pl}$$

After the M_{pl} (the limiting slab restraining moment) was reached the joint rotation increased at approximately a constant moment equal to M_{pl}. Sahlin found that there is an ultimate joint rotation, θ_{ult}, that the joint can reach before the wall fails due to instability, caused by the prying apart of the walls because of the large slab rotation. He found this ultimate rotation of the joint to vary linearly with the wall axial loads. Fig. 2.1 gives the relationship between θ_{ult} and the applied moment.

Sahlin defined three possible failure modes for the wall-slab specimens:

1. $\theta = 0$. $(\phi_v = \phi_h)$. $0 \leq M \leq M_{pl}$ $\sigma_{edge} = \sigma_{ult}$ axial.
   Failure occurs when the ultimate edge stress is reached before the limiting slab restraining moment is attained. The joint remains rigid ($\theta = 0$) and the wall fails due to buckling or due to eccentric loading two or three bricks below the slab. The negative moment can be evaluated by considering frame action and reduced stiffness of the wall due to cracking.
2. $0 < \theta < \theta_{ult}$ $M = M_{pl}$ $\sigma_{edge} = \sigma_{ult}$ axial.
   Failure occurs when the ultimate edge stress is reached after

the limiting slab restraining moment is attained. The joint becomes "plastified" ($\theta > 0$). Above M_{pl} the joint begins to rotate with the moment remaining constant or decreasing. If the slab is stiff enough to prevent large end rotations, the joint remains intact and failure occurs when the load reaches the ultimate capacity of the wall. Since the moment remains constant, increasing the slab load will increase the compressive load on the wall. Since the slab moment and wall load are known, the eccentricity, e, can easily be calculated.

3. $0 < \theta = \theta_{ult}$ $M = M_{pl}$ $\sigma_{edge} < \sigma_{ult}$ axial.
Failure occurs when the limiting joint rotation is reached. The joint has become "plastified", and failure is localized at the joint and crushing of the blocks immediately above and below the joint results. Although the failure is separate from the failure of the wall, the rotation capacity of the joint is governed by the axial load on the wall. The ultimate rotation capacity of the joint decreases as the axial load on the wall increases.

Sahlin[4] provided a theoretical explanation of the interaction and developed equations for the calculation of the wall, slab, and joint rotations. These equations are very complex and require a knowledge of θ_{ult} and M_{pl} before they can be used. Thus the values of θ_{ult} and M_{pl} must be determined experimentally before the failure mode and the failure load can be calculated for the given wall-slab combination.

The effect of precompression load and mortar strength on the joint behavior was investigated by Maurenbrecher and Hendry[5]. They found that for a given mortar strength the initial slope of the moment

versus slab rotation plots were linear and had the same slope regardless of the precompression load. The slope of the moment-slab rotation plots decreased for decreasing mortar strengths. Because most of the rotation occurred in the mortar joint and the lower strength mortar was easily crushed, M_{pl} decreased as the mortar strength decreased. For larger precompression loads less ultimate rotation of the slab end occurred, resulting in larger moments in the walls. For walls with small precompression loads, failure resulted from the slab prying apart the walls and cracking the joint. They concluded that as long as the joint remains elastic the level of precompression has little effect on the degree of fixity of the joint.

Further tests by Colville and Hendry[6] on two storey single bay load bearing brick masonry structures also indicated that increasing wall precompression increased joint rigidity. It was found that up to 75% of full fixity can be developed by the joint. Other conclusions from their tests were that the rigidity of the joint is not linearly related to increases in wall precompression, and at high precompressions the magnitude of the floor loading does not have a significant effect on the degree of fixity.

Carlsen[7] tested a small number of joints between a precast concrete floor slab and a brickwall to study the effect of the length of bearing of the slabs on the bearing capacity of the joint and the ultimate slab restraining moment. He found that the bearing capacity of the wall is not affected by the bearing length of the slabs, and a reduction in bearing length reduces the ultimate slab moment.

Risager[8] also investigated the effect of the interaction of wall-floor slabs on the bearing capacity of masonry walls. He considered that the angle of rotation of the slab and wall had no influence on the bearing capacity of the wall and is a problem which can be investigated

separately. However, the behavior of the wall-slab joint determined the amount of eccentricity of the wall load and the deflected shape of the wall.

Sinha and Hendry[9] found that the equivalent eccentricities they calculated from their test results were less than theoretical values due to partial fixity of the joints and non-uniformity of strains.

Germanio and Macchi[10] tested ceramic block-concrete slab frames. They suggested that a joint could be evaluated as a 'partial hinge' transferring a limited moment to the wall. The characteristics of the 'partial hinge' depend upon the axial load on the wall. For joints having small axial load (upper floors of the building) the assumption of an ideal hinge can be very near to reality. For joints subject to large wall loads (lower floors in the building) the joints can be assumed to be fully fixed even in the ultimate condition. They did not, however, suggest a means of evaluating the partial moment for a case between the two extremes. They also found that the assumption of zero tensile strength in the walls seems acceptable. They concluded that rigid frame analysis techniques can model a masonry wall-slab frame providing the joint is rigid and the cracked stiffnesses of the members are used.

Tests in which the wall was axially loaded and then end moments were applied were conducted by Furler and Thurliman[11]. They discovered that as the axial load increased, the wall failed with lower end rotations.

The most recent research on the interaction of concrete block masonry bearing walls with concrete floor slabs was conducted by Ferguson[12] at the University of Alberta. The experimental portion of study consisted of full scale wall-slab combinations, with both cast-in-place and precast concrete slabs. The effect of the wall precompression load on the behavior

of the joint for various joint details was studied. The analytical portion of the study involved modeling the specimens as rigid frames. The test results were compared with analytical results and existing theories of joint performance.

Ferguson concluded that precast slab joints can be assumed to be hinged, and that this detail greatly reduces the load carrying capacity of the wall due to the asbestos pad under the slab.

For cast-in-place slabs, Ferguson found that the specimens behaved as described by Sahlin[3]. He discovered that the joint can be considered a rigid connection up until the ultimate moment capacity of the wall is reached, at which point the wall fails. Ferguson also concluded that the degree of fixity of the rigid joint of the cast-in-place slabs is a function of the stiffness of the masonry walls; as the wall stiffness increased, so did the resistance to rotation of the slab end. This stiffness, dependent on the equivalent moment of inertia and modulus of elasticity of the cracked wall, decreased as the level of axial load on the wall decreased and as the moment transferred to the wall increased, due to cracking of the wall.

Ferguson also discovered that the structural analysis of a structure consisting of load bearing masonry walls and cast-in-place concrete slabs can be carried out using existing rigid frame analysis methods.

2.2.2 Wall Behavior

The behavior of eccentrically loaded masonry walls is important in the understanding of joint behavior in frames. The amount of moment that is transferred from the floor to the walls is a function of the stiffness of both the walls and the floor slab. Although the walls

and slabs can be designed independently, their interaction is fundamental to the frame analysis of a structure.

Large amounts of research have been conducted over the past two decades to evaluate the behavior of masonry walls under concentric and eccentric loads, the most recent being that by Hatzinikolas[13] at the University of Alberta. From his tests on full scale walls, Hatzinikolas developed a moment magnifier method that accounts for wall slenderness and eccentricity of load to evaluate the strength or capacity of a masonry block wall. He first had to develop a means to calculate the stiffness of the cracked wall before the moment magnifier method could be applied. It is the cracked wall stiffness that must be known in order to analyze a structure using existing rigid frame analysis methods.

2.3 Present Design Practice

Most present day building codes for masonry construction give detailed, yet simple, procedures for the design of masonry walls subjected to eccentric loading. These codes do not recommend a method, or give guidelines, for determining the eccentricity to be used in the wall design. The designer must rely on his own judgment in assessing the interaction of the structure and its joints.

The problem the designer faces is whether to assume complete fixity of the joints, to assume the joints are pure hinges, to assume a value of simple eccentricity, or to ignore the possibility of any eccentricity and assume pure axial loading of the wall. Many buildings exist where the problem has been successfully ignored, but this is illogical and could be dangerous.

Germanio and Macchi[10] recommended some assumptions to be used in determining the eccentricity. These assumptions are quite conservative,

with the wall-floor connection assumed to be either fully fixed or ideally hinged, depending upon the location of the joint in the building and the method of construction of the connection. The error in these assumptions is a result of the actual connections providing neither complete restraint nor a complete hinged condition, although in some cases the assumptions may be very nearly correct. For joints having a small axial load (upper floors in a building) the connections are assumed to be hinges. The joints of the floors with a high axial wall load (lower floors in a building) are assumed to be fully fixed connections. The two assumptions are very near to reality and therefore will yield satisfactory results. The intermediate floors (where the joint is deformable but can resist a limited moment) are very difficult to model. This present study will investigate this intermediate condition.

Germanio and Macchi noted that the upper floor joints may crack to such an extent that moisture penetration through these horizontal cracks may be a significant problem. They recommended creating a "real" hinge in these joints to avoid this problem.

Gross, Dikkers, and Grogan[14] consider the sequence of construction in modelling the joints as hinged or fixed, as well as the location of the floor in the building. If the slab is placed with no support except at the wall joints prior to the construction of any upper walls or floors, then the joint is considered to be hinged for its own dead load, but fixed for any live load that the floor will be subjected to. This results from the slab being able to rotate freely under its own dead-load prior to any upper wall construction.

Gross, Dikkers, and Grogan defined the values of eccentricity and moments to be applied to the walls from the floor. For the "hinged" joint, a triangular stress distribution under the bearing area is assumed.

The moment and eccentricity can be easily calculated, with the eccentricity being the distance from the centerline of the wall to the centroid of the triangle, and the moment being this eccentricity times the floor load. The moment can then be distributed to the wall above and below the slab in accordance to their relative stiffness. This distributes approximately one-half of the bending moment to the wall immediately above the slab and one-half to the wall immediately below the slab.

For the fixed or fully restrained joint Gross, Dikkers, and Grogan assumed the moment in the floor slab at the face of the support to be $1/16\ wl^2$. This moment is then distributed into the wall in proportion to the relative stiffness of the wall above and below the slab. The magnitude of the bending moment may also be determined by a more exact method, such as Moment Distribution. The eccentricity is equal to the distributed moment on the wall divided by the wall's axial load.

Knowing the vertical loads and the appropriate eccentricities for all the walls in the structure, the adequacy of the wall designs can be checked.

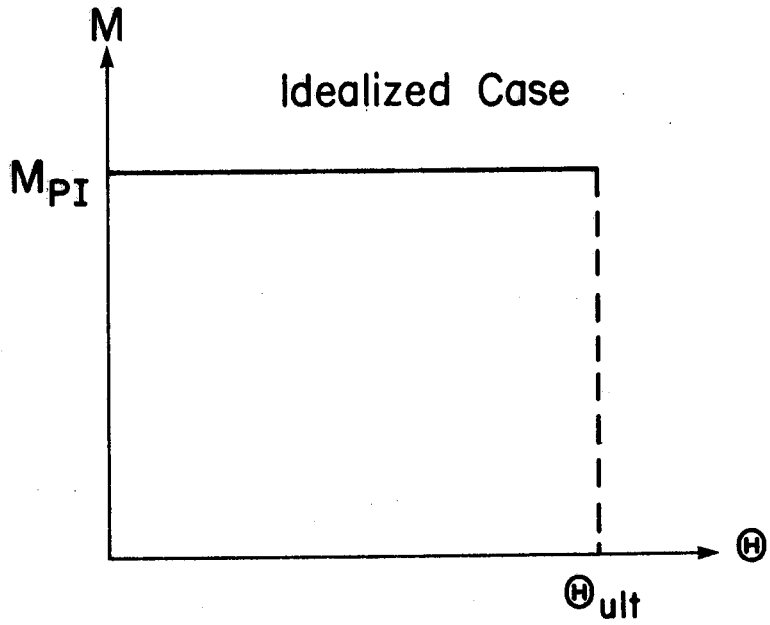

Fig. 2.1 Moment Versus Joint Rotation

CHAPTER III

EXPERIMENTAL PROGRAM

3.1 Materials

Materials used in the construction of the various test specimens are typical of those that are currently being used in masonry construction in the Edmonton area.

3.1.1 Concrete Block Units

Nine common concrete block units were used in the construction of the prisms and walls. The nine types of units are grouped into three categories: 10-inch blocks, 8-inch blocks, and the slab blocks. The 10-inch units consisted of Corner Sash and Standard blocks with a nominal size of 10 x 8 x 16 in., and Half blocks with a nominal size of 10 x 8 x 8 in. The 8-inch units consisted of 8 x 8 x 16 inch Corner Sash and Standard blocks, and 8 x 8 x 8 in. Half blocks. The slab units were 2 x 8 x 16 in. Solid Slab blocks. The units are shown schematically in Fig. 3.1 and Fig. 3.2. The physical properties of the units are listed in Table 3.1.

3.1.2 Mortar

The mortar used throughout the test program was mixed according to the specifications for Type S mortar given in CSA Standard A179M-1976[15]. The mix specifications call for the following volume proportions: 1 part Normal portland cement, 1/2 part hydrated lime, and 4 parts masonry sand. The mortar was mixed by hand in approximately 1/18 cubic yard batches with water added according to the mason's directions.

Two types of sand, each with a different fineness modulus were used. The results from the sieve analysis on the two sands are shown in Fig. 3.3. One of the sands, (B), was too fine and did not meet the grading requirements given by ASTM C144[16].

Two inch test cubes were made from the various mortar mixes for both types of sands. After making the cubes, the molds were placed under wetted burlap for 24 hours, after which the molds were stripped and the cubes were left to cure for 28 days, either in a lime saturated water solution or totally exposed to the air in the lab.

The cubes made using sand A (i.e. with the sand that met the ASTM C144 requirements) gave a lime saturated solution strength of 2170 psi (average of 21 cubes), and an average air cured strength of 1000 psi (3 cubes). The cubes made using sand B gave a lime saturated solution strength of 1160 psi (average of 18 cubes), and an average air cured strength of 950 psi (5 cubes).

3.1.3 Grout

The grout used in the reinforced walls consisted of a mixture of Normal portland cement, concrete sand, and 3/8 in. pea gravel. The mix proportions by weight were as follows: 88 lbs cement, 345 lbs sand, 245 lbs gravel, and a w/c ratio of 1. These proportions were in accordance with CSA Standard A179M-1976[15] and yielded a 5 cubic foot mix. Twenty-nine 3 x 3 x 6 inch grout specimens were prepared and cured according to CSA Standard A179M-1976. The average 28 day compressive strength of the grout test prisms was 2990 psi.

3.1.4 Concrete

All the slabs were cast-in-place with a concrete mixture of Normal portland cement, concrete sand, and 3/4" crushed aggregate. The mix proportions by weight were: 257 lbs cement, 379 lbs sand, 567 lbs gravel

and a w/c ratio of 0.44. These proportions yielded a 9 cubic foot mix volume. Seventeen 6 in. diameter test cylinders were constructed, cured and tested according to CSA Standard CAN3-A23.2-M77[17]. The average 28 day compressive strength of the cylinders was 5650 psi.

3.1.5 Reinforcing Steel

The tension reinforcing steel in the slabs consisted of #5 Imperial bars, while #3 Imperial bars were used for the shear stirrups. The vertical wall reinforcement varied depending upon the wall thickness. No. 10 Metric bars were used for the 10 in. block walls, while #3 Imperial bars were used for the 8 in. block walls. The stress-strain relationships for the vertical wall reinforcement are given in Fig. 3.4. The physical properties of the bars are given in Table 3.2.

3.2 Test Specimens

3.2.1 Prisms

Twenty-one prisms of varying block type, mortar type, and dimensions were constructed and tested. All the prisms had face shell mortar bedding with tooled joints.

Only 8 in. block prisms were constructed using mortar B (i.e. mortar mixed using sand B). The dimensions of the prisms are shown in Fig. 3.5 and Fig. 3.6(a). Nine stack bonded prisms consisting of one 8 in. Standard block per course were built; 4 being two blocks high, 5 - three blocks high and 2 - five blocks high. Also built with mortar B were 4 prisms with running bond consisting of 5 courses of block with one 8 in. Corner Sash and one 8 in. Half block per course.

Six prisms were built using mortar A (i.e. mortar mixed using sand A). These prisms were constructed in running bond, with one Corner

Sash and one Half block in each of the five courses. Of these 6 prisms, 3 were built using 8 in. block and 3 using 10 in. block. The dimensions of the prisms are shown in Fig. 3.6.

3.2.2 Full Scale Wall Specimens

Sixteen full scale wall specimens were constructed. Fourteen of these walls had slabs extending out from the wall at mid-height, while the remaining two walls had no slabs. The wall specimens were constructed and cured in a laboratory environment, at a temperature of 73°F and a relative humidity of 41%.

All walls were constructed by experienced masons using techniques typical of good workmanship and supervision. Each course consisted of one Standard, one Corner Sash, and one Half block in running bond. The bed and head joints were 3/8 inch face shell mortar, which were cut flush and then tooled. The first course was laid in a mortar joint on the laboratory floor to assure a smooth, uniform surface at the bottom of the walls. A thin sheet of paper was initially placed down to prevent the mortar from bonding to the concrete floor. The mason continued building the walls using a horizontal line and level to keep the walls straight and plumb.

The reinforced walls were constructed with clean out holes at the bottom of each wall void that was to be grouted. The reinforced walls were grouted in one lift and vibrated using a one inch diameter vibrator. The top and bottom courses of all walls were fully grouted to avoid damage during transportation and local damage from the loading channels.

The variables introduced in the tests were: wall thickness, mortar strength, vertical reinforcing, degree of slab penetration, tie back effect, and wall precompression load. Table 3.3 gives a summary of the variables of the walls. The nominal slenderness ratio (h/t) for all the walls with slabs was 16, and 15 for

all the walls without slabs (Series F). All the slabs were cast-in-place, 8 inches thick, and the same width as the walls. The length of the slabs was such that a 48 inch moment arm could be applied to the centerline of the wall by the slab load cell, with another 2 inch extension on the slab to prevent local failure at the point of the slab load. All the slabs were sufficiently reinforced to assure a failure of the wall before a failure of the slab.

As is the case in a real structure, the slabs were prevented from translating horizontally but were free to rotate about the line formed by the intersection of the wall's center plane with the slab's center plane. These characteristics were achieved by casting 1 in. diameter rods into the line of intersection of the slab and wall, and then using 3/4 inch diameter rod to tie the 1 inch bar to an independent, but fixed frame. The rotational freedom was brought about by connecting to the end of the 3/4 inch rod, a 2 inch diameter bar with a 1 1/32 inch diameter hole which would slide over the bar cast in the slab. Plate 3.1 shows the detail of this tie system.

For the reinforced walls, the area of vertical reinforcement gave an Av/Ag ratio of 0.00157 for both the 8 in. and 10 in. walls. There was no horizontal reinforcement in any of the walls.

3.2.2.1 Type A Specimens

The four Type A specimens consisted of seven courses of 8 inch block both above and below the 8 inch cast-in-place slab. The walls contained no vertical reinforcement and were constructed using mortar B. The slab penetrated through the entire wall cross-section.

The construction sequence was as follows:

a. The bottom seven courses of the walls were laid with the bottom course completely grouted solid.

b. Slab forms were placed and the slabs were cast. The concrete was prevented from flowing into the wall voids. The slabs were cured under polyethylene sheets for seven days after which the forms were removed.

c. The final seven courses of the wall were laid; with the top course grouted solid.

3.2.2.2 Type B Specimens

The four Type B specimens were identical to the four Type A specimens except for the presence of vertical reinforcement in the walls. Three - #3 Imperial bars, one in each of the outside voids and one in the middle void, were grouted over the entire length of the wall. The construction sequence was as follows:

a. The bottom course was laid with clean out holes in the three voids designated for reinforcement. All other voids in this course were grouted solid.

b. The remaining six courses of the bottom wall were laid.

c. The cleanout holes were cleaned and the vertical reinforcement was placed (at the center of the voids) and grout was vibrated into the reinforced cores to the top of the walls.

d. Slab forms were placed and the slabs were cast. The concrete was allowed to flow into the top course of the ungrouted cores. The slabs were cured for seven days under polyethylene sheets after which the forms were removed.

e. The final seven courses of the walls were laid with the clean out holes in the appropriate locations.

f. The vertical reinforcement for the top walls was placed and grouted. A lap splice of 12 inches was provided above the slab to give continuity of the vertical reinforcement, as well

as easy laying of the top wall blocks. The top course was grouted solid.

3.2.2.3 Type C Specimens

The two Type C specimens consisted of nine courses of 10 inch block both above and below the 8 inch thick cast-in-place slab. The slab covered the entire cross-section of the wall which was 9 5/8 in. wide by 39 5/8 in. long. Three - No. 10 Metric bars ran vertically through the entire wall length in the outside two voids and the center void. Mortar A was used for this series of walls.

The construction sequence was the same as for Type B specimens with the exception that the top and bottom walls contained 9 courses of 10 inch block instead of 7 courses of 8 inch block.

3.2.2.4 Type D Specimens

The two Type D specimens, like the Type C specimens, consisted of nine courses of 10 inch block both above and below the cast-in-place slab, with 3 - No. 10 Metric bars running vertically through the walls. Mortar A was also used for this series. The only difference between the Type C and Type D specimens was that the Type D walls had slabs that only partially covered the wall cross-sections. For the Type D specimens, a 1 1/2 inch thick Solid Slab block was placed behind the slab. This gives the exterior face of such a wall a continuous block finish appearance, as opposed to one in which the floor slabs disrupt the block pattern.

The construction sequence was as follows:

a. The bottom course was laid with clean out holes in the three voids designated for reinforcement. All other voids in this course were grouted solid.

b. The remaining eight courses of the bottom wall were laid.

c. The mortar droppings were removed from the clean out holes,

the vertical reinforcement was placed, and grout vibrated to the top of the walls.

d. Slab forms were placed around the entire back edge of the wall. The slab blocks were then mortared to the wall at the back of the slab. The slab was then cast with the concrete being allowed to flow into the voids of the top course and up against the inside face of the slab blocks. The slabs were cured for seven days under wetted burlap covered with polyethylene sheets, after which the forms were removed.

e. One course of blocks was laid on the slab around the lower wall's reinforcement that projected 300 mm (≃ 12 in.) above the slab to form the lap splice. Clean out holes were placed in the appropriate voids.

f. The final eight courses were laid.

g. The vertical reinforcement was placed with grout vibrated to the top of the walls in the reinforced voids only. This assured a 300 mm lap splice of the upper and lower reinforcement. The top course was grouted solid.

3.2.2.5 Type E Specimens

The two Type E specimens were constructed of 8 in. block, with mortar A, but no vertical reinforcement. The 8 inch thick cast-in-place slab completely covered the wall cross-section. The masonry wall consisted of seven courses of block both above and below the slab. The construction sequence was the same as for the Type A specimens.

Joint details for Type A, B, C and E walls are shown in Fig. 3.7. Joint details for Type D walls are shown in Fig. 3.8.

3.2.2.6 Type F Specimens

The two Type F specimens were constructed of 8 inch block. The

walls were built 14 courses high using mortar A. Three - #3 Imperial bars were grouted into the entire wall length, one in each of the outside cores and one in the center core. The construction sequence was as follows:

a. The bottom course was laid with clean out holes in the three voids that were to be reinforced. All other voids in this course were grouted solid.

b. The remaining 13 courses of the wall were laid.

c. The mortar droppings were removed from the clean out holes, the vertical reinforcement was placed, and grout was vibrated to the top of the walls. All voids in the top course were filled with grout.

3.3 Loading Apparatus

The walls of the specimens were loaded in compression through a channel-roller system shown in Fig. 3.9. The weight of the channel-roller system was 475 lbs for the 8 inch walls and 625 lbs for the 10 inch walls. This system was used to simulate a pin-ended condition representing points of zero bending moment in the real structure. The vertical load on the wall was applied by an MTS hydraulic testing machine with a capacity of 1.5 million pounds in compression, and capability of maintaining a preset load to ± 10 lbs.

The vertical load on the slab was applied through a hydraulic center pull ram. The ram had a load capacity of 60 kips with a stroke of 2 1/2 inches. It was mounted under the 26 inch thick load floor in front of the MTS machine and was connected through a loading apparatus to a channel used to apply a line load to the slab. The line load was placed at 48 inches from the centerline of the wall. The weight of the loading apparatus was 225 lbs. A diagram of the slab loading apparatus is shown in Fig. 3.10.

3.4 Instrumentation

3.4.1 Prisms

Prisms were tested in vertical compression using the MTS hydraulic testing machine. Vertical deformations were monitored to 1/1000 inches by the movement of the head of the MTS machine. For more accurate vertical strain measurements, linear variable differential transducers (LVDT's) calibrated to read increments of 1/10,000 inches/inch were mounted on the faces of the prisms. Plate 3.2 shows a typical LVDT set-up.

3.4.2 Full Scale Wall Specimens

Horizontal deflections of the walls were measured at points along the height of the wall using LVDT's calibrated to read in increments of 1/1000 inches. Horizontal deflections were read at 10 points over the height of the wall for walls with slabs, and at 14 points for the walls without slabs. The location of the LVDT's on the walls are shown in Fig. 3.11 for the walls with slabs and Fig. 3.12 for the walls without slabs. The LVDT's were mounted on an independent frame and connected to the walls with light gauge wires. This was to prevent damage to the LVDT's upon failure of the walls.

Rotations of specific elements in the specimens were not measured directly but calculated from horizontal displacements. The rotation of the block above the slab, the block below the slab, and the slab itself were computed from the readings of the two LVDT's attached to each of these elements. The rotations were calculated by taking the inverse sine of the difference in the two adjacent LVDT measurements divided by the vertical distance between the gauge points.

Vertical deflections of the slab were measured at 16 inches and

36 inches from the face of the wall using LVDT's. These readings were also used to give the rotation of the slab, which was found to be more reliable than the rotation given by the LVDT's on the back of the slab since the back of the slab would sometimes crack or spall causing one of the LVDT connections to fall off of the slab.

Vertical deformations and strains were measured by LVDT's by the same means as was used for the measurement of the vertical strains of the prisms as shown in Plate 3.2. These vertical strain measuring LVDT's were located at 6 places on the walls as shown in Fig. 3.11 for the walls with slabs, and Fig. 3.12 for the walls without slabs.

The strains in the vertical reinforcing bars in the walls were measured by strain gauges mounted on the reinforcement. For the walls with slabs, gauges were mounted at one mortar joint above and below the slab, and at the mid-height of each of the upper and lower walls. For the walls without slabs, gauges were mounted on the bars at their quarter-points. See Fig. 3.11 and Fig. 3.12 for gauge locations.

Vertical load on the wall was read directly from the MTS machine. Vertical load on the slab was measured using a 30 kip load cell.

The location of the tie back pin in the slab was monitored using the horizontal deflection measurements of the LVDT's attached to the back of the slab. The forces in the tie back rods were computed using load cells (previously calibrated) mounted on the 3/4 inch tie rods.

The measuring devices (strain gauges, load cells, and LVDT's) were powered by a common six-volt power supply that produced output in the range of ± 0.001 volts. The analog signals from the devices were converted into digital form by a digital voltmeter controlled by an interactive Fortran program in the Nova computer. This allowed the measurements to be monitored and read into storage during testing. At a

particular load level, all output was measured and recorded automatically within 5 seconds. The interactive Fortran program allowed the test supervisor to determine, during the test, the increments of loading at which data was to be read and stored. After completion of testing, the data was printed on a hard copy terminal, stored on a digital cassette tape and later transferred to the AMDAHL 470 computer for further processing.

3.5 Testing Procedures

3.5.1 Prisms

All prisms were tested in axial compression. They were capped top and bottom with 1/2 inch fibre board, and 1/4 inch steel plates were placed so that the load was applied uniformly over the total area of the prisms.

3.5.2 Full Scale Wall Specimens

3.5.2.1 Placement of Specimen

The specimens were transported to the testing machine in a clamping device consisting of two frames connected with steel rods. The frames were constructed from C7 x 9.8 channel sections, with a shape identical to the shape of the wall profile. The frames were placed on the two sides of the wall and a compressive force was applied by tightening bolts on the rods. Rubber pads were placed between the channels and the specimen at various locations to prevent damage to the wall from the steel channels. The specimens were then lifted by a 10 ton overhead crane through the use of four chains located at the top of the wall and the end of the slab on each side of the specimen. The lengths of the chains were adjusted prior to lifting to maintain the slab in a horizontal

position when the wall was lifted.

The specimens were guided into the testing machine using the overhead crane and two 1 ton chain hoists. The bottom channel-roller assembly was covered with about a 3/8 inch layer of plaster of paris to ensure that the load was distributed evenly. The wall was set in the bottom channel assembly in a plumb configuration and the plaster was allowed to set.

A steel HSS-4 x 3 x 0.25 in. section was placed under the slab to provide stability to the wall. The clamping frames were removed and the top channel-roller assembly was plastered into place. A 3 kip load was applied to the channel to provide an even set of the plaster and overall stability of the specimen. The slab loading apparatus, the slab tie back assembly, and the measuring devices were then connected. Plate 3.3 shows a specimen ready for testing.

3.5.2.2 Application of the Loads

A nylon sling connected to the MTS machine frame was used to support the slab and ensure safety while the necessary bolts were removed from the channel-roller assemblies to make them pin-ended joints. With the 3 kips still applied to the wall to ensure stability the slab supporting HSS section was removed. The wall was then loaded to 10 kips, where upon the sling supporting the slab was removed. At this point, the readings on all the gauges and LVDT's were initialized as being equal to zero. The wall load was then increased in suitable increments up to the predetermined level, with instrumentation readings being taken at each increment. The tie back rods were adjusted when necessary to keep the tie bar in the slab at zero horizontal deflection. This was done by a continuous monitoring of the horizontal deflections by the Nova computer.

After the required axial load on the wall was reached the loading

of the slab was started. The load cell of the slab loading apparatus was monitored and instrumentation readings were taken at every 0.5 kip load increment up to the maximum slab load. If the walls did not become unstable at the maximum slab load then the deflections of the slab were monitored and the stroke of the slab center pull ram was increased. Measurements were recorded at various intervals as the slab deflection increased until complete instability of the walls occurred. The tie back rods were continually adjusted throughout the slab loading, to prevent horizontal movement of the slab tie bar.

Table 3.4 lists the magnitude of axial load and the degree of out of plumb of the walls for all test specimens.

TABLE 3.1 DIMENSIONS AND PHYSICAL PROPERTIES OF CONCRETE BLOCK UNITS

Masonry Unit	Width (in.)	Length (in.)	Height (in.)	Moisture Content %	Absorption %	Gross Area ($in.^2$)	Effective Net Solid Area		Compressive Strength (Ksi)	
							(%)	($in.^2$)	Gross Area	Net Area
8 in. Standard	7 5/8	15 5/8	7 5/8	8.4	12.9	119.1	48.1	57.3	1.61	3.34
8 in. Corner Sash	7 5.8	15 5/8	7 5/8	6.5	18.0	119.1	52.5	62.5	1.39	2.66
8 in. Half	7 5/8	7 5/8	7 5/8	7.9	14.6	58.1	55.6	32.3	1.98	3.57
10 in. Standard	9 5/8	15 5/8	7 5/8	36.5	18.0	150.4	53.0	79.7	1.63	3.08
10 in. Corner Sash	9 5/8	15 5/8	7 5/8	36.8	11.4	150.4	58.1	87.4	1.94	3.34
10 in. Half	9 5/8	7 5/8	7 5/8	32.7	15.2	73.4	65.9	48.4	2.32	3.51
Solid Slab	1 1/2	15 5/8	7 5/8	-	-	23.4	100	23.4	-	-

TABLE 3.2 PHYSICAL PROPERTIES OF REINFORCING STEEL

Bar	Yield Stress σ_y, (Ksi)	Yield Strain E_y, (in/in)	Ultimate Stress σ_{ult}, (Ksi)	Modulus of Elasticity E_s, (Ksi)
#3 Imperial Series B	54.8	0.00199	78.1	27.5×10^3
#3 Imperial Series F	82.6	0.00269	129.8	30.7×10^3
No. 10 Metric Series C & D	60.6	0.00205	92.6	29.6×10^3

TABLE 3.3 VARIABLES IN FULL SCALE WALLS

Wall Series	Number of Walls	Wall Thickness		Vertical Reinforcement			Slab Penetration			Mortar	
		8 in.	10 in.	Plain	3#3	3 No.10	Full	Partial	No Slab	Good Sand	Poor Sand
A	4	✓		✓			✓				✓
B	4	✓			✓		✓				✓
C	2		✓			✓	✓			✓	
D	2		✓			✓		✓		✓	
E	2	✓		✓			✓			✓	
F	2	✓			✓				✓	✓	

TABLE 3.4 LOADING DETAILS FOR TEST SPECIMENS

Specimen Number	Axial Load (kips)	Out of Plumb[1] (in)		
		Top Wall	Bottom Wall	Total Specimen
A 50	50	+ 1/2	Plumb	+ 3/8
A100	100	+ 1/4	+ 3/16	+ 5/8
A101	100	- 5/16	- 1/16	- 3/8
A150	150	+ 5/16	+ 1/8	+ 9/16
B 50	50	Plumb	Plumb	Plumb
B150	150	+ 1/4	+ 1/8	+ 3/8
B200	200	+ 1/16	Plumb	+ 1/16
B320	324	+ 1/8	Plumb	+ 3/16
C200	200	+ 1/8	+ 1/16	+ 3/16
C300	300	+ 1/16	Plumb	+ 1/8
D200	200	+ 3/16	- 1/8	- 1/8
D300	300	+ 3/16	- 1/16	+ 1/8
E 50	50	Plumb	- 1/4	- 5/16
E100	100	+ 1/16	Plumb	+ 1/8
E150	150	Plumb	- 1/4	- 5/16
F 1	313	-	-	+ 1/16
F 2	328	-	-	Plumb

1. A positive out of plumb indicates that the top of the wall leaned towards the slab.

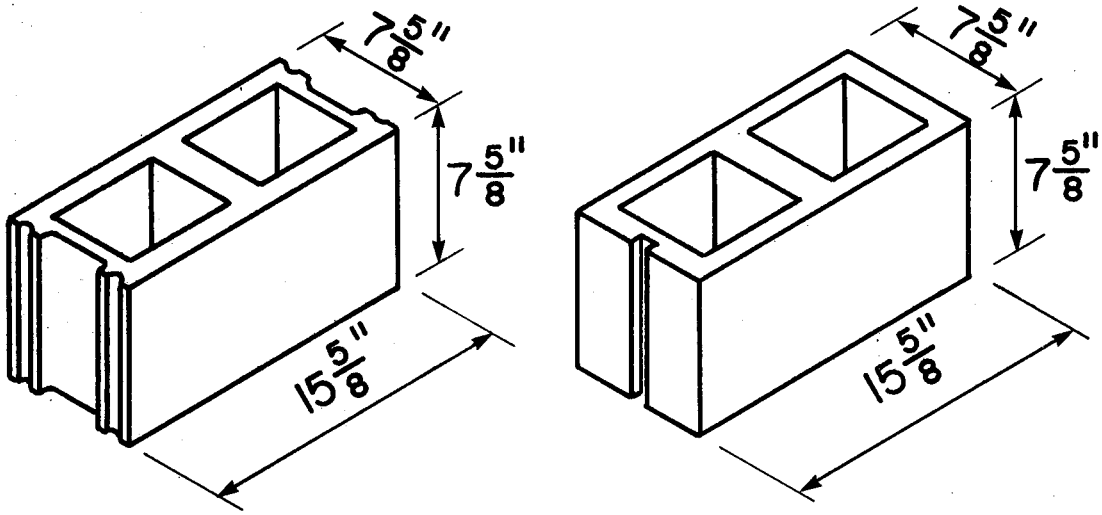

(a) 8 in. Standard

(b) 8 in. Corner Sash

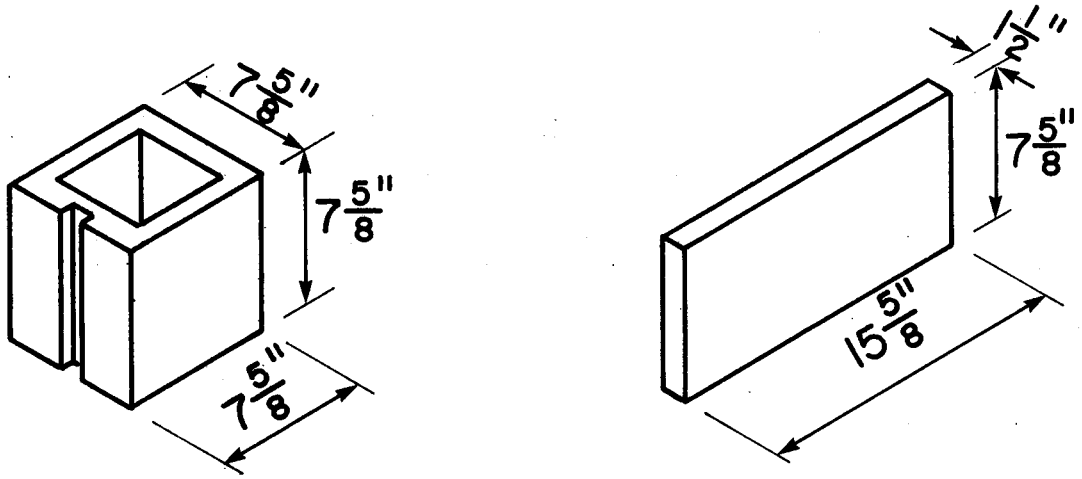

(c) 8 in. Half

(d) Solid Slab

Fig. 3.1 Masonry Units

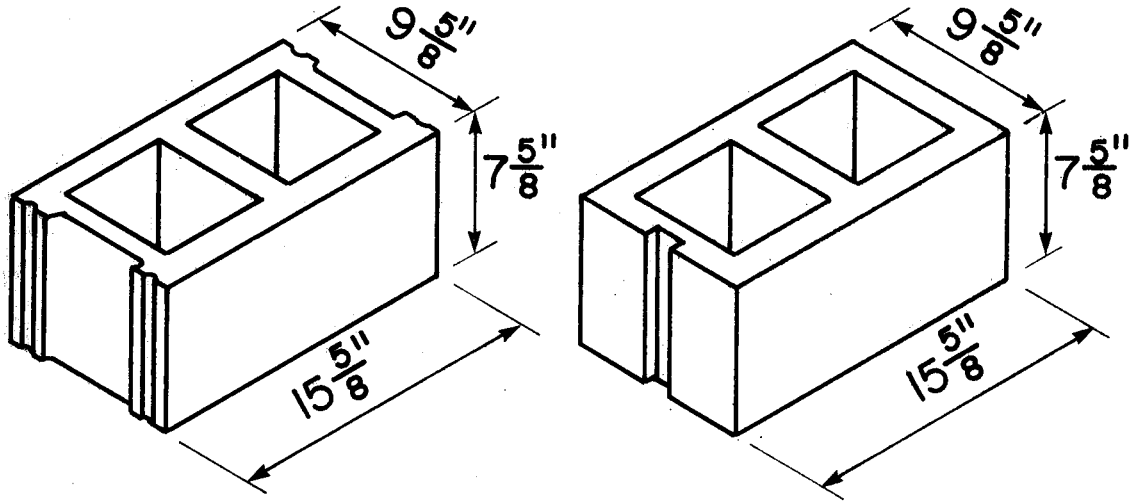

(e) 10 in. Standard (f) 10 in. Corner Sash

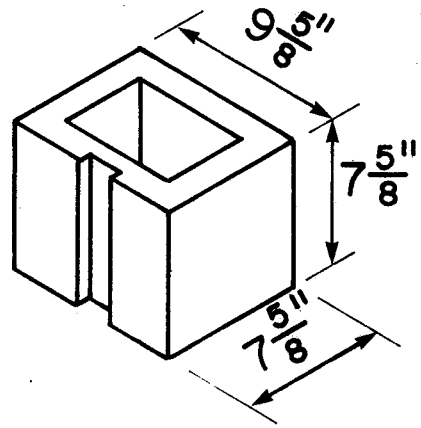

(g) 10 in. Half

Fig. 3.2 Masonry Units

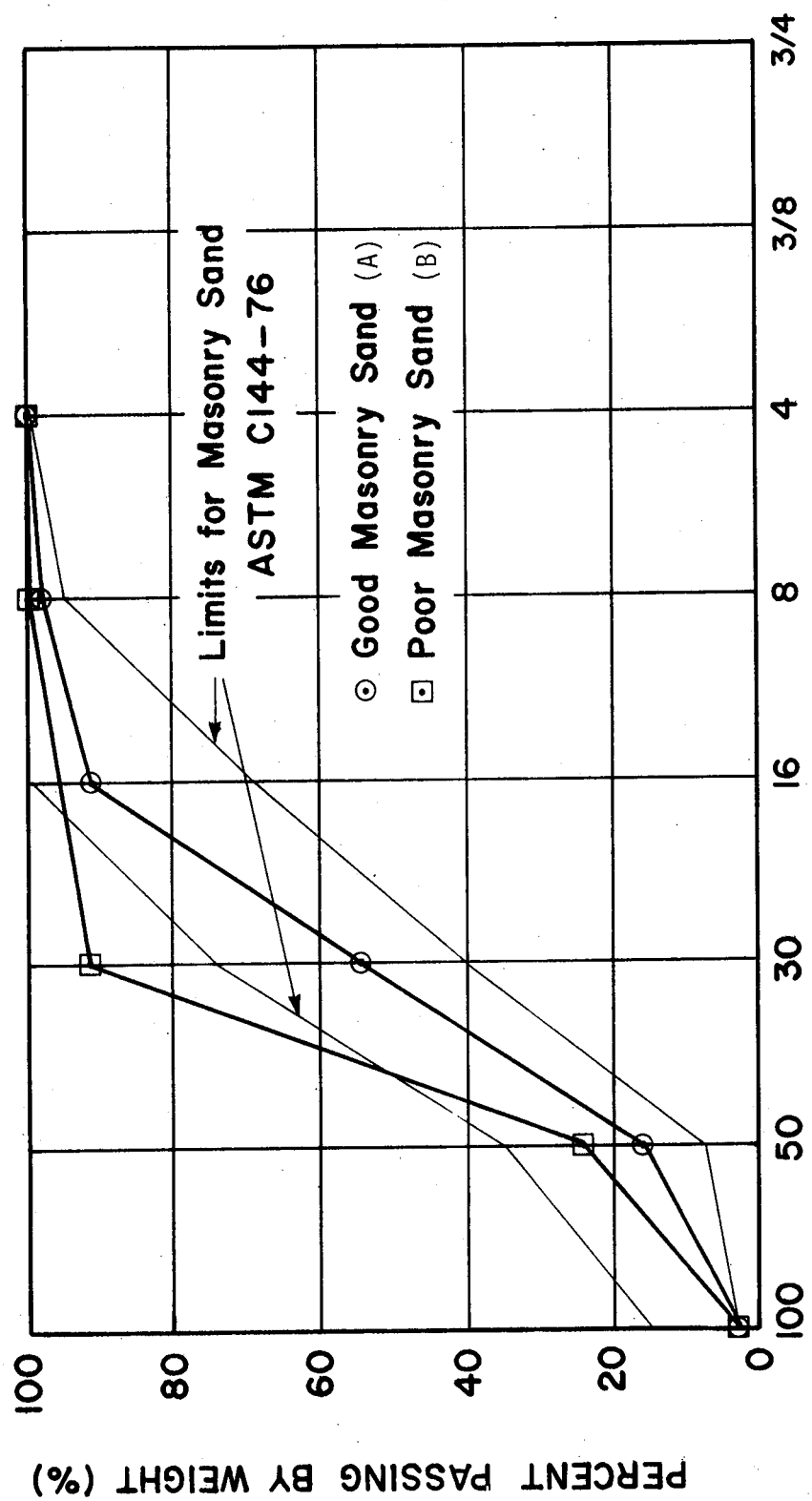

Fig. 3.3 Masonry Sand Sieve Analysis

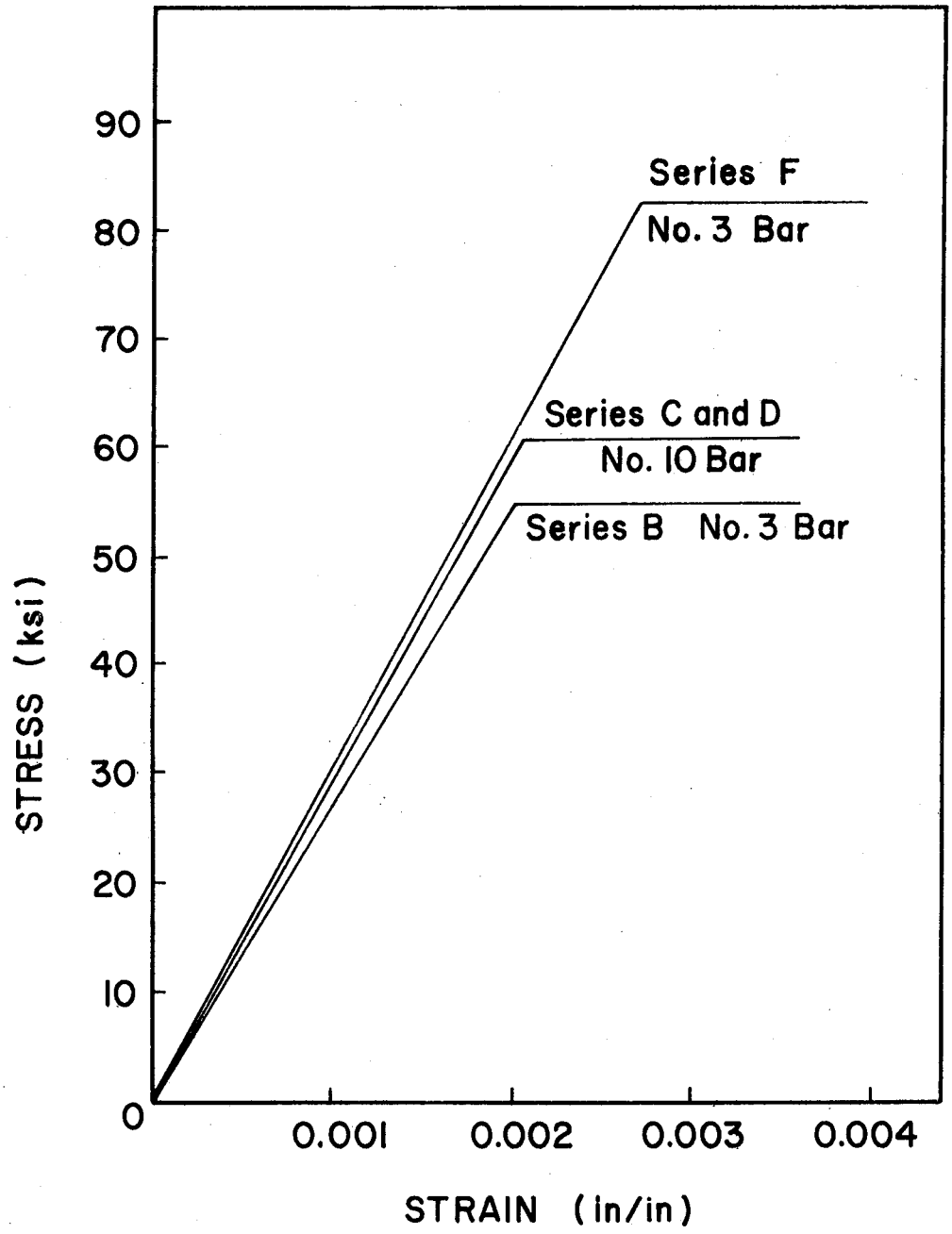

Fig. 3.4 Stress-Strain Relationship for Reinforcing Steel

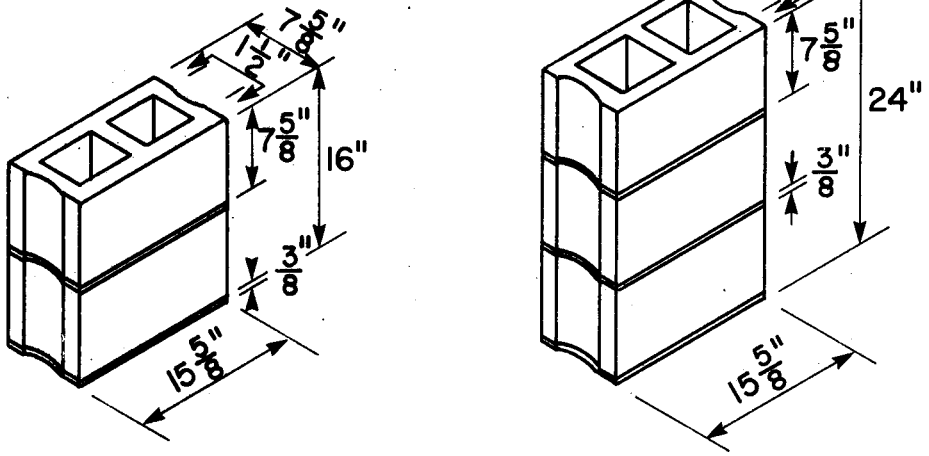

(a) 8in. Standard - 2 courses

(b) 8 in. Standard - 3courses

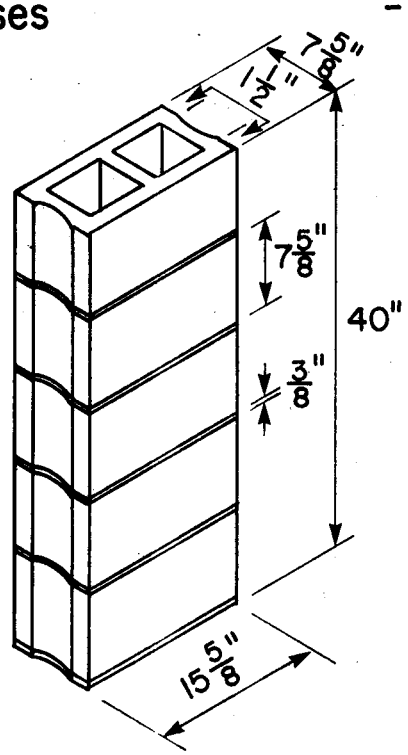

(c) 8 in. Standard - 5 courses

Fig. 3.5 Prisms

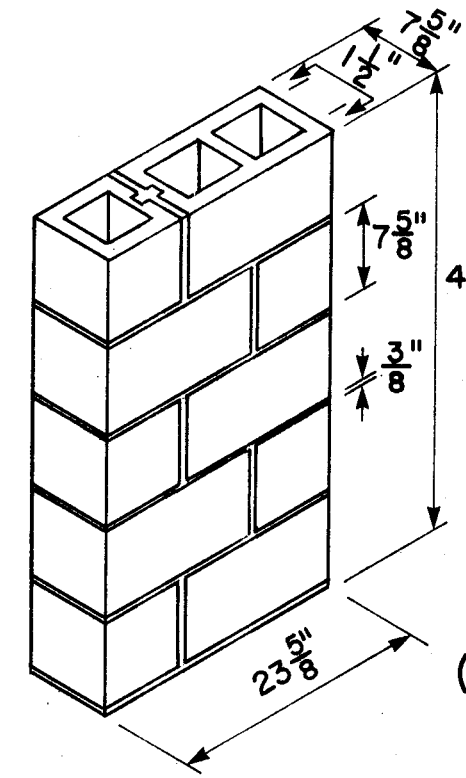

(a) 8 in. Corner Sash
+Half -5 courses

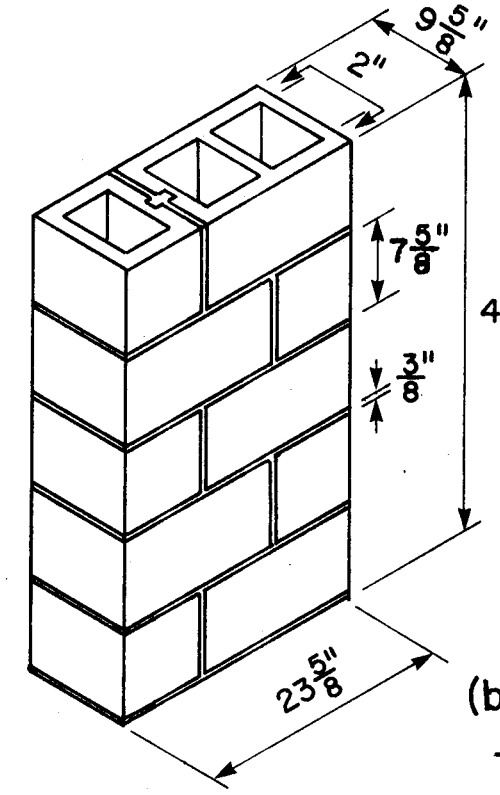

(b) 10 in. Corner Sash
+Half -5 courses

Fig. 3.6 Prisms

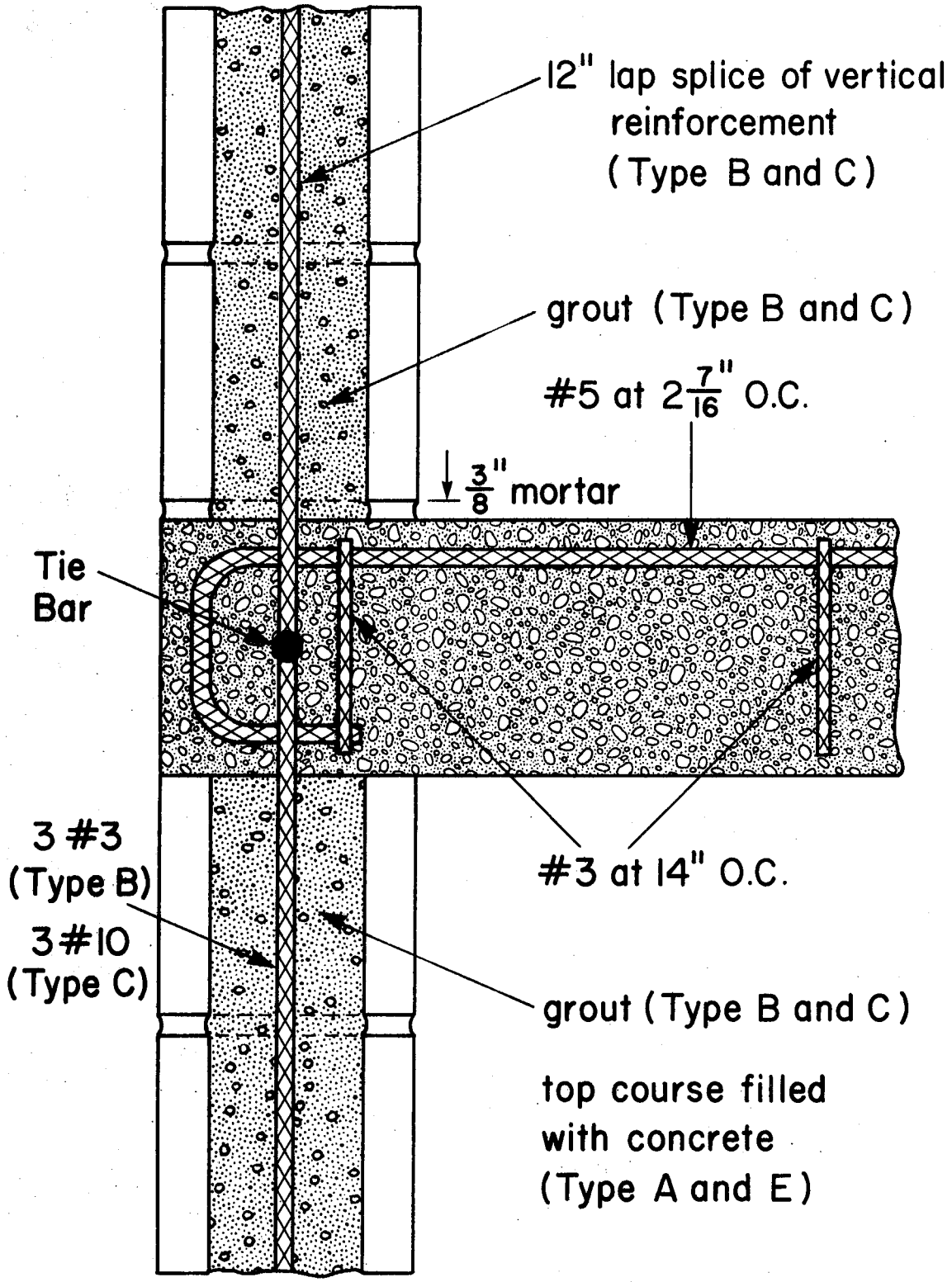

Fig. 3.7 Joint Details for Specimens A, B, C & E

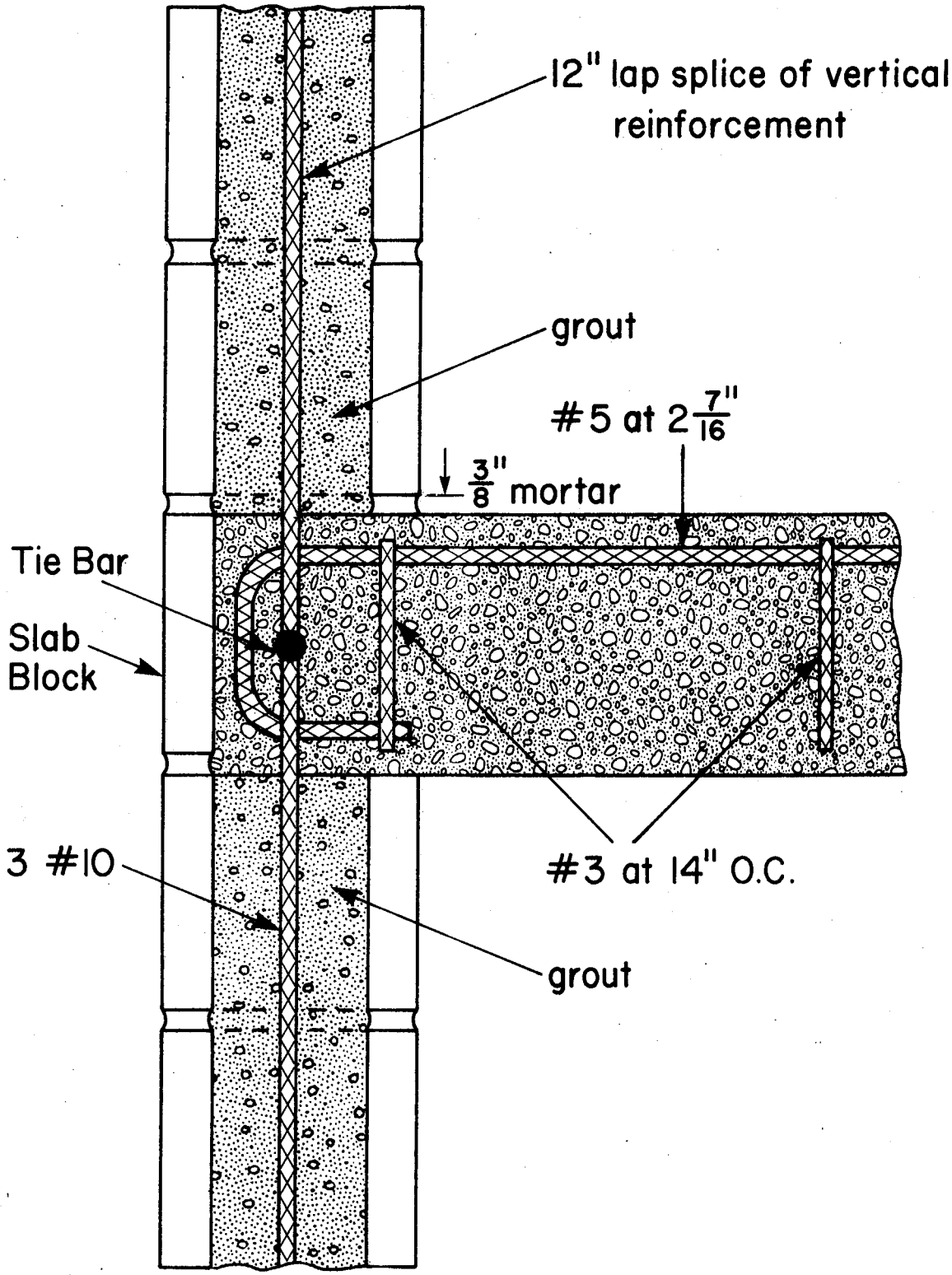

Fig. 3.8 Joint Detail for Specimens D

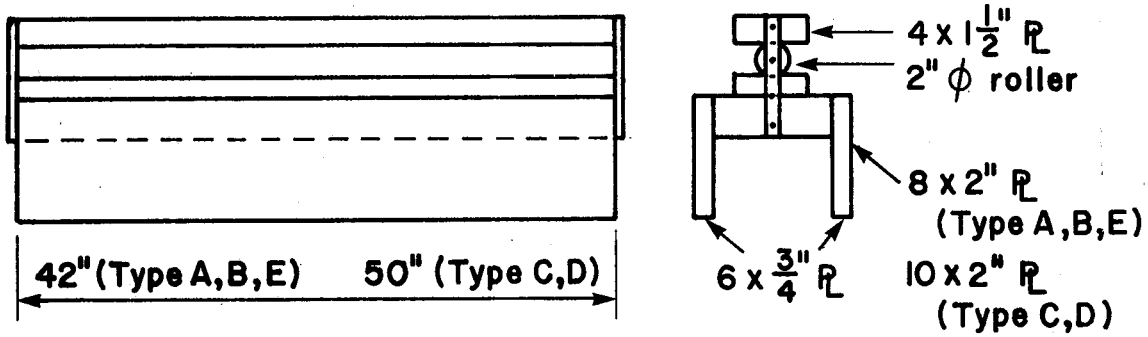

Fig. 3.9 Channel-Roller Assembly

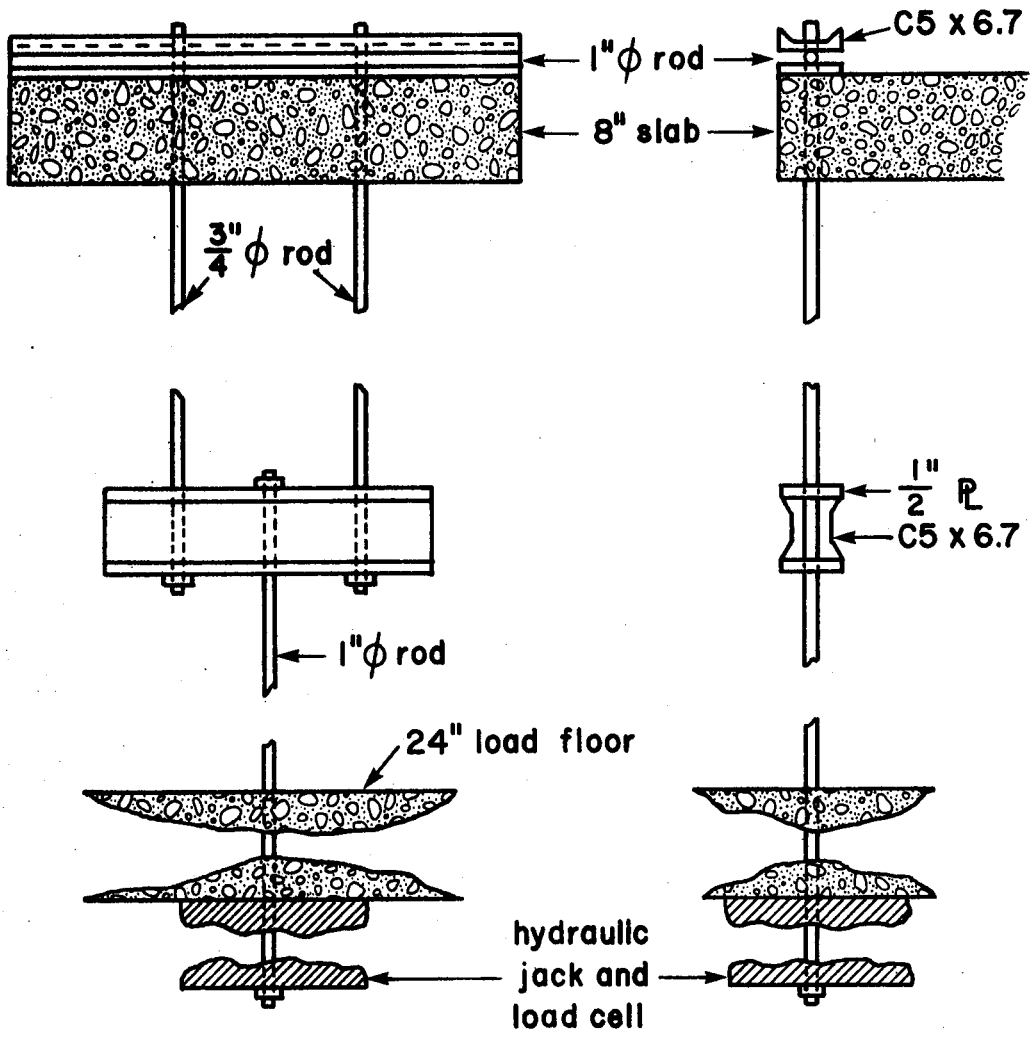

Fig. 3.10 Slab Loading Apparatus

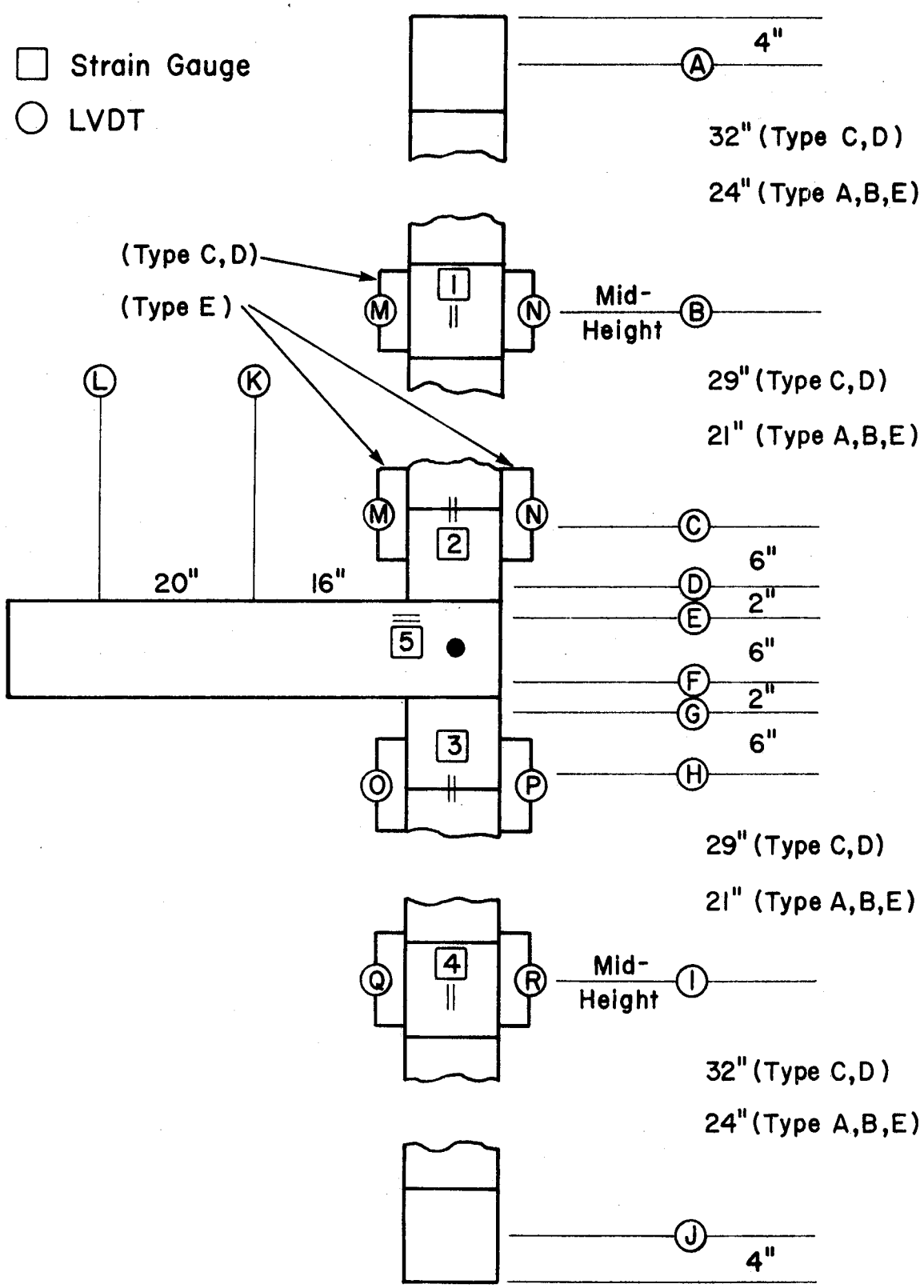

Fig. 3.11 Location of Instrumentation for Walls With Slabs (Series A,B,C,D & E)

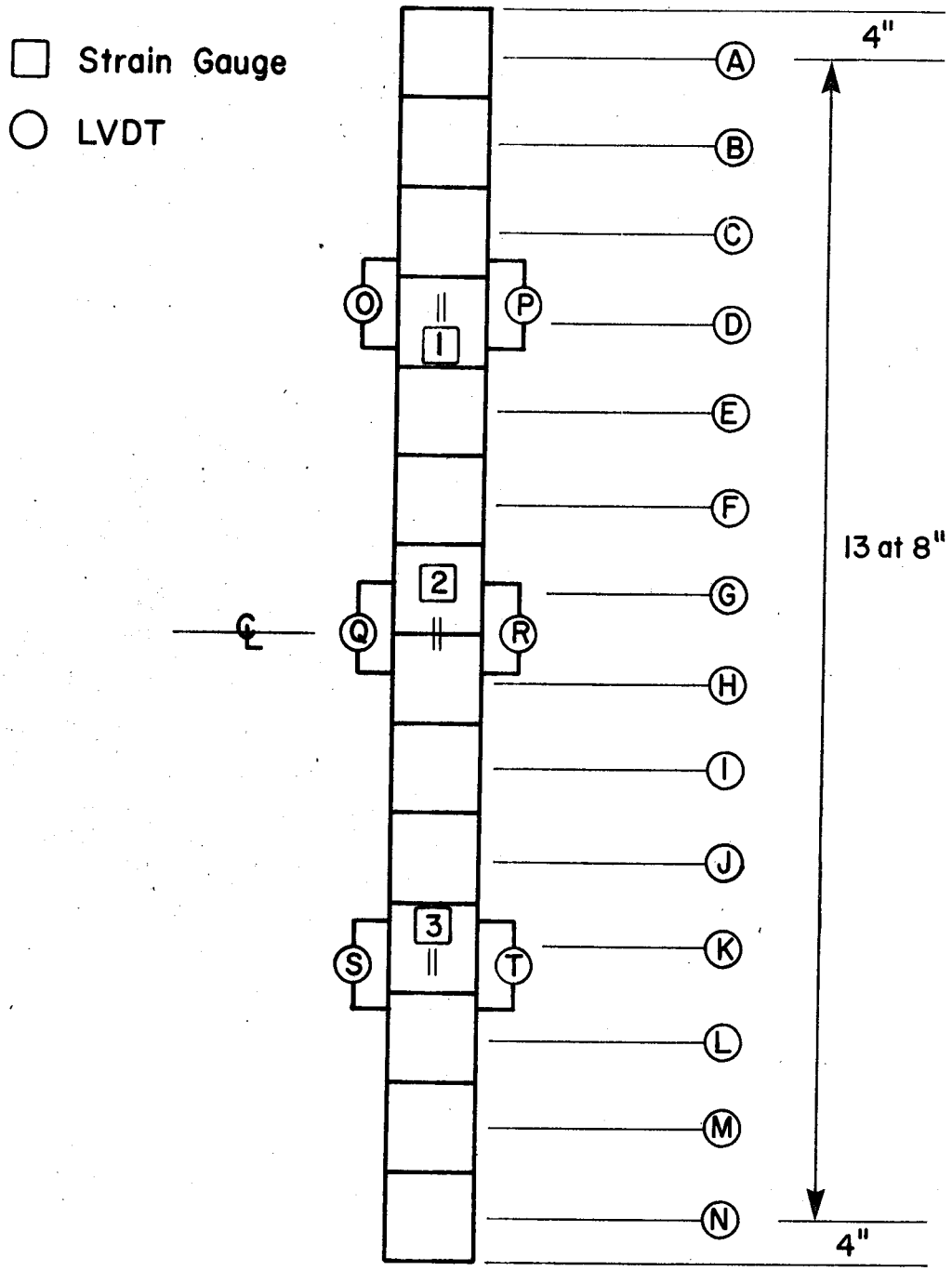

Fig. 3.12 Location of Instrumentation for Walls Without Slabs (Series F)

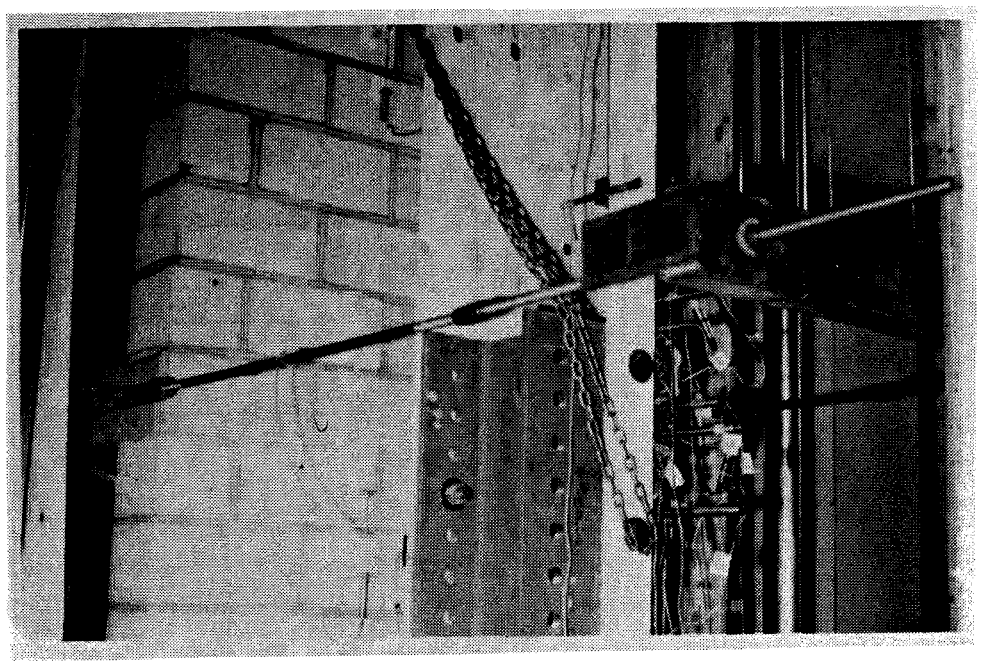

Plate 3.1 Tie Back System

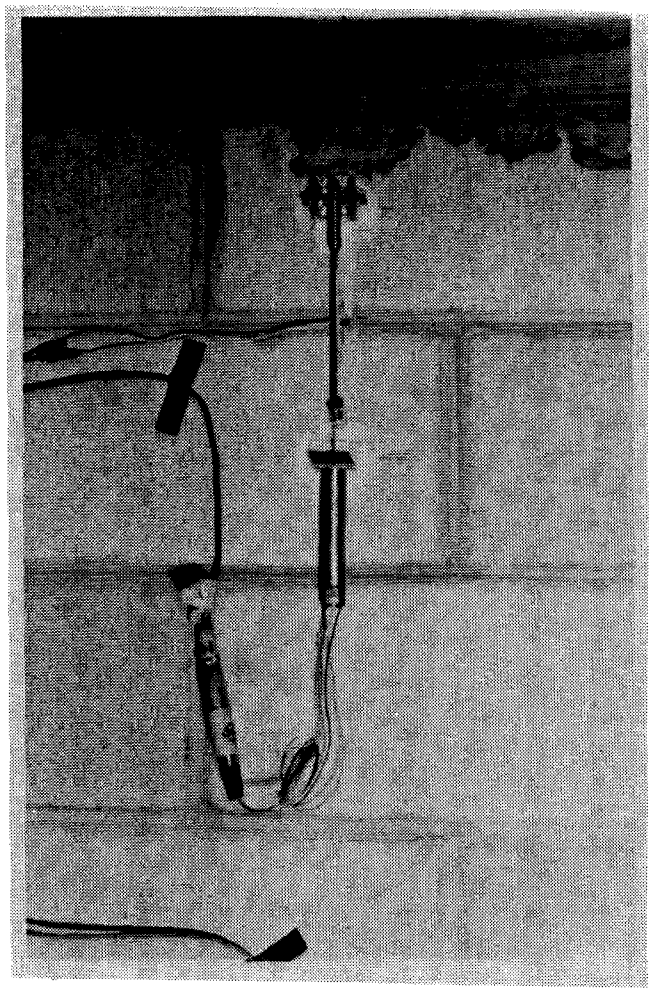

Plate 3.2 LVDT Strain Measuring Apparatus

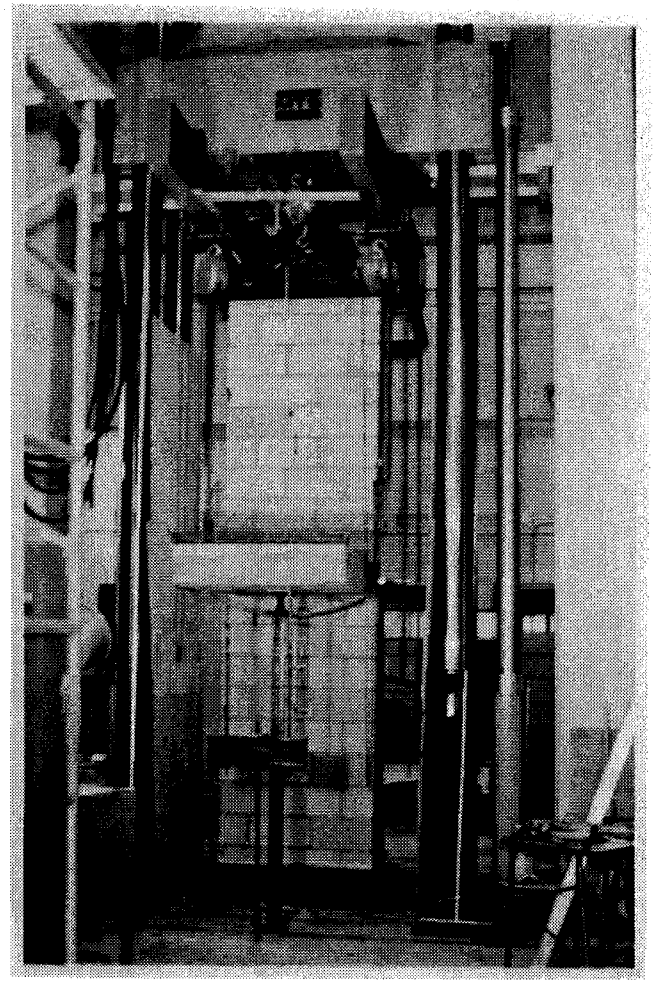

Plate 3.3 Specimen Ready for Testing

CHAPTER IV

TEST RESULTS

4.1 Introduction

The results of the tests on prisms and full scale wall specimens with and without slabs are summarized and presented in this chapter in tabular, graphic, and photographic form.

4.2 Compressive Strength Masonry

4.2.1 Unit-Mortar Method

The Unit-Mortar method for determining the ultimate compressive strength of masonry at 28 days, f'_m , is presented in clause 4.3.3 of CSA Standard S302-1977[1]. "Masonry Design and Construction for Buildings". The fifteen 8 inch units tested yielded an average compressive strength of 3120 psi. The six 10 inch units tested yielded an average compressive strength of 3420 psi. For Type S mortar, Table 3 of CSA Standard S304-1977 yields f'_m values for the 8 inch masonry and the 10 inch masonry of 1740 psi and 1830 psi, respectively.

4.2.2 Prism Test Method

The Prism method for determining f'_m is outlined in clause 4.3.2 of CSA Standard S304-1977[1]. Table 4.1 gives a summary of the prisms tested. The code does not allow for prisms with h/t values greater than 3. The correction factor for an h/t of 3 was used for all prisms with an h/t ratio larger than 3. The compressive strength, f'_m, of Type A and B, Type C and D, and Type E and F specimens were 1850 psi, 1730 psi, and

1900 psi, respectively. Mortar A gave a slightly higher value for f'_m than did mortar B. This was shown by the f'_m value for Type A and B prisms, and for Type E and F prisms being 1850 psi, and 1900 psi, respectively. The fineness of the sand used in the mortar does not appear to have any effect on the compressive strength of a short wall. Additional tests must be conducted before a definite conclusion can be reached.

The compressive strength values for the 8 inch block prisms and the 10 inch block prisms were fairly close. It appears that the compressive strength is governed by the net area of the concrete block.

All prisms failed with a vertical splitting down the center plane of the prisms. This is due to the higher modulus of elasticity of the block units as compared to the modulus of elasticity of the mortar. This difference makes the mortar want to "flow" outwards out of the joints. This tendency of the mortar to "flow" causes shear forces to develop between the block units and the mortar, with the shear forces tending to pull the units apart. The prism walls split vertically down the center plane once the tensile strength of the webs of the blocks were exceeded. Plate 4.1 shows a typical splitting failure of a compressively loaded prism.

4.3 Modulus of Elasticity of Masonry

4.3.1 Prisms

Six prisms were mounted with vertical strain measuring LVDT's. Three 8 inch and three 10 inch block prisms were monitored. These prisms were five courses high with a Corner Sash and a Half block per course in running bond. The strains were measured over 4 complete unit-mortar

courses to give a reasonable average. This gave a gauge length of 32 inches. The 8 inch block prisms yielded an average modulus of elasticity, E_m, of 1,260 Ksi; while the 10 inch block prisms yielded an average E_m of 1,200 Ksi. The results of the tests are plotted in Fig. 4.1 and Fig. 4.2 where only the average value of E are shown. It must be noted that although the tests indicate a linear relationship for stress versus strain up to about 80% of the ultimate stress, it cannot be assumed the linearity continues beyond this point. Measurements had to be stopped at this level of load to avert damage to the LVDT's during the explosive prism failures.

4.4 Summary of Test Results of Full Scale Wall Specimens

4.4.1 Specimens With Slabs

The cast-in-place slab specimens failed in two distinct modes depending on the magnitude of axial load on the wall. The overall failure mode was independent of whether or not the wall was reinforced. The axial load at which the mode of failure changes is defined as the balanced load, P_b. For loads higher than the balanced load, a compressive strength failure of the wall occurs. The failure mode of walls subjected to axial loads less than the balanced load is a tensile failure. This behavior will be discussed in more detail in Chapter 5. Thus the walls fall into two categories: those with axial loads higher than P_b, and those with axial loads lower than P_b.

Although the failure modes of all the wall types were the same and were governed by the value of the axial load relative to P_b, the value of P_b for each wall type varied depending upon the block size and whether or not the walls were reinforced. In calculating the balanced

load it was assumed that cross-sections which were plane prior to loading remained plane after the load was applied, and that sufficient bonding of the grout to the reinforcing bars was developed to prevent slipping between the two materials. The second assumption ensures that the strain in the embedded bar is the same as that of the surrounding grout. With these assumptions and the data obtained from the prism tests, the balanced load, P_b, for Series A, Series B, Series C & D, and Series E were calculated to be 100 kips, 210 kips, 300 kips, and 95 kips respectively.

4.4.1.1 Walls Subjected to a Low Axial Load

The walls subjected to a low axial load, i.e., less than P_b, had a tension type failure. No distress in the walls were observed until approximately 80% of M_{max} (the maximum applied bending moment which the joint was able to resist) was applied to the system. At this point, horizontal cracks opened up in the mortar joints on the tension sides of the wall immediately above and/or below the slab. The size of the crack increased with increasing moment until M_{max} was reached. This was due to the slab end rotating more than the blocks above and below the slab. The cracks, at M_{max}, were more than 1/4 inch wide.

At this point, the blocks above and below the slab stopped rotating, while the slab end rotation greatly increased, as the wall maintained a constant moment equal to M_{max}. The slab end continued rotating until the joint failed by reaching its ultimate rotation capacity ($\theta = \theta_{ult}$). Throughout the entire test no vertical splitting cracks were detected in either the top or bottom wall.

4.4.1.2 Walls Subject to a High Axial Load

The walls subjected to a high axial load had a compressive mode of failure. The moment versus rotation behavior was similar to that for walls

subjected to lower loads until M_{max} was reached. But upon reaching M_{max}, the walls failed suddenly, with no significant difference of rotation between the slab end and the blocks above and/or below the slab (i.e. $\theta = 0$).

No large tensile cracks were observed in these walls, but many large vertical splitting cracks were found. Spalling of the mortar joint immediately above the slab and of the block immediately below the slab on the compression face of the walls was observed as M_{max} was approached.

The moment versus rotation relationships for the walls are summarized and presented graphically for the 8 inch unreinforced walls in Fig. 4.3 and Fig. 4.4, for the 8 inch reinforced walls in Fig. 4.5 and Fig. 4.6, and for the 10 inch reinforced walls in Fig. 4.7 and Fig. 4.8.

A photograph of wall E50 at failure, a typical tension type failure of an unreinforced wall, is presented in Plate 4.2. A photograph of wall E100 at failure, a typical compression failure of an unreinforced wall, is presented in Plate 4.3. A photograph of wall B50 at failure, a typical tension type failure of a reinforced wall, is presented in Plate 4.4. A photograph of wall B200 at failure, a typical compression failure of a reinforced wall, is shown in Plate 4.5.

4.4.2 Specimens Without Slabs

The failure of the walls without slabs occurred when the compressive strength of the unit was reached on the compression side of the wall. When the strength of the mortar was reached on the compressive side, pieces of the mortar fell off the wall but the wall supported additional load before failing.

Vertical splitting cracks formed as early as 50% of the maximum applied load. With increasing vertical load, these cracks opened up in width and propagated throughout the entire wall height. New vertical cracks

also appeared and grew in size as load was applied.

At failure the crushing of the compression side was accompanied simultaneously by separation of the blocks on the opposite side. This separation on the tension side resulted in the opening up of horizontal cracks as well as the spalling off of block and mortar from the wall. Plate 4.6 and Plate 4.7 show the compressive and the tensile faces of wall F1 at failure.

4.5 Unreinforced 8 Inch Walls With Slabs

4.5.1 Wall A50

Horizontal cracks opened up in the first mortar joints above and below the slab on the tension face of the top and bottom walls at 84% of M_{max}. The two cracks were approximately 1/16 inch wide when first observed. As load was applied the cracks widened to about 1/4 inch at M_{max}. The specimen continued to resist M_{max} as deflection of the slab was increased. The top and bottom walls experienced no further rotation of the blocks which were adjacent to the slab. The slab end continued to rotate until the difference between the rotation of the blocks above and below the slab, and the rotation of the slab end, θ, reached 1.66 degrees. At this θ value, the walls exploded. Except for the horizontal cracks at the first mortar joints above and below the slab, the top and bottom walls experienced no signs of distress during the test until the failure of the specimen. After the failure the mortar from the joint consisting of the slab and the block above the slab was bonded only to the slab. This indicates that the mortar bonds better to the slab concrete than the masonry block. The rotations of the walls and slab end together with the corresponding loads and moments are tabulated in Table 4.2 and the deflected shape is presented graphically in Fig. 4.9.

4.5.2 Wall A100

No cracks were detected in either the top or bottom walls before the sudden explosive failure. The tie back rods were too tight initially which induced the wall to deflect horizontally in the direction of the tie force. At failure, both top and bottom walls exploded. Seventy-five percent of the mortar from the first joint above the slab was bonded to the slab after failure. The rotations of the walls and slab end together with the corresponding loads and moments are tabulated in Table 4.3, and the deflected shape is presented graphically in Fig. 4.10.

4.5.3 Wall A101

A vertical splitting crack formed in the bottom wall at 90% M_{max}. No horizontal cracks were observed until M_{max} was reached. The failure was sudden, coming very soon after M_{max} was reached, with the bottom wall exploding. The top wall was intact after failure and showed no signs of distress. The rotation of the walls and slab end together with the corresponding loads and moments are listed in Table 4.4. The deflected shape is presented graphically in Fig. 4.11.

4.5.4 Wall A150

No horizontal cracks or vertical splitting cracks were detected during the test. The wall rotations followed the slab end rotation throughout the test. The failure was sudden, with the bottom wall exploding immediately upon reaching M_{max}. The top wall remained intact with no evidence of cracks at failure. Table 4.5 lists the rotations of the wall and slab end together with the corresponding loads and moments. Fig. 4.15 graphically presents the deflected shape.

4.5.5 Wall E50

Horizontal cracks opened up at the first mortar joints above and below the slab on the tension face of the walls at 76% of M_{max}. The

cracks were small at first but widened to 1/4 inch at M_{max}. No distress was detected, i.e. no mortar crushing or spalling, on the compressive face side of the wall at the mortar joint that was opening up. Plate 4.2 shows a side view of the specimen at M_{max}.

The behavior of the specimen after M_{max} was reached was identical to that of Wall A50. The specimen continued to resist M_{max} as deflection of the slab increased. The walls experienced no further rotation of the blocks which were adjacent to the slab. The slab continued to rotate until a θ value of 1.74 degrees was reached.

Throughout the test, the top and bottom walls experienced no sign of distress, except for the horizontal cracks in the first mortar joints above and below the slab. The mortar was bonded partly to the slab and partly to the block above the slab when the joint above the slab opened up.

The rotations of the walls and slab end along with the respective loads and moments are tabulated in Table 4.14, and the deflected shape is shown in Fig. 4.21.

4.5.6 Wall E100

No horizontal cracks were detected in the walls during the test. Vertical splitting cracks were observed in the top wall faces and in the sides of the slab at about 90% M_{max}. The vertical cracks in the wall faces were barely detectable and ran down the blocks in the bottom two courses of the top wall. The vertical cracks in the sides of the specimen started in the slab and progressed up through the three courses above the slab. The side cracks were 3/16 inch wide at M_{max}. Plate 4.3 shows Wall E100 at M_{max}.

Table 4.15 lists the rotations of the walls and the slab end along with the corresponding loads and moments. Fig. 4.22 presents the deflected shape of the specimen.

4.5.7 Wall E150

No horizontal or vertical cracks were detected during the test. The wall rotations followed the slab end rotation throughout the test. The failure was sudden, with the bottom wall exploding immediately upon reaching M_{max}. The top wall remained intact and showed no signs of distress after failure.

Table 4.16 lists the rotations of the wall and slab end together with the corresponding loads and moments. Fig. 4.23 graphically presents the deflected shape of the specimen.

4.6 Reinforced 8 Inch Walls With Slabs

4.6.1 Wall B50

At 81% of M_{max}, tensile cracks opened up between the slab and the block below the slab on the tension (back side) face of the lower wall. The horizontal crack opened up to approximately 1/4 inch at M_{max}. Horizontal cracks opened up on the tensile face of the walls just prior to M_{max}, in the first mortar joint above the slab, and in the joint between the first and second blocks below the slab. These cracks opened wider as M_{max} was achieved. The specimen was able to sustain M_{max} as θ increased from 0.61 degrees to 1.25 degrees. Once θ reached 1.25 degrees the moment capacity of the specimen drastically dropped off. The rotations of the walls and the slab end together with the corresponding loads and moments are listed in Table 4.6, and the deflected shape is graphically presented in Fig. 4.13.

4.6.2 Wall B150

At 70% of M_{max} vertical cracks were observed in the middle of the front and back face of the top wall. As more moment was applied vertical

cracks opened on the side faces of the specimen, running from the block below the slab up through the slab and to the top of the block immediately above the slab. These vertical side cracks grew to 1/2 inch wide at M_{max}. A horizontal crack appeared prior to M_{max} on the tension face of the top wall, two joints above the slab. Crushing of the block below the slab began prior to M_{max}. The crushing occurred 1 inch below the slab and extended across the entire front face of the bottom wall. Failure occurred immediately upon reaching M_{max}. The rotations of the walls and the slab end together with the corresponding loads and moments are listed in Table 4.7. The deflected shape is shown in Fig. 4.14.

4.6.3 Wall B200

No horizontal tensile cracks were detected during the test. A vertical crack opened up at 70% of M_{max} in the top wall just above the slab. The crack propagated to the top of the wall upon further loading. Several vertical cracks opened in the bottom wall as shown in Plate 4.5. Crushing in the block below the slab was observed. The crushing was only detected over an eight inch length on the front face. The failure of the specimen occurred at M_{max}. Table 4.8 lists the rotations of the wall and the slab end along with the corresponding loads and moments. Fig. 4.15 graphically shows the deflected shape of the specimen.

4.6.4 Wall B320

A vertical crack appeared in the center three courses of the top wall at 45% of P_{max} (the maximum applied vertical wall load). This crack widened with increased loads. No new cracks appeared until 95% of P_{max} was reached. The new cracks were vertical cracks in the lower back portion of the top wall.

At P_{max} the top wall suddenly failed. The back portion failed in compression as the compressive strength of the units was reached. The

sudden failure buckled the reinforcement in the third course from the top, causing the removal of the block facing on the tension face.

The rotations of the wall blocks and the slab end along with the respective loads and moments are tabulated in Table 4.9. The deflected shape of the specimen is presented graphically in Fig. 4.16.

4.7 Reinforced 10 Inch Walls With Full Penetration Slabs

4.7.1 Wall C200

A vertical hairline crack opened on the side of the slab at 20% M_{max}. This crack eventually spread vertically through the block below the slab and through the four blocks above the slab. At M_{max}, the crack was 1/8 inch wide. Vertical cracks opened on the front face of the top wall at 75% of M_{max}. These cracks started in the first two courses above the slab and propagated up through the next two courses as further loading was applied. The largest vertical crack on the top face at failure was 1/16 inch wide. No vertical or horizontal cracks developed in the bottom wall. Upon reaching M_{max}, the moment capacity significantly dropped to about 75% M_{max}. The rotations of the walls and slab end together with the corresponding loads and moments are tabulated in Table 4.10, and the deflected shape is presented graphically in Fig. 4.17.

4.7.2 Wall C300

Vertical cracks in the sides of the slab appeared at 50% of M_{max}. These cracks extended one block above and below the slab, and widened to 1/16 inch at M_{max}. At 70% of M_{max} vertical cracks began to form on the front and sides of the top wall. The cracks on the front were extremely narrow and ran the entire length of each vertical mortar joint. The vertical cracks on the sides of the top wall were 1/8 inch wide and

propagated through the center of the bottom five courses of the top wall.

The moment capacity of the wall dropped to 85% of M_{max} upon reaching failure. The rotations of the walls and slab end along with the respective loads and moments are listed in Table 4.11, and the deflected shape is shown in Fig. 4.18.

4.8 Reinforced 10 Inch Walls With Partial Penetration Slabs

4.8.1 Wall D200

At 60% of M_{max}, vertical cracks opened between the slab and the slab block. Initially, these cracks ran through the slab and the block above the slab and were very narrow. These cracks eventually propagated down through the course immediately below the slab and were 1/4 inch wide upon reaching M_{max}. Several vertical cracks appeared in the front and back faces of the top wall soon after the cracks in the slab appeared. Initially these cracks were hairline in size and were only one or two courses long. As M_{max} was approached the cracks grew in length to run the entire length of the top wall along vertical mortar joint lines, and were up to 1/8 inch wide. The bottom wall had no cracks of any kind, except for the two vertical cracks on the sides of the top course that had propagated down from the crack between the slab and the slab block.

Upon reaching M_{max}, the moment carrying capacity of the specimen dropped to about 80% of M_{max}. Table 4.12 lists the rotations of the walls and the slab end together with the corresponding loads and moments. Fig. 4.19 graphically presents the deflected shape of the specimen.

4.8.2 Wall D300

Wall D300 behaved the same as Wall D200. Cracks between the slab and

the slab block appeared first and propagated up two blocks into the top wall and two blocks down into the bottom wall as M_{max} was reached. The cracks grew to a maximum size of 1/8 inch in width.

Vertical cracks appeared in the front and back face of the top wall, running along the vertical mortar joint lines. With increasing moment being applied the cracks grew to 1/16 inch in width, and ran the entire wall length.

The bottom wall showed no signs of distress on the front and back faces. The rotation of the walls and slab end together with the associated moments and loads are listed in Table 4.13. The deflected shape is presented graphically in Fig. 4.20.

4.9 Reinforced 8 Inch Walls Without Slabs

4.9.1 Wall F1

No cracks formed in the wall prior to 70% of P_{max}. At this point, a vertical crack formed along one of the vertical mortar joint lines and penetrated through the entire 8 inch thickness of the wall. No more cracks appeared until 95% of P_{max} when two more sets of vertical cracks, like the first set, opened up. The width of the cracks when they first opened were approximately 1/8 inch.

At P_{max} the wall failed due to the compressive strength of the units being exceeded on the compressive side of the wall. The explosive failure resulted in the spalling off of mortar and blocks from the compressive side of the wall, as well as the dislodging of the block shells from the tensile side of the wall.

Fig. 4.24 graphically presents the deflected shape of the specimen.

4.9.2 Wall F2

Wall F2 behaved the same as Wall F1. The only difference between the two walls was that Wall F2 failed at a load 3% higher than that of Wall F1, and the vertical cracks opened up at different loads.

The first vertical crack in Wall F2 developed at 50% of P_{max} and the second and last vertical crack opened up at 95% of P_{max}. The first crack propagated through the entire length of the wall and was 3/16 inch wide just prior to failure. The second crack to form was only 1/32 inch wide and three blocks high (24 inches long) prior to failure. Fig. 4.25 shows the deflected shape of the wall.

Plate 4.6 shows the compressive face of Wall F1 after failure, and Plate 4.7 shows the tensile face of Wall F1 after failure. These photographs are typical of both Series F wall failures.

TABLE 4.1 COMPRESSIVE STRENGTH OF MASONRY FROM PRISM TESTS

Type of Prism		Series	No. of Prisms Tested	$\frac{h}{t}$	Net Area (in^2)	Ultimate Load (kips)	h/t Correction Factor[1]	f'_m (psi)
Block Size	Blocks Used Per Course							
8 inch	1 Standard	A,B	4	2.05	58	131.4	1.01	2290
8 inch	1 Standard	A,B	5	3.10	58	120.4	1.20	2490
8 inch	1 Standard	A,B	2	5.20	58	113.4	1.20	2350
8 inch	1 Corner + 1 Half	A,B	4	5.25	98	151.0	1.20	1820
8 inch	1 Corner + 1 Half	E,F	3	5.25	98	155.6	1.20	1900
10 inch	1 Corner + 1 Half	C,D	3	4.16	135	194.3	1.20	1730

1 Table 1 CSA Standard S304-1977

TABLE 4.2 MOMENTS, LOADS, AND ROTATIONS FOR WALL A50

M_{slab} Kip-In	T Kips	M_{wall} Kip-In	P_{wall} Kips	ϕ_v Degrees	ϕ_h Degrees	θ Degrees
48	4.94	27	51	0.00	0.00	0.00
97	4.74	50	51	0.00	0.00	0.00
147	4.51	85	51	0.04	0.04	0.00
192	4.19	109	51	0.10	0.10	0.00
237	4.29	136	51	0.13	0.14	0.01
297	3.37	169	51	0.18	0.19	0.01
351	1.01	200	51	0.23	0.25	0.02
394	0.09	191	51	0.28	0.28	0.00
448	0.00	213	51	0.32	0.40	0.08
467	-0.02	225	51	0.35	1.14	0.79
460	-0.04	224	51	0.35	1.63	1.28
451	-0.07	220	51	0.34	2.00	1.66

TABLE 4.3 MOMENTS, LOADS, AND ROTATIONS FOR WALL A100

M_{slab} Kip-In	T Kips	M_{wall} Kip-In	P_{wall} Kips	ϕ_v Degrees	ϕ_h Degrees	ϕ Degrees
48	6.14	194	103	-0.06	0.00	0.06
98	9.63	334	104	-0.08	0.03	0.11
146	9.28	346	105	-0.04	0.02	0.06
192	8.84	356	106	-0.01	0.00	0.01
245	8.14	360	107	0.03	0.01	-0.02
293	7.41	362	108	0.08	-0.01	-0.09
343	6.82	370	109	0.13	-0.03	-0.16
410	5.92	378	110	0.20	-0.03	-0.23
437	5.58	381	111	0.22	-0.05	-0.27
504	4.59	387	112	0.29	-0.07	-0.36
554	3.86	391	113	0.34	-0.08	-0.42

TABLE 4.4 MOMENTS, LOADS, AND ROTATIONS FOR WALL A1Q1

M_{slab} Kip-In	T Kips	M_{wall} Kip-In	P_{wall} Kips	ϕ_v Degrees	ϕ_h Degrees	θ Degrees
48	0.92	56	103	-0.03	-0.01	0.02
98	0.41	51	104	-0.02	0.03	0.05
142	0.24	80	105	-0.01	0.05	0.06
206	0.24	110	106	0.01	+0.08	0.07
244	0.27	129	107	0.03	0.12	0.09
287	0.27	149	108	0.04	0.13	0.09
340	0.30	175	109	0.06	0.14	0.08
412	0.33	209	111	0.08	0.19	0.11
459	0.38	232	112	0.09	0.23	0.14
502	0.40	253	112	0.10	0.24	0.14
560	0.47	281	114	0.12	0.29	0.17
600	0.60	304	115	0.12	0.33	0.21
657	0.80	336	116	0.13	0.38	0.25
697	1.13	363	117	0.13	0.44	0.31
752	1.28	394	118	0.13	0.56	0.43
670	0.15	327	116	0.19	0.73	0.54

TABLE 4.5 MOMENTS, LOADS, AND ROTATIONS FOR WALL A150

M_{slab} Kip-In	T Kips	M_{wall} Kip-In	P_{wall} Kips	ϕ_v Degrees	ϕ_h Degrees	θ Degrees
47	0.00	61	153	0.00	0.00	0.00
95	0.62	106	154	0.00	0.00	0.00
203	0.64	158	156	0.06	0.05	0.01
312	0.71	212	158	0.10	0.11	0.01
408	0.80	259	160	0.12	0.14	0.02
501	0.84	304	162	0.16	0.22	0.04
602	0.90	354	164	0.22	0.30	0.08
703	0.95	403	167	0.27	0.39	0.12
719	0.94	410	167	0.29	0.41	0.12

TABLE 4.6 MOMENTS, LOADS, AND ROTATIONS FOR WALL B50

M_{slab} Kip-In	T Kips	M_{wall} Kip-In	P_{wall} Kips	ϕ_v Degrees	ϕ_h Degrees	θ Degrees
48	2.54	96	53	-0.03	-0.03	0.00
97	4.40	182	54	-0.02	0.00	0.02
151	4.14	200	56	0.01	0.04	0.03
201	3.86	216	57	0.03	0.07	0.04
247	3.52	227	58	0.05	0.10	0.05
313	3.02	244	59	0.08	0.15	0.07
358	2.66	255	60	0.10	0.18	0.08
407	2.06	261	61	0.16	0.25	0.09
459	1.59	272	62	0.21	0.34	0.13
508	0.98	278	63	0.26	0.43	0.17
552	0.40	283	64	0.29	0.60	0.31
600	0.63	315	65	0.34	0.95	0.61
617	0.32	315	65	0.38	1.18	0.80
608	0.39	314	65	0.39	1.43	1.04
570	1.89	314	64	0.39	1.64	1.25
530	0.18	279	64	0.42	1.65	1.23

TABLE 4.7 MOMENTS, LOADS, AND ROTATIONS FOR WALL B150

M_{slab} Kip-In	T Kips	M_{wall} Kip-In	P_{wall} Kips	ϕ_v Degrees	ϕ_h Degrees	θ Degrees
47	1.58	60	153	0.02	0.02	0.00
98	1.63	85	154	0.02	0.04	0.02
193	1.65	128	156	0.05	0.07	0.02
290	1.70	175	158	0.07	0.10	0.03
408	1.79	233	161	0.11	0.16	0.05
503	1.86	279	163	0.14	0.20	0.06
601	1.96	327	165	0.16	0.25	0.09
696	1.97	371	167	0.20	0.30	0.10
792	2.07	419	169	0.23	0.37	0.14
914	2.09	477	171	0.27	0.49	0.22
1008	2.12	520	173	0.33	0.63	0.30
1094	2.27	565	175	0.38	0.81	0.43
1123	2.38	583	176	0.40	0.89	0.49

TABLE 4.8 MOMENTS, LOADS, AND ROTATIONS FOR WALL B200

M_{slab}	T	M_{wall}	P_{wall}	ϕ_v	ϕ_h	θ
Kip-In	Kips	Kip-In	Kips	Degrees	Degrees	Degrees
50	3.33	102	203	-0.02	-0.01	0.01
110	3.36	131	205	0.00	0.01	0.01
195	3.40	171	206	0.01	0.02	0.01
289	3.47	216	208	0.03	0.06	0.03
413	3.63	278	211	0.06	0.11	0.05
483	3.66	311	212	0.08	0.13	0.05
601	3.76	369	215	0.11	0.20	0.09
699	3.82	417	217	0.14	0.25	0.09
797	3.82	462	219	0.18	0.33	0.15
891	3.77	505	221	0.21	0.41	0.20
1010	3.36	552	224	0.28	0.60	0.32
1106	2.60	580	226	0.35	0.72	0.37
1128	2.20	581	226	0.41	0.80	0.39
1076	0.59	520	225	0.49	0.89	0.40

TABLE 4.9 MOMENTS, LOADS, AND ROTATIONS FOR WALL B320

M_{slab} Kip-In	T Kips	M_{wall} Kip-In	P_{wall} Kips	ϕ_v Degrees	ϕ_h Degrees	0 Degrees
48	2.05	80	53	-0.02	-0.02	0.00
48	2.83	98	103	-0.02	0.00	0.02
48	3.31	107	154	-0.02	0.01	0.03
48	9.07	293	203	0.05	0.05	0.00
48	8.93	289	243	0.04	0.04	0.00
49	8.56	279	304	0.02	0.02	0.00
48	8.40	276	324	0.01	0.01	0.00

TABLE 4.10 MOMENTS, LOADS, AND ROTATIONS FOR WALL C200

M_{slab} Kip-In	T Kips	M_{wall} Kip-In	P_{wall} Kips	ϕ_v Degrees	ϕ_h Degrees	θ Degrees
46	-0.08	18	204	0.00	-0.01	-0.01
100	-0.08	44	206	0.00	0.02	0.02
198	-0.08	90	208	0.03	0.04	0.01
295	-0.08	136	210	0.06	0.05	-0.01
371	0.87	211	211	0.04	0.07	0.03
486	0.85	264	214	0.09	0.08	-0.01
576	1.52	334	216	0.07	0.16	0.09
708	2.51	435	218	0.14	0.27	0.13
803	2.47	479	220	0.13	0.31	0.18
891	2.44	519	222	0.17	0.38	0.21
1021	2.33	576	225	0.20	0.49	0.29
1104	2.25	612	227	0.22	0.54	0.32
1035	2.70	596	225	0.26	0.71	0.45
848	2.87	525	221	0.12	1.26	1.14
560	2.41	374	215	0.05	1.00	0.95
273	2.06	226	209	0.02	0.58	0.56
50	1.91	115	205	-0.03	0.32	0.35

TABLE 4.11 MOMENTS, LOADS, AND ROTATIONS FOR WALL C300

M_{slab} Kip-In	T Kips	M_{wall} Kip-In	P_{wall} Kips	ϕ_v Degrees	ϕ_h Degrees	θ Degrees
46	1.13	68	303	0.00	0.00	0.00
142	1.14	114	303	0.02	0.04	0.02
289	1.13	187	303	0.03	0.07	0.04
435	1.14	259	303	0.06	0.13	0.07
548	2.05	345	303	0.09	0.15	0.06
672	2.08	408	303	0.11	0.24	0.13
778	2.13	463	303	0.13	0.31	0.18
908	2.23	533	303	0.14	0.42	0.28
942	3.80	595	303	0.23	0.59	0.36
907	2.13	515	303	0.23	0.85	0.52
857	2.26	485	303	0.20	1.10	0.90
745	2.27	415	303	0.10	1.25	1.15

TABLE 4.12 MOMENTS, LOADS, AND ROTATIONS FOR WALL D200

M_{slab} Kip-In	T Kips	M_{wall} Kip-In	P_{wall} Kips	ϕ_v Degrees	ϕ_h Degrees	θ Degrees
48	-0.02	18	202	0.00	0.00	0.00
141	-0.02	62	203	0.01	0.00	-0.01
223	-0.02	102	203	0.02	0.06	0.04
298	-0.02	139	203	0.04	0.05	0.01
412	-0.02	195	203	0.06	0.10	0.04
506	-0.02	241	203	0.07	0.11	0.04
607	-0.01	289	203	0.09	0.17	0.08
680	0.00	325	202	0.12	0.27	0.15
819	0.04	391	203	0.20	0.48	0.28
911	0.21	430	203	0.25	0.66	0.41
807	0.76	354	202	0.34	1.06	0.72
748	0.82	321	203	0.33	1.17	0.84
514	0.04	218	203	0.07	0.22	0.15

TABLE 4.13 MOMENTS, LOADS, AND ROTATIONS FOR WALL D300

M_{slab} Kip-In	T Kips	M_{wall} Kip-In	P_{wall} Kips	ϕ_v Degrees	ϕ_h Degrees	θ Degrees
49	0.04	29	305	0.00	0.00	0.00
99	0.04	54	306	0.01	0.04	0.03
196	0.07	101	308	0.08	0.11	0.03
292	0.10	147	310	0.11	0.10	-0.01
390	0.15	195	312	0.15	0.17	0.02
487	0.21	241	314	0.19	0.16	-0.03
580	0.25	287	316	0.22	0.22	0.00
724	0.39	360	319	0.30	0.31	0.01
821	0.55	413	321	0.36	0.56	0.20
868	0.56	439	322	0.41	0.63	0.22
796	0.75	424	320	0.49	0.85	0.36
733	0.82	400	319	0.48	0.92	0.44

TABLE 4.14 MOMENTS, LOADS, AND ROTATIONS FOR WALL E50

M_{slab} Kip-In	T Kips	M_{wall} Kip-In	P_{wall} Kips	ϕ_v Degrees	ϕ_h Degrees	θ Degrees
50	1.29	-13	51	-0.07	-0.05	0.02
98	2.65	-33	51	0.01	0.00	-0.01
152	2.61	- 7	51	-0.01	0.06	0.05
207	2.44	24	51	-0.01	0.09	0.08
257	2.17	56	51	0.02	0.19	0.17
292	1.88	80	51	0.08	0.23	0.15
354	1.23	128	51	0.21	0.34	0.13
396	0.81	160	51	0.28	0.53	0.25
450	0.15	207	51	0.24	1.09	0.85
464	0.10	216	51	0.25	1.74	1.49
446	0.06	209	51	0.24	1.97	1.73
429	0.04	202	51	0.24	1.98	1.74

TABLE 4.15 MOMENTS, LOADS,AND ROTATIONS FOR WALL E100

M_{slab} Kip-In	T Kips	M_{wall} Kip-In	P_{wall} Kips	ϕ_v Degrees	ϕ_h Degrees	θ Degrees
48	-0.01	27	103	0.00	0.00	0.00
135	0.60	88	105	0.03	0.02	-0.01
153	0.51	96	105	0.02	0.02	0.00
203	0.50	117	106	0.04	0.03	-0.01
242	0.48	135	107	0.07	0.06	-0.01
299	0.50	162	108	0.09	0.10	0.01
347	0.52	185	109	0.10	0.16	0.06
388	0.55	205	110	0.11	0.15	0.04
436	0.61	230	111	0.12	0.24	0.12
501	0.61	261	112	0.15	0.39	0.24
536	0.64	279	113	0.17	0.42	0.25
581	0.70	302	114	0.19	0.48	0.29
671	0.72	345	116	0.22	0.64	0.42
703	0.74	361	117	0.23	0.71	0.48
741	0.87	383	117	0.24	0.84	0.60
234	1.23	160	107	0.31	1.35	1.04

TABLE 4.16 MOMENTS, LOADS, AND ROTATIONS FOR WALL E150

M_{slab} Kip-In	T Kips	M_{wall} Kip-In	P_{wall} Kips	ϕ_v Degrees	ϕ_h Degrees	θ Degrees
49	2.08	92	153	0.00	0.00	0.00
114	2.11	123	155	0.00	-0.01	-0.01
152	2.13	142	155	-0.03	-0.02	0.01
201	2.18	166	156	-0.03	-0.03	0.00
239	2.22	185	157	-0.02	0.03	0.05
293	2.30	213	158	0.00	0.05	0.05
363	2.37	248	160	0.04	0.08	0.04
391	2.38	261	160	0.05	0.10	0.05
467	2.45	299	162	0.09	0.17	0.08
494	2.48	313	163	0.10	0.17	0.07
535	2.51	333	163	0.12	0.21	0.09
600	2.57	365	165	0.14	0.25	0.11
619	2.24	365	165	0.18	0.32	0.14

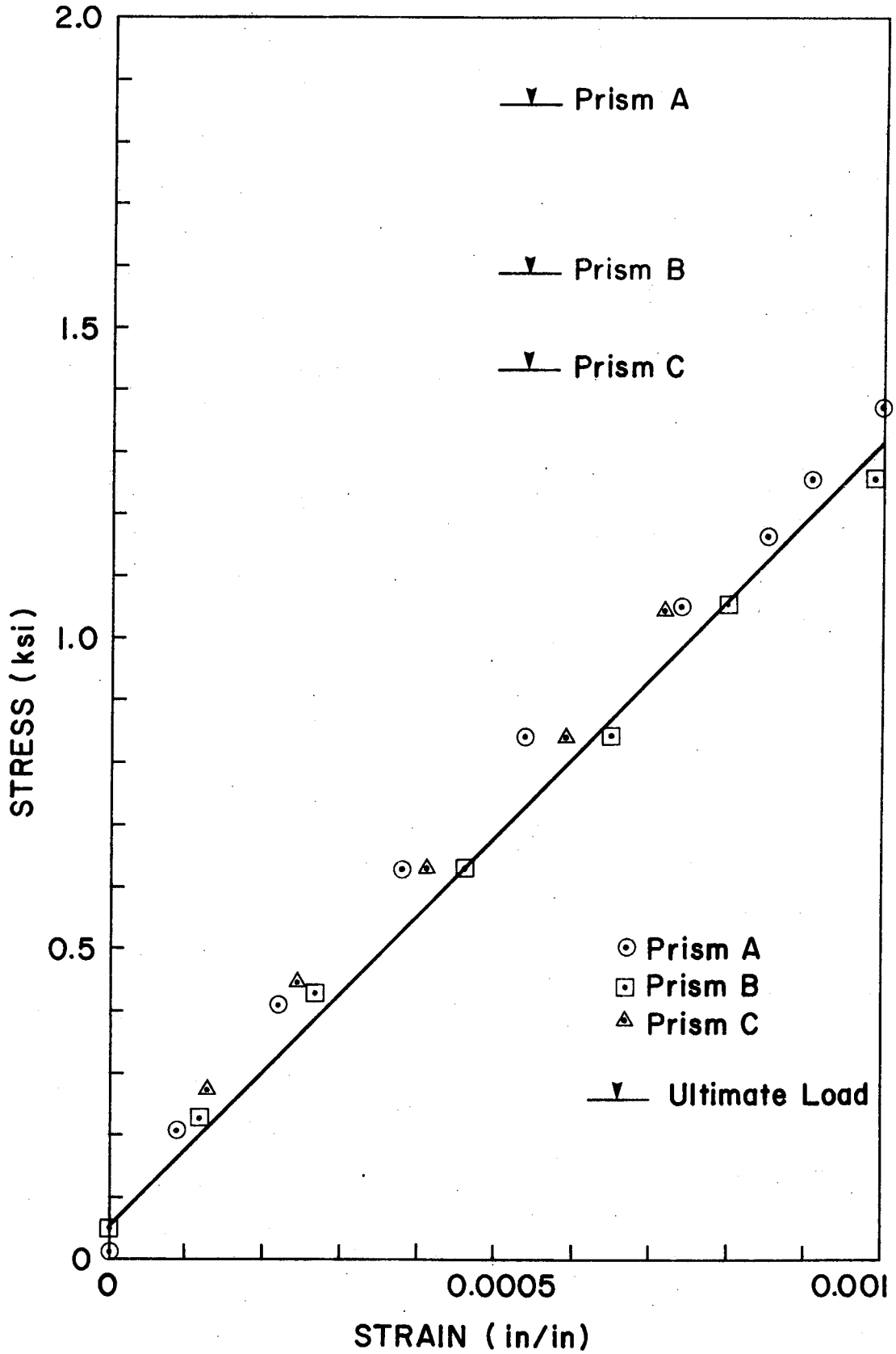

Fig. 4.1 Stress Versus Strain for 8 Inch Prisms

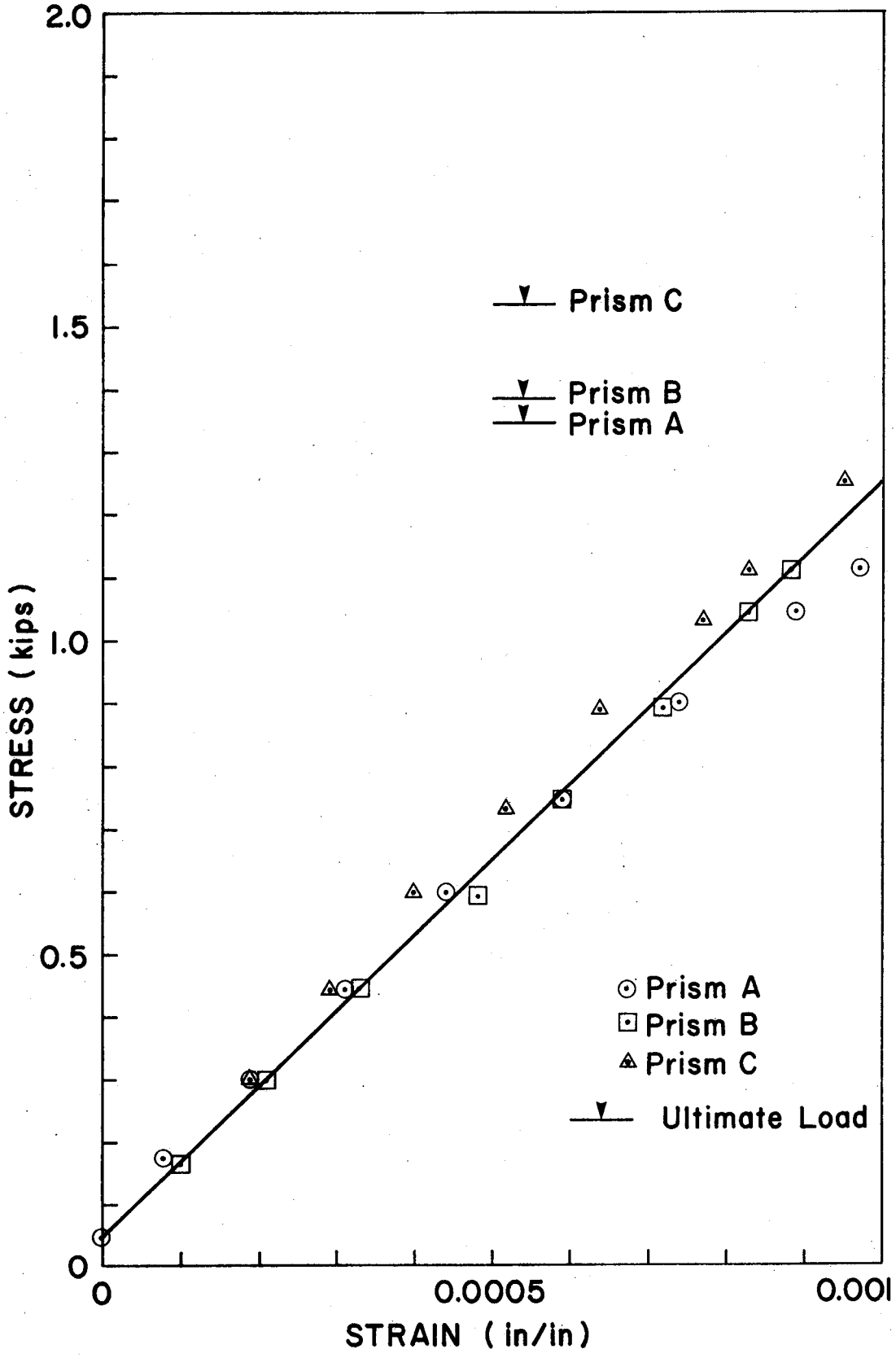

Fig. 4.2 Stress versus Strain for 10 Inch Prisms

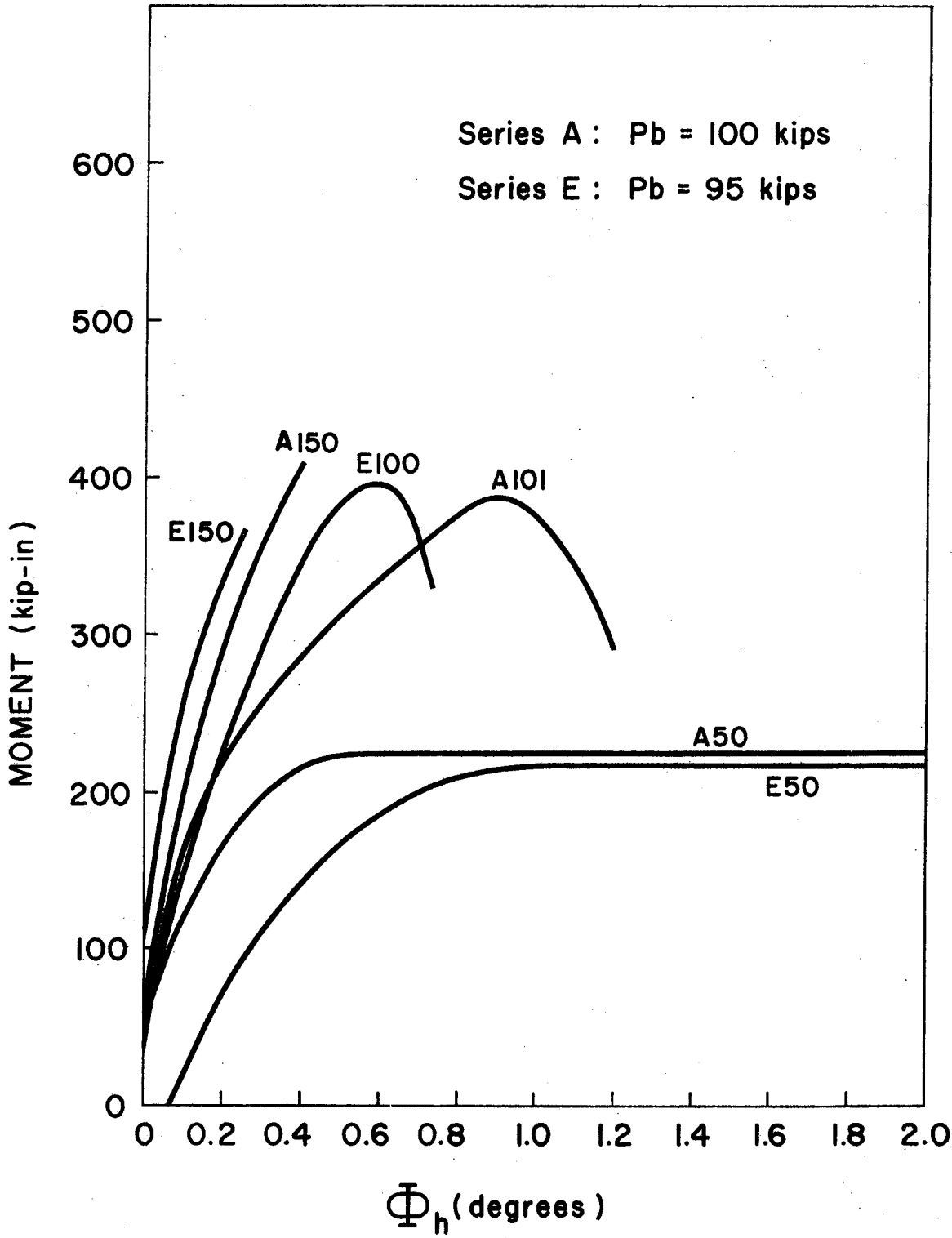

Fig. 4.3 Slab Rotation versus Moment for Unreinforced 8 Inch Walls

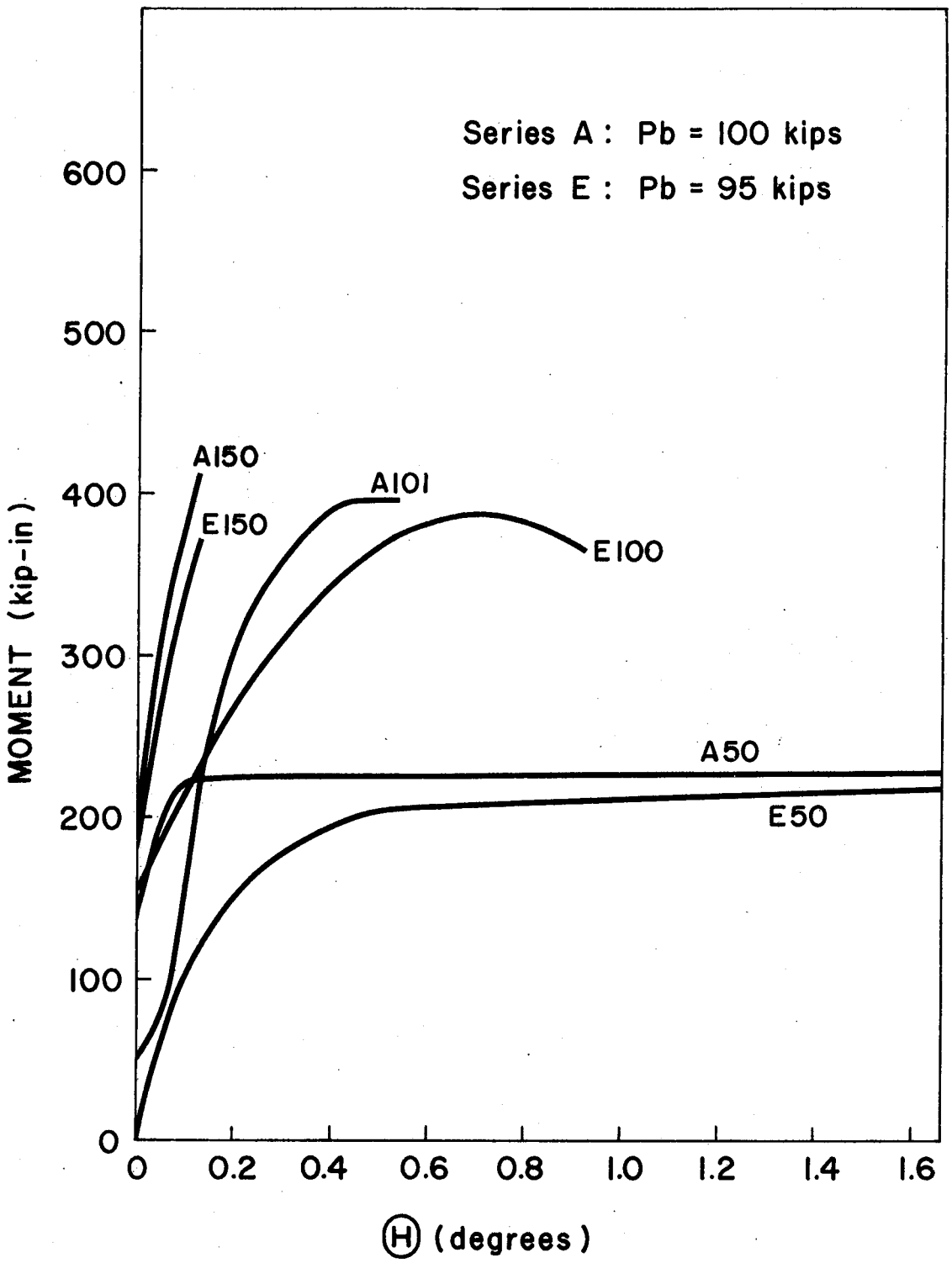

Fig. 4.4 Joint Rotation versus Moment for Unreinforced 8 Inch Walls

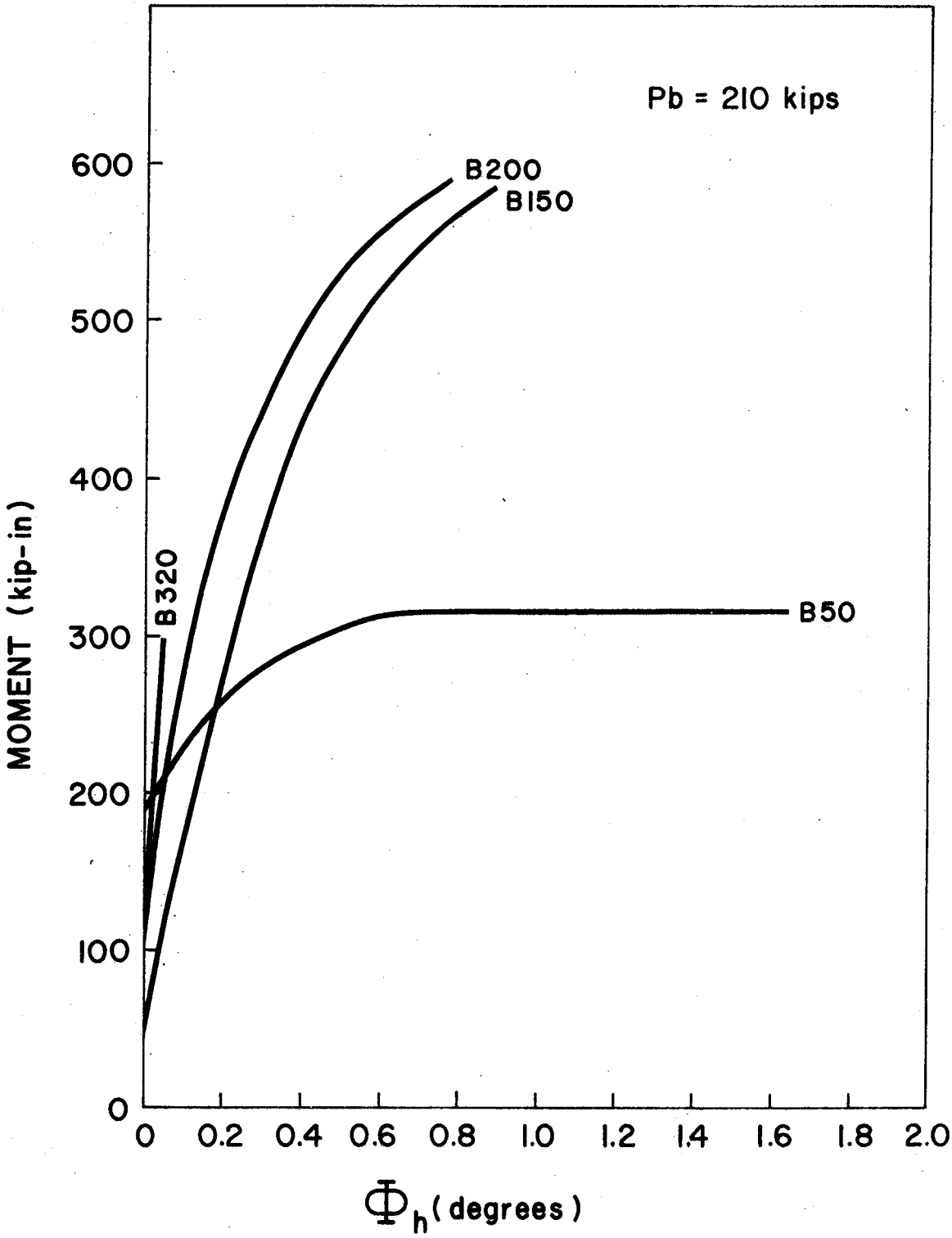

Fig. 4.5 Slab Rotation versus Moment for Reinforced 8 Inch Walls

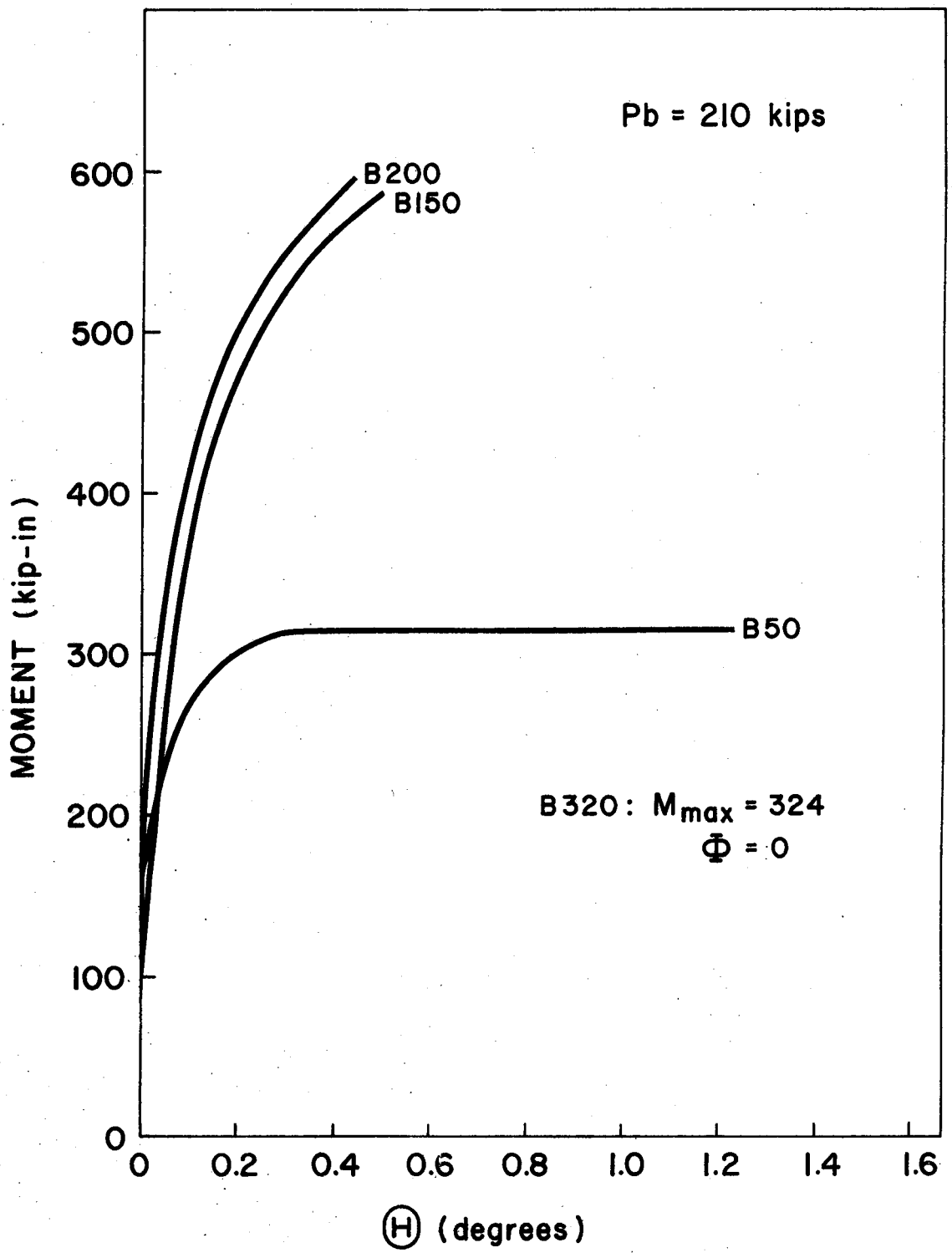

Fig. 4.6 Joint Rotation versus Moment for Reinforced 8 Inch Walls

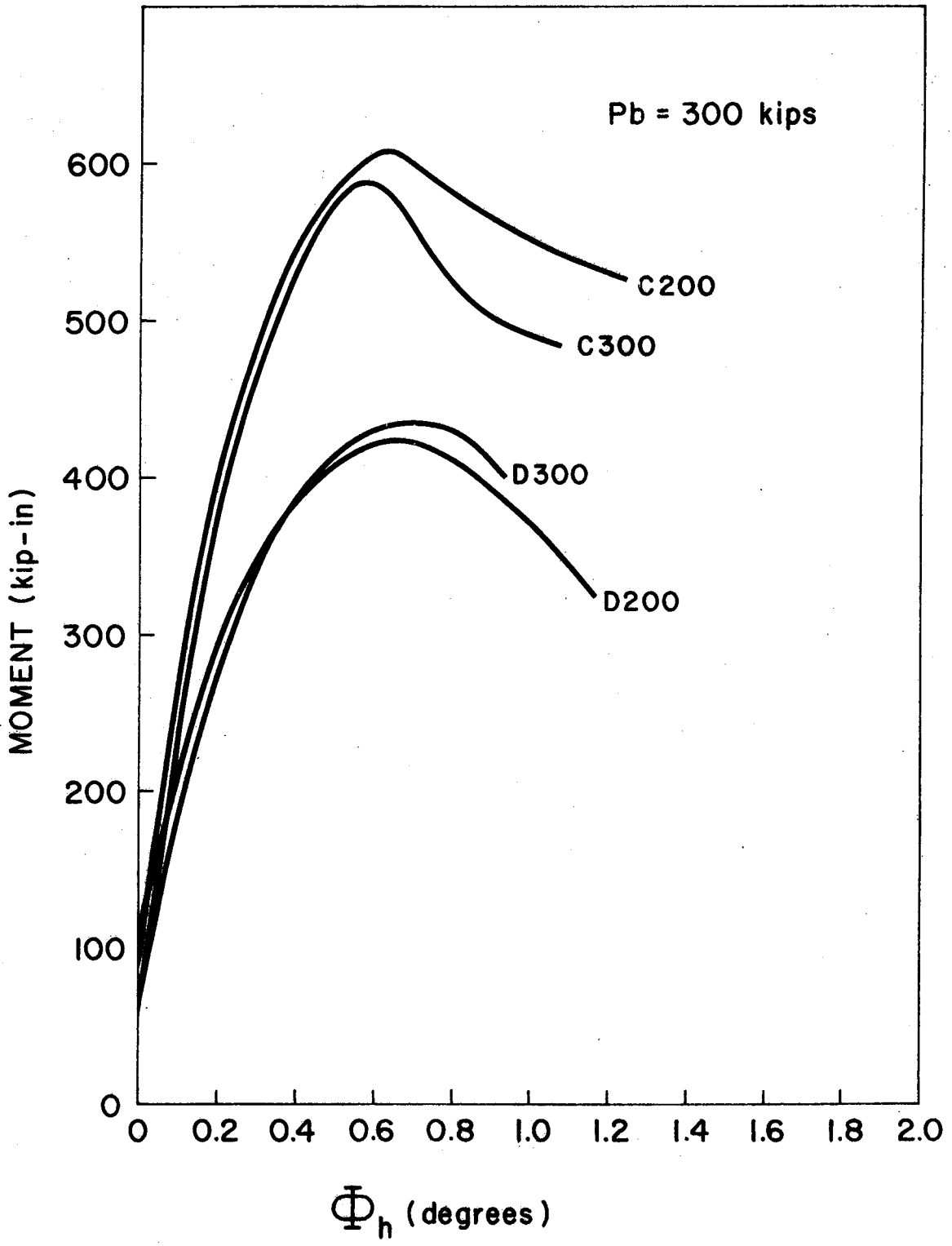

Fig. 4.7 Slab Rotation versus Moment for Reinforced 10 Inch Walls

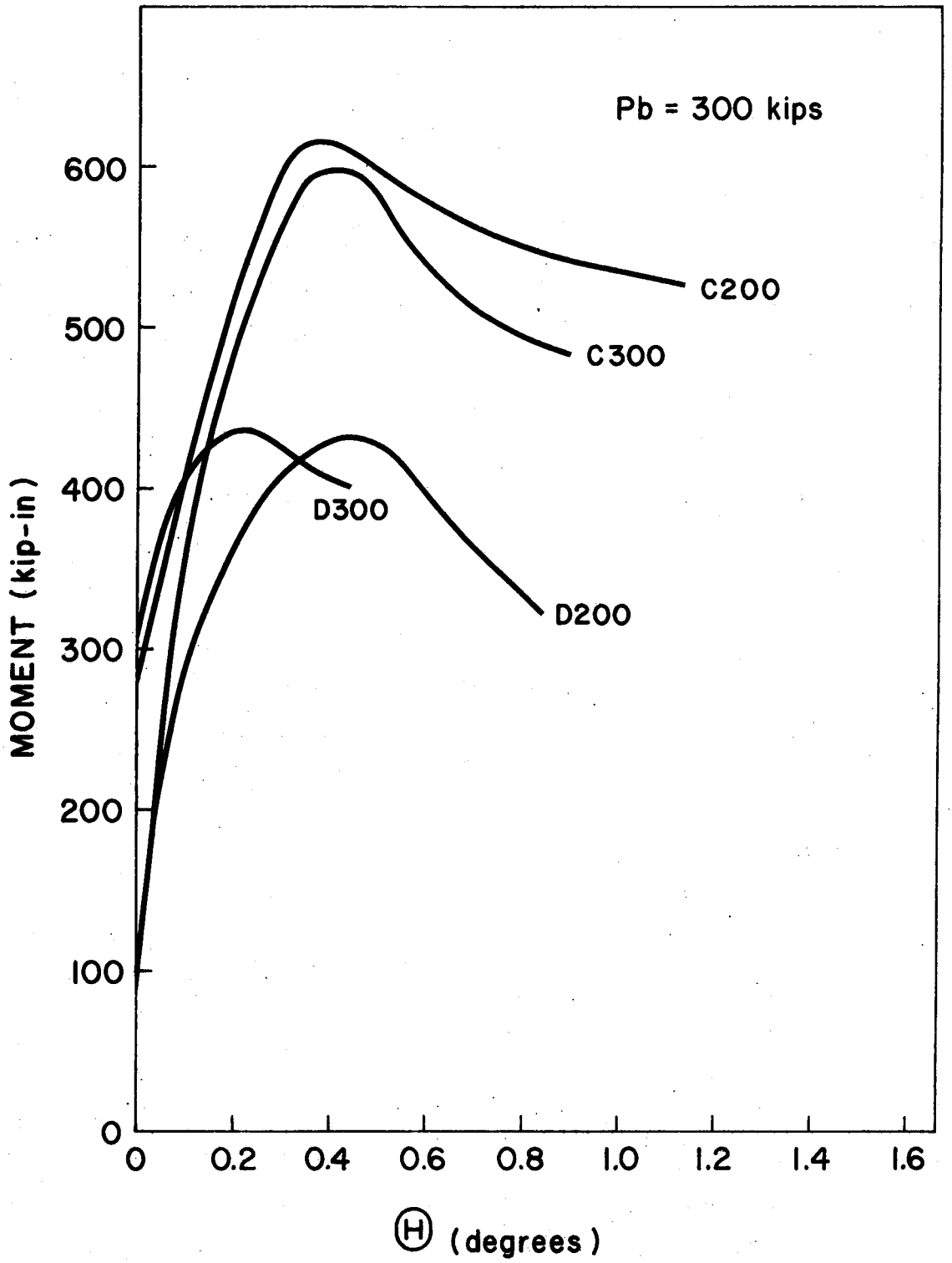

Fig. 4.8 Joint Rotation versus Moment for Reinforced 10 Inch Walls

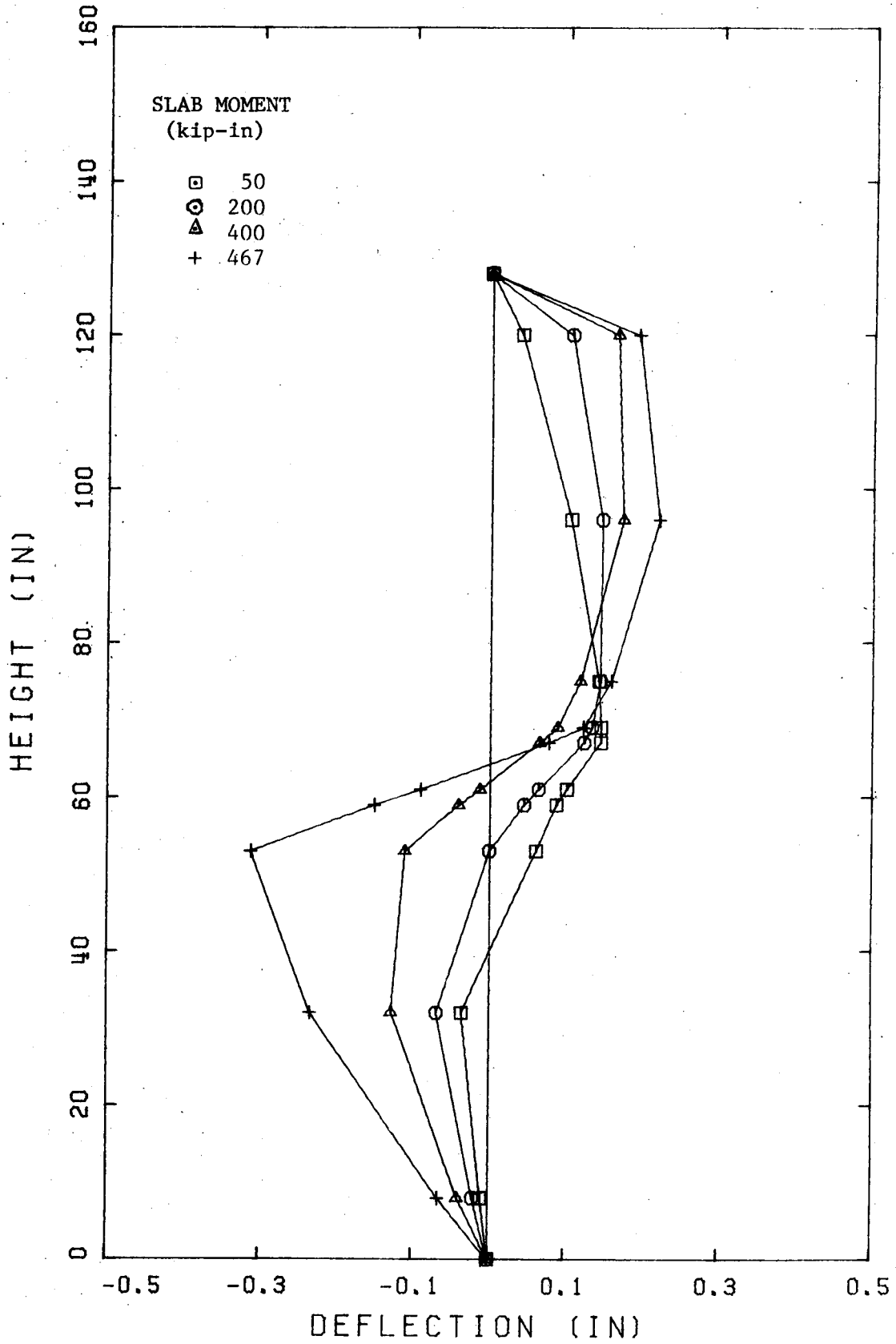

Fig. 4.9 Deflected Shape of Wall A50

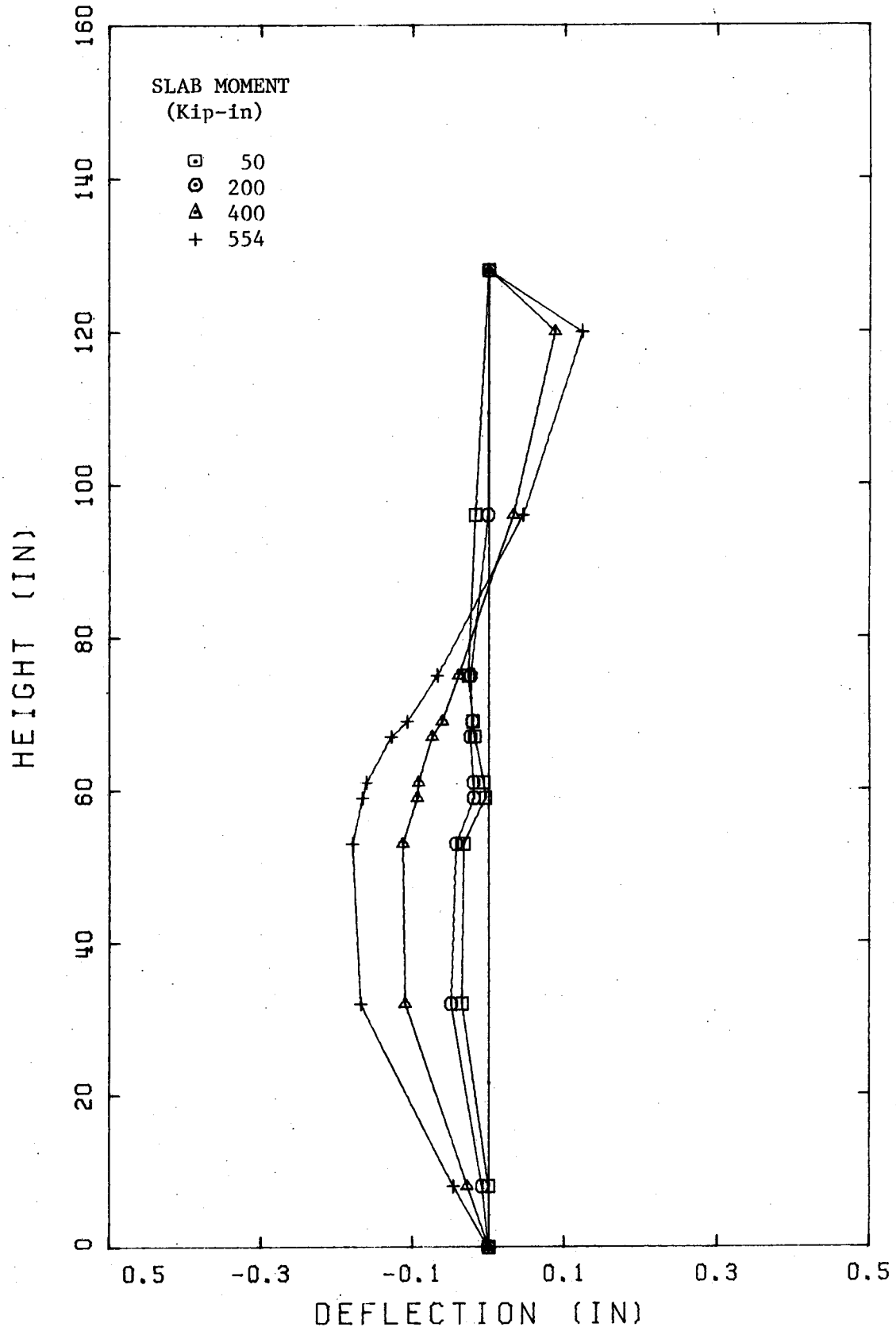

Fig. 4.10 Deflected Shape of Wall A100

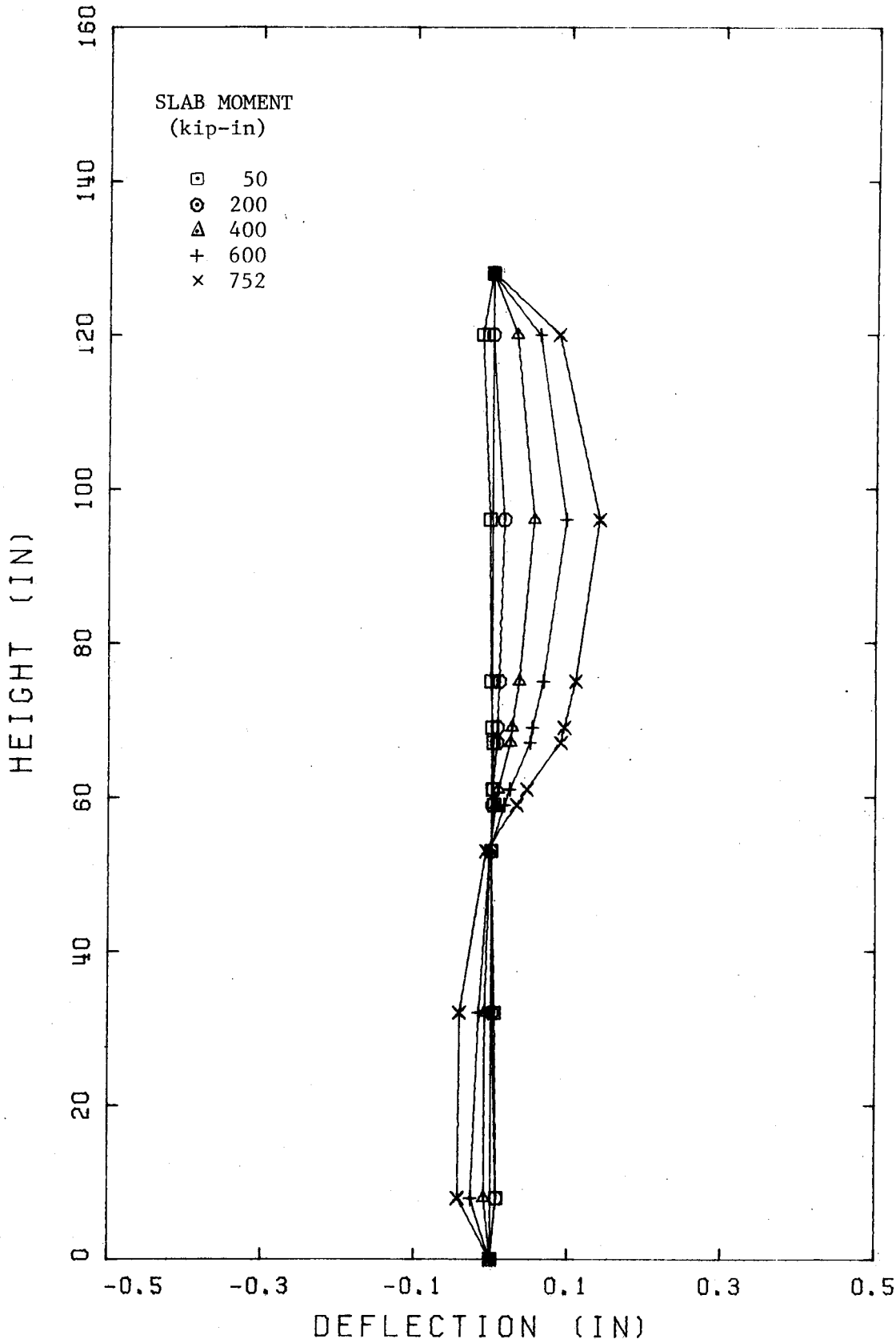

Fig. 4.11 Deflected Shape of Wall A101

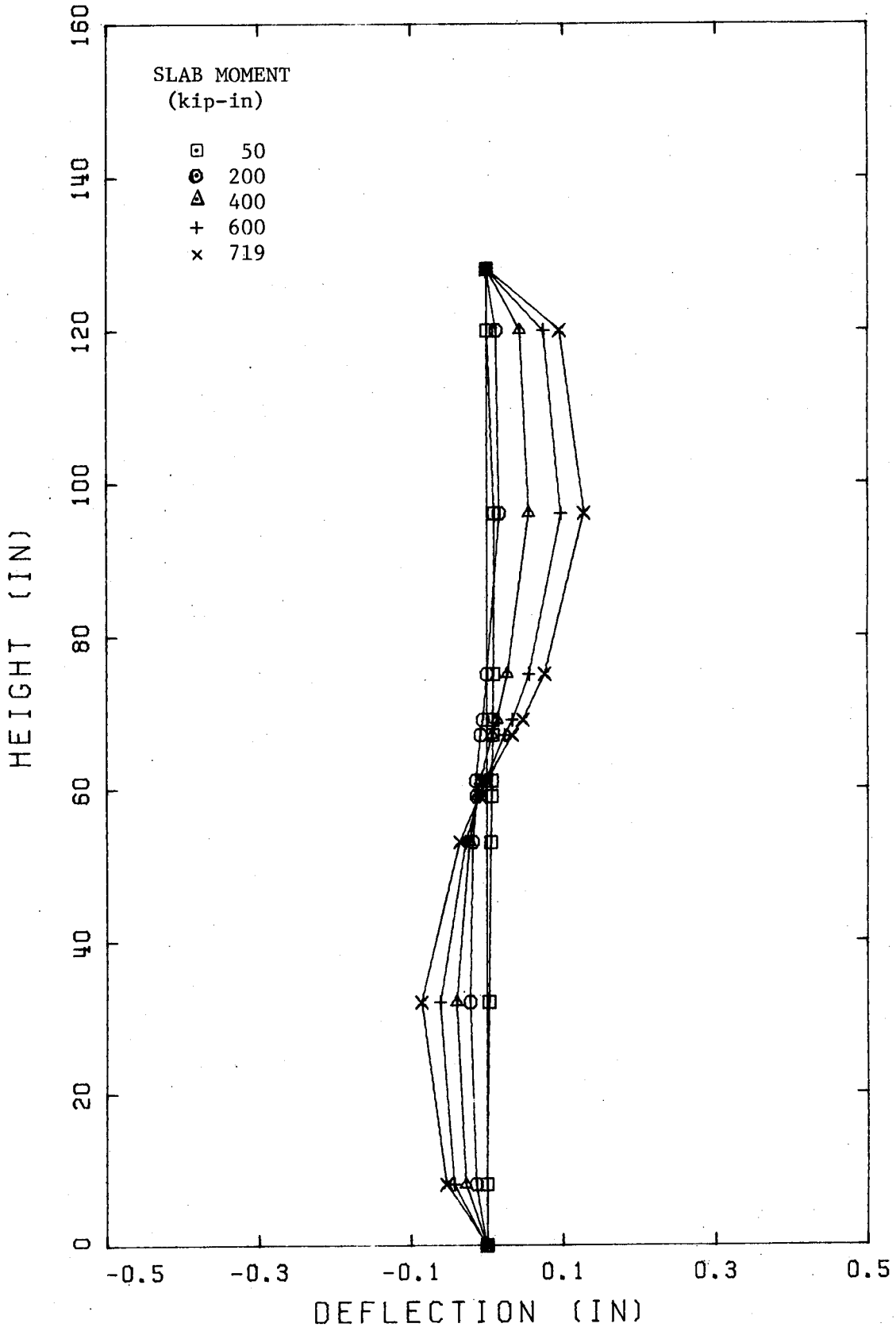

Fig. 4.12 Deflected Shape of Wall A150

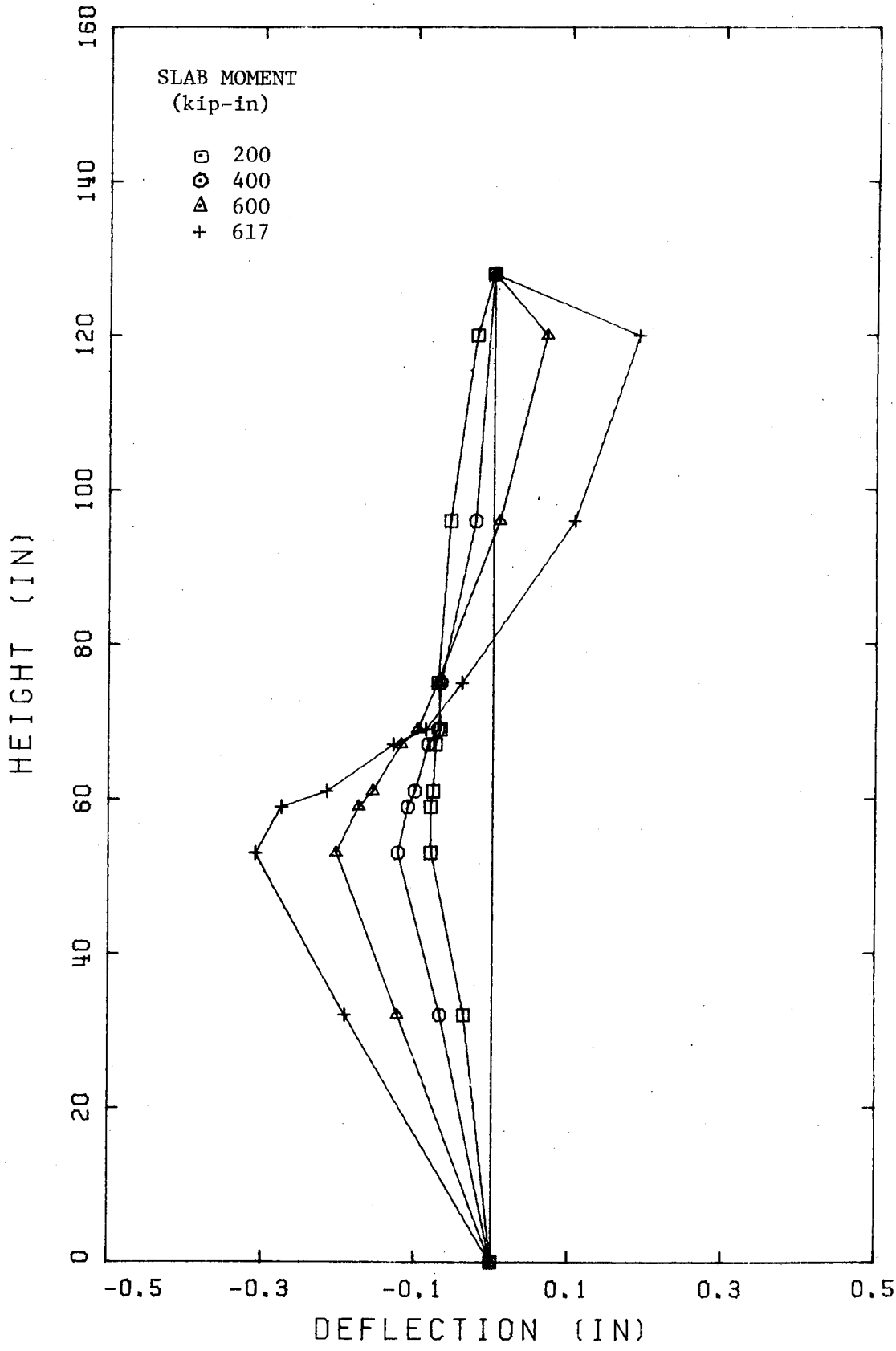

Fig. 4.13 Deflected Shape of Wall B50

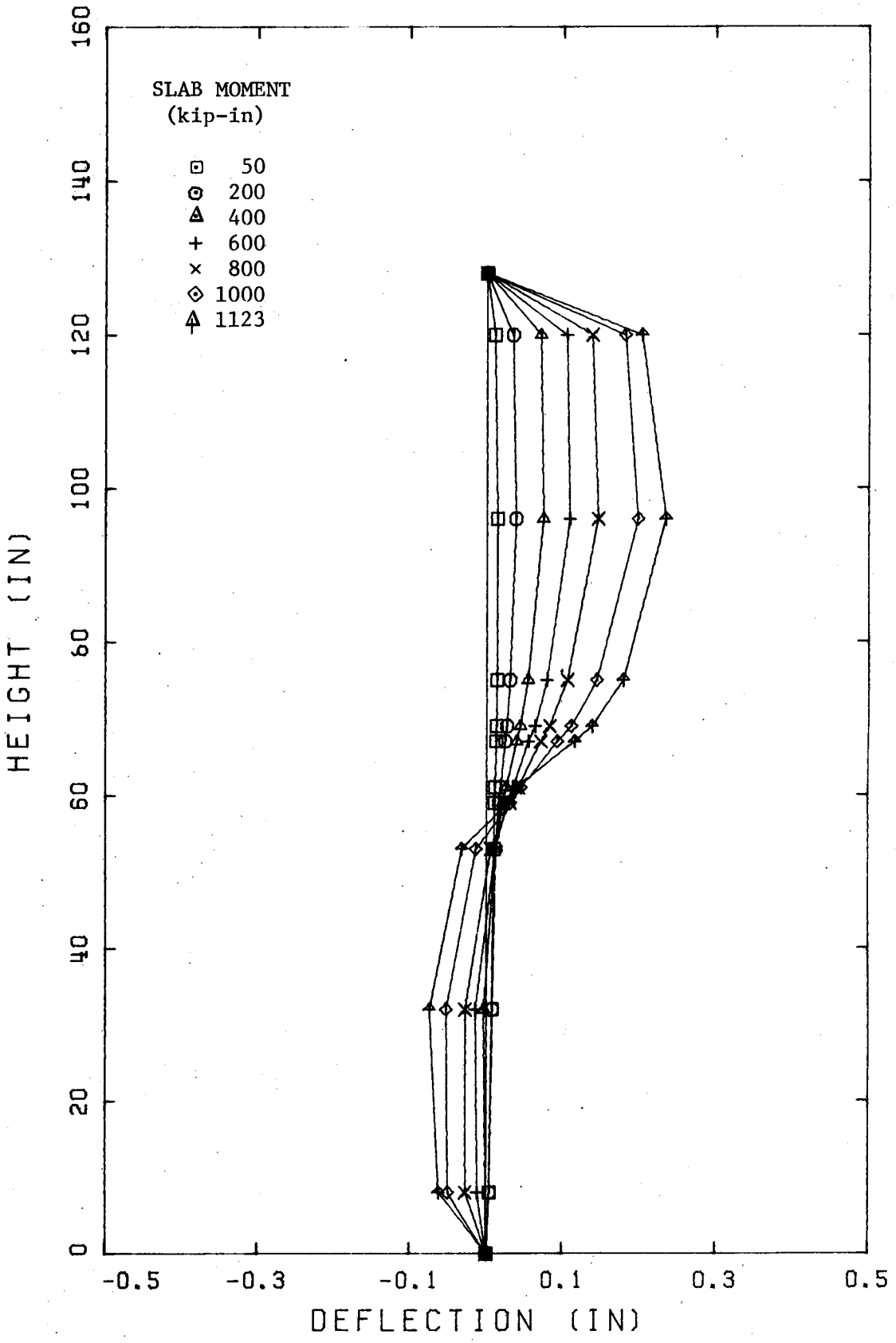

Fig. 4.14 Deflected Shape of Wall B150

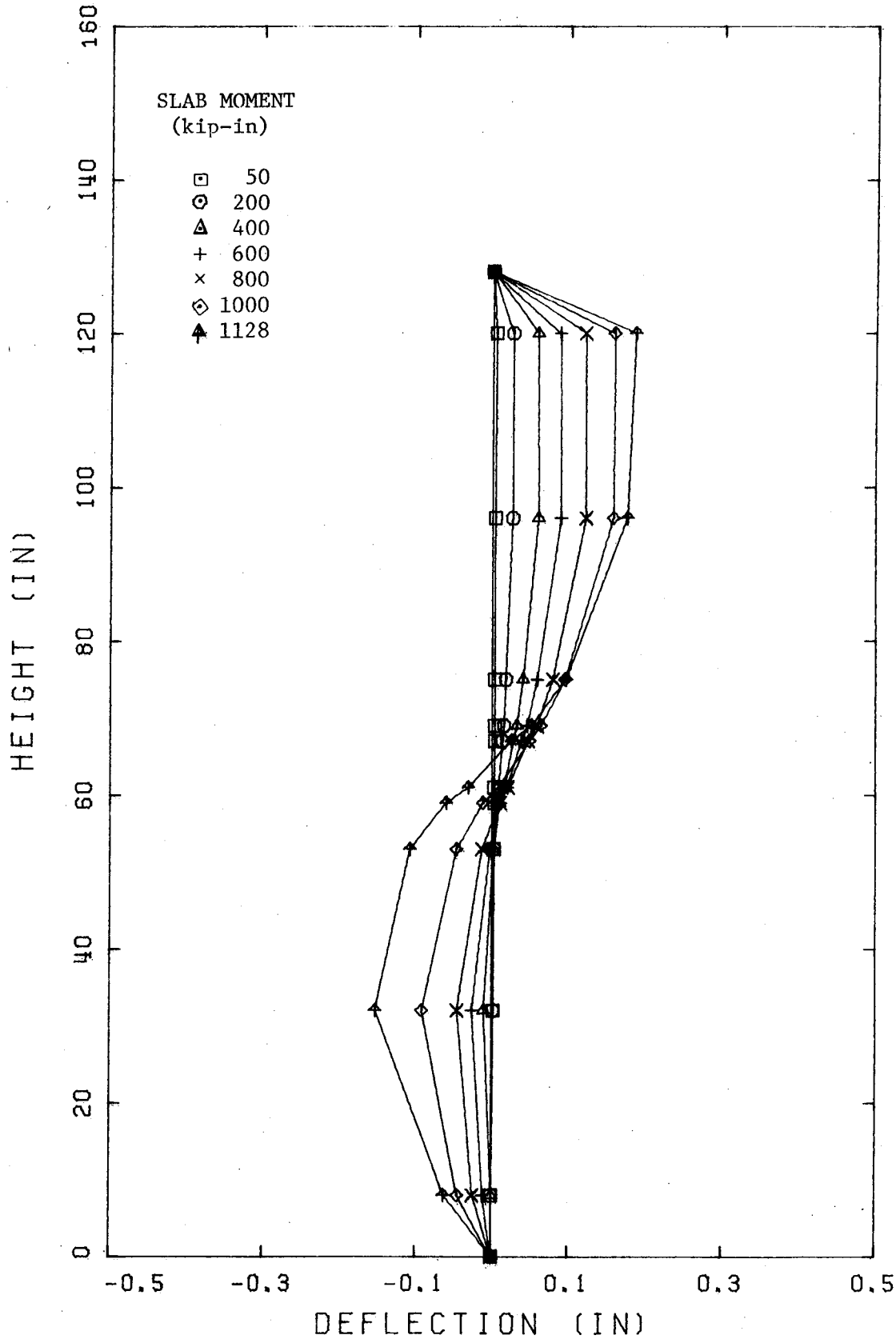

Fig. 4.15 Deflected Shape of Wall B200

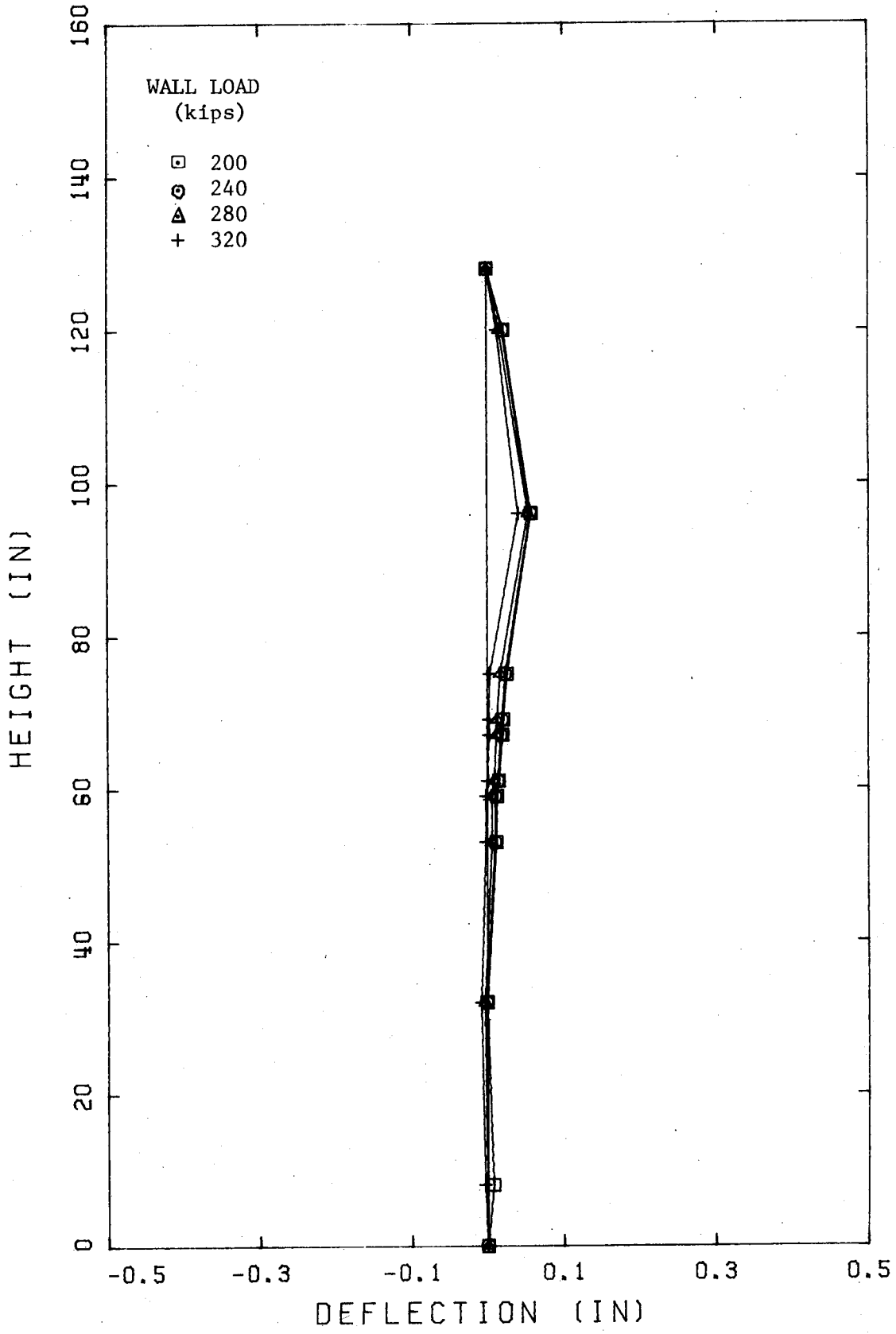

Fig. 4.16 Deflected Shape of Wall B320

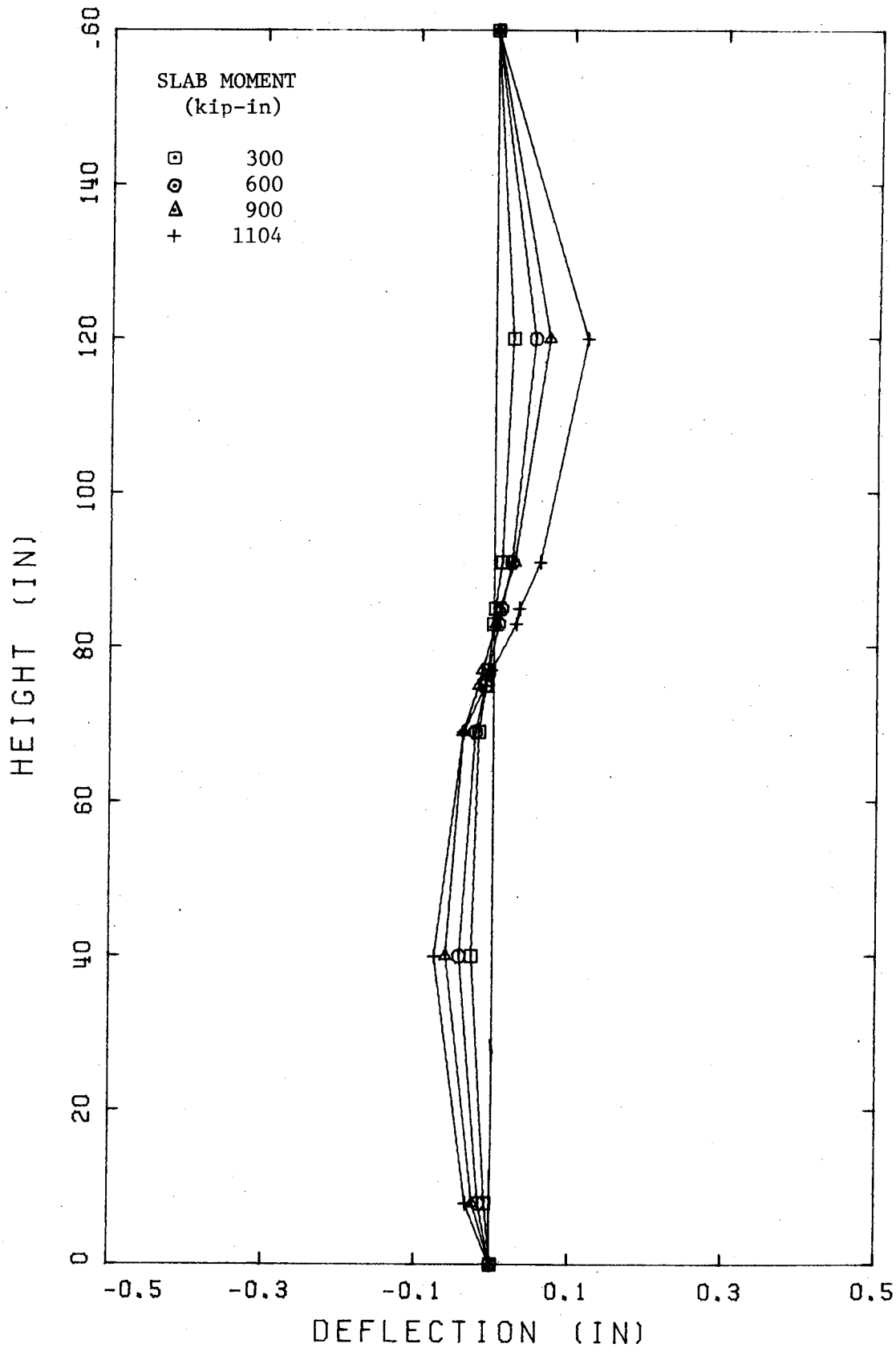

Fig. 4.17 Deflected Shape of Wall C200

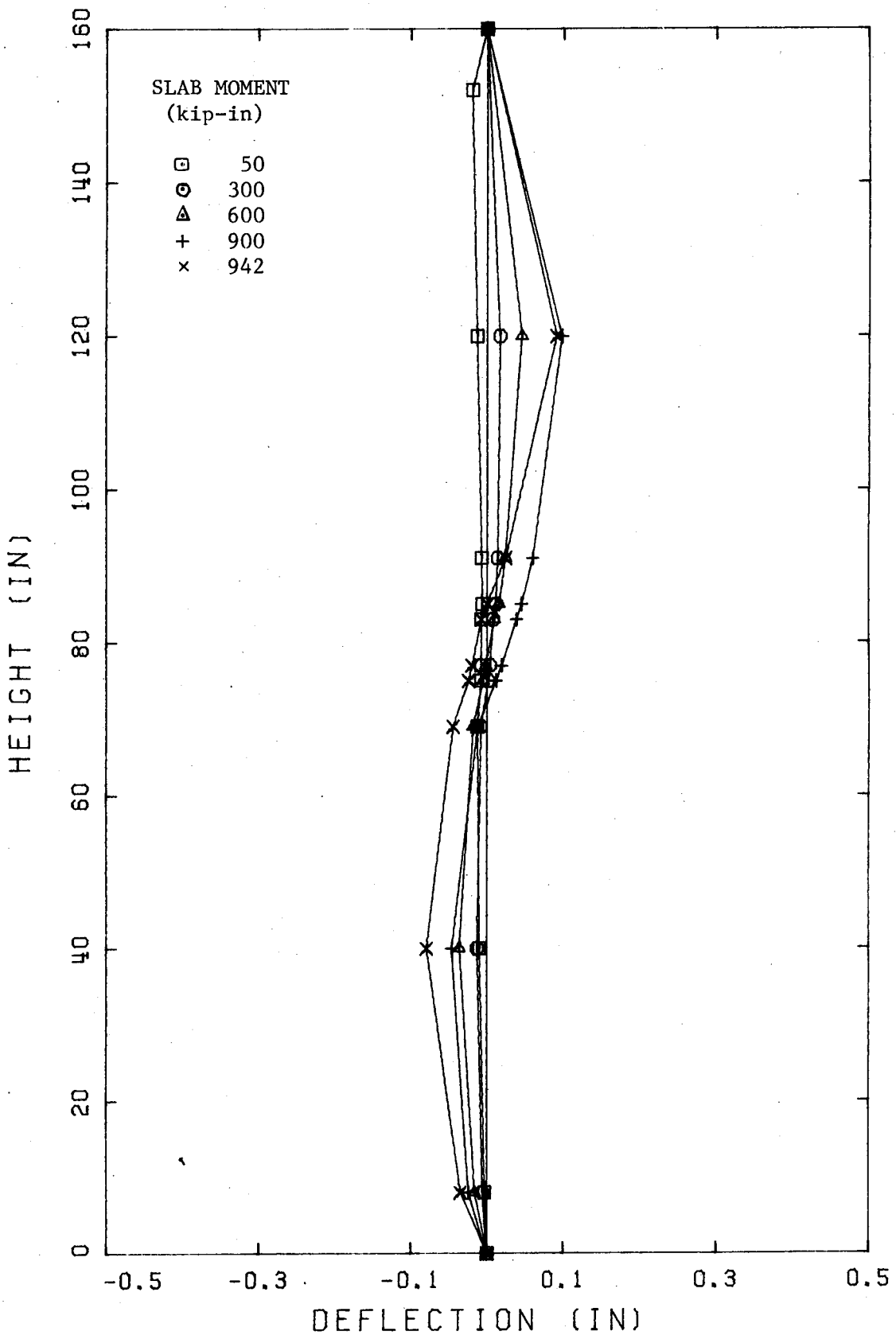

Fig. 4.18 Deflected Shape of Wall C300

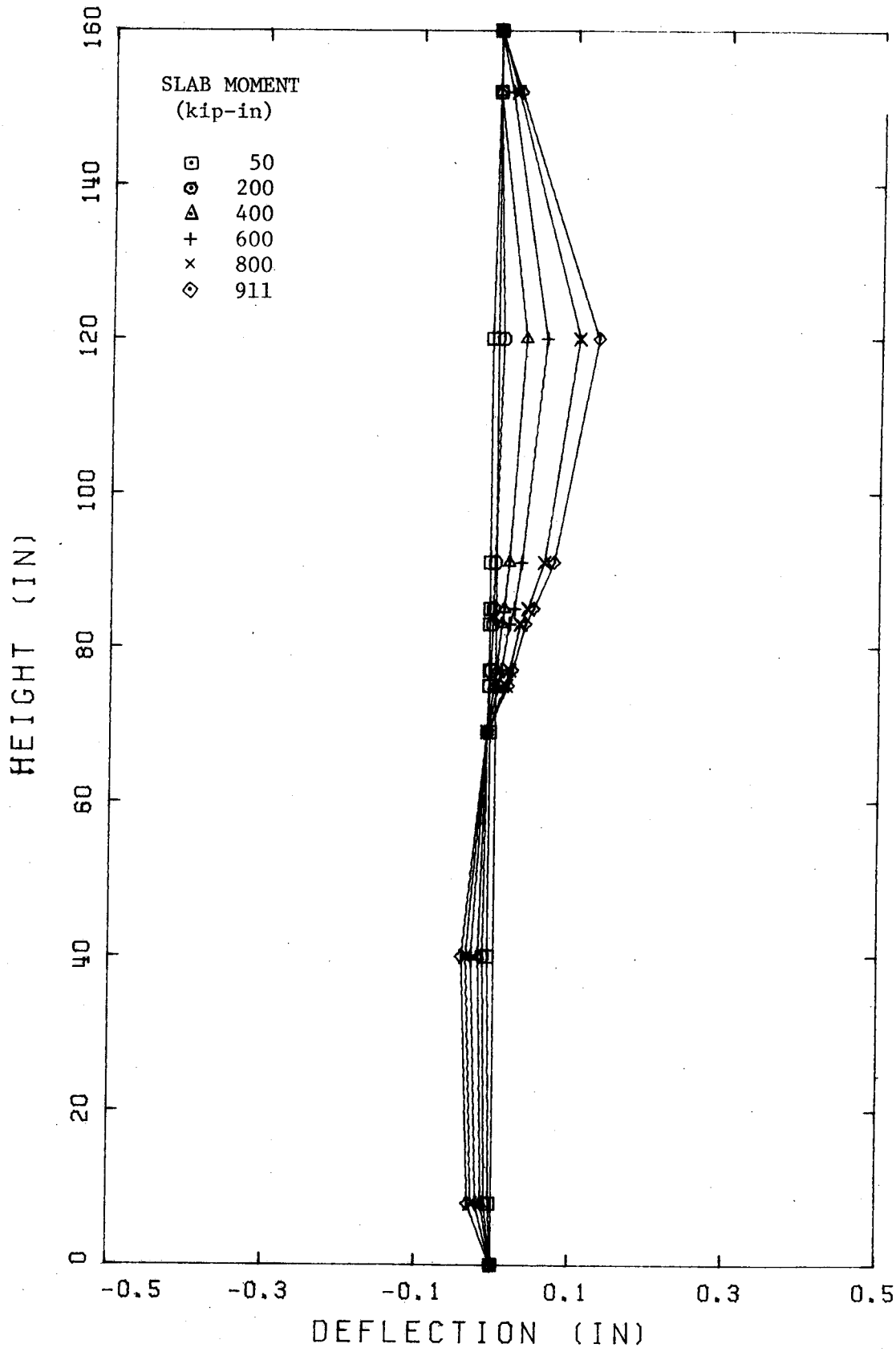

Fig. 4.19 Deflected Shape of Wall D200

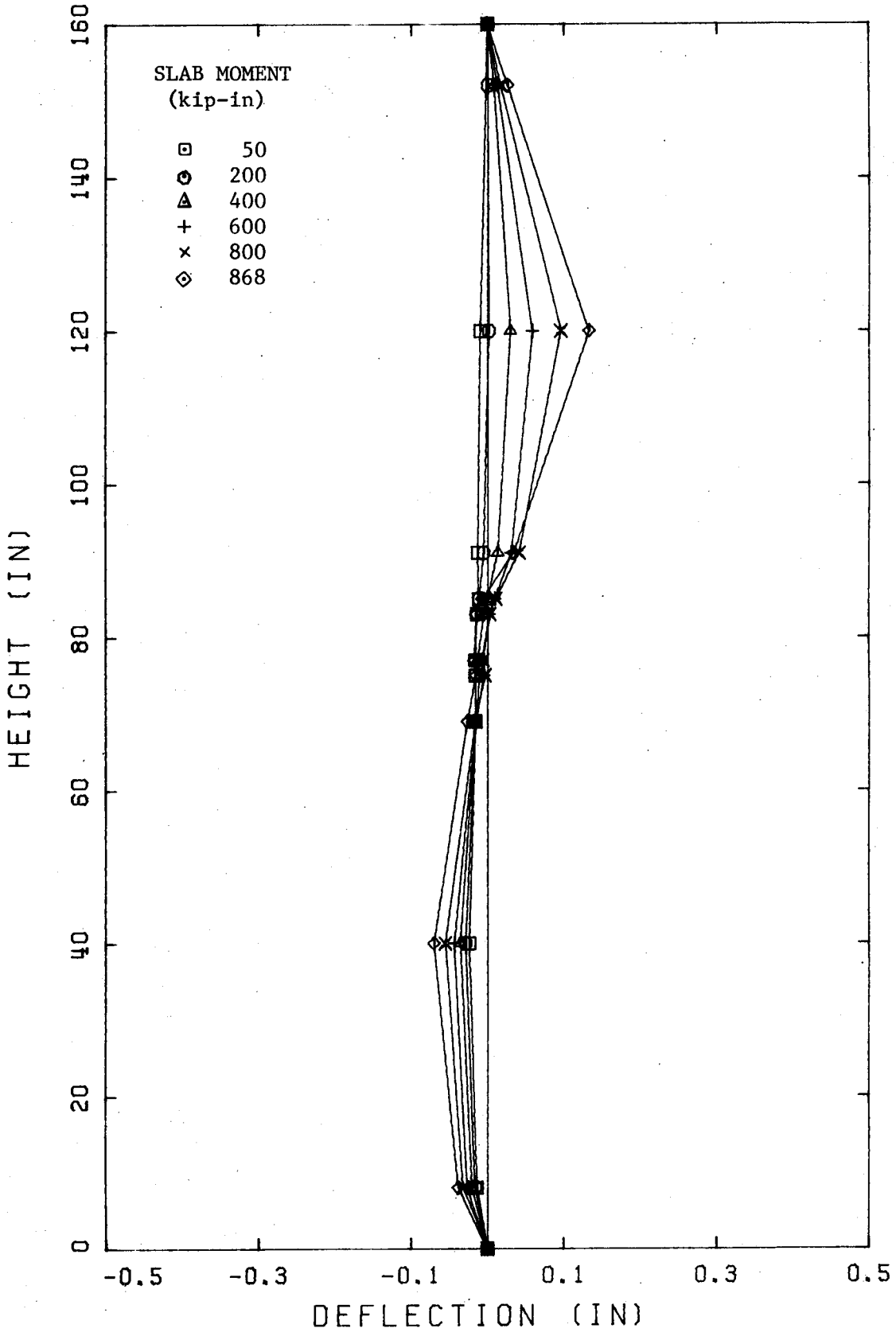

Fig. 4.20 Deflected Shape of Wall D300

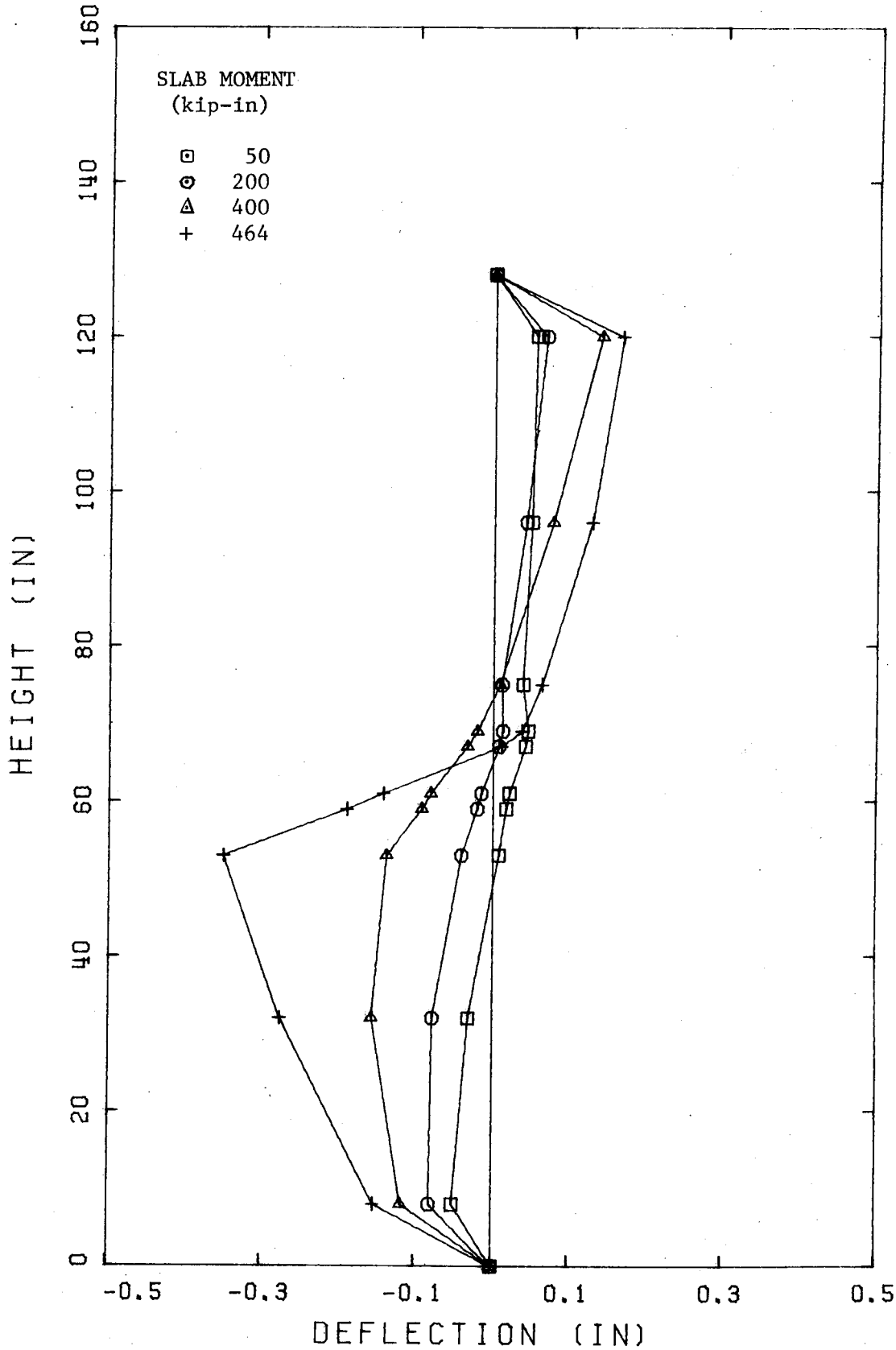

Fig. 4.21 Deflected Shape of Wall E50

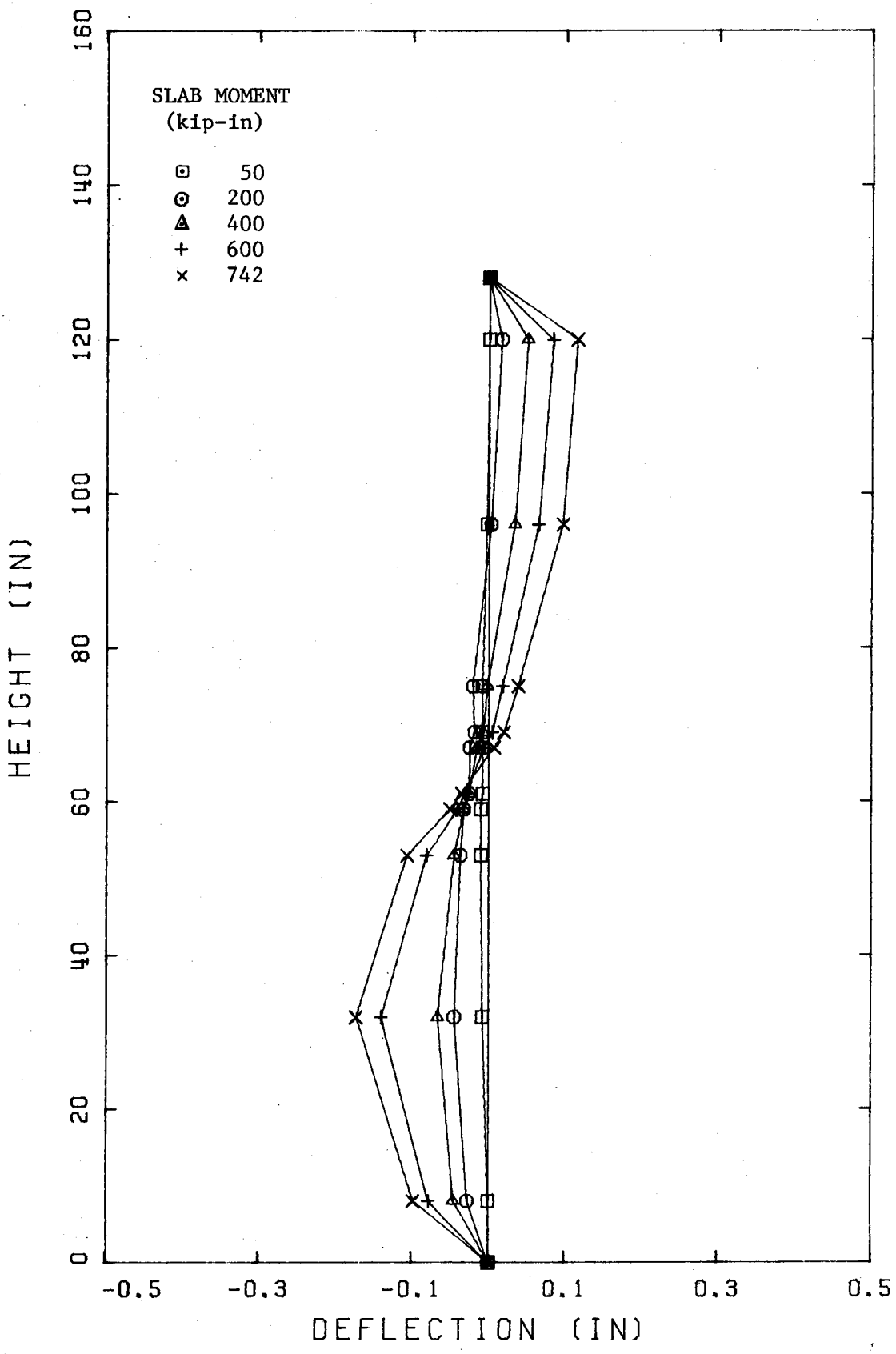

Fig. 4.22 Deflected Shape of Wall E100

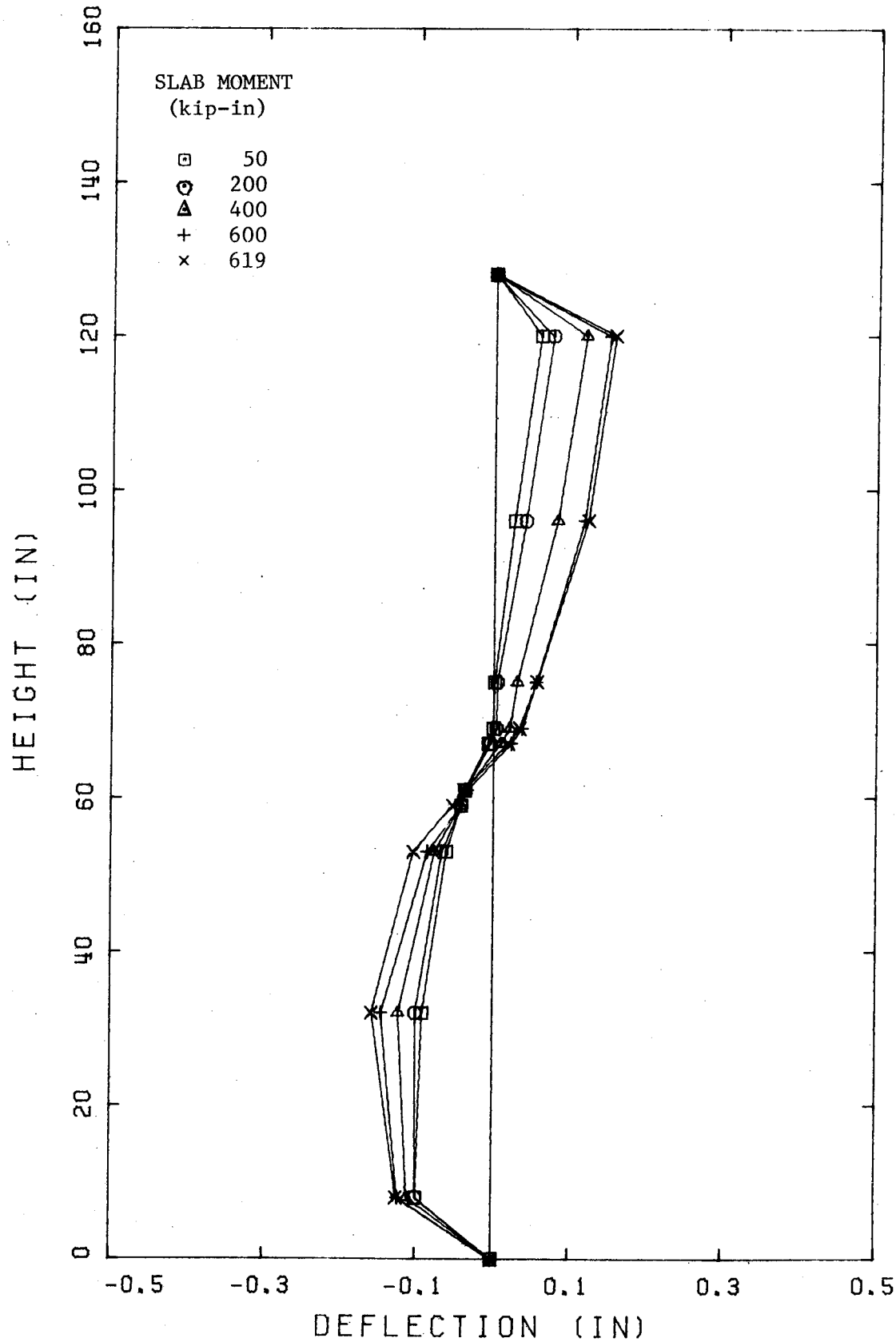

Fig. 4.23 Deflected Shape of Wall E150

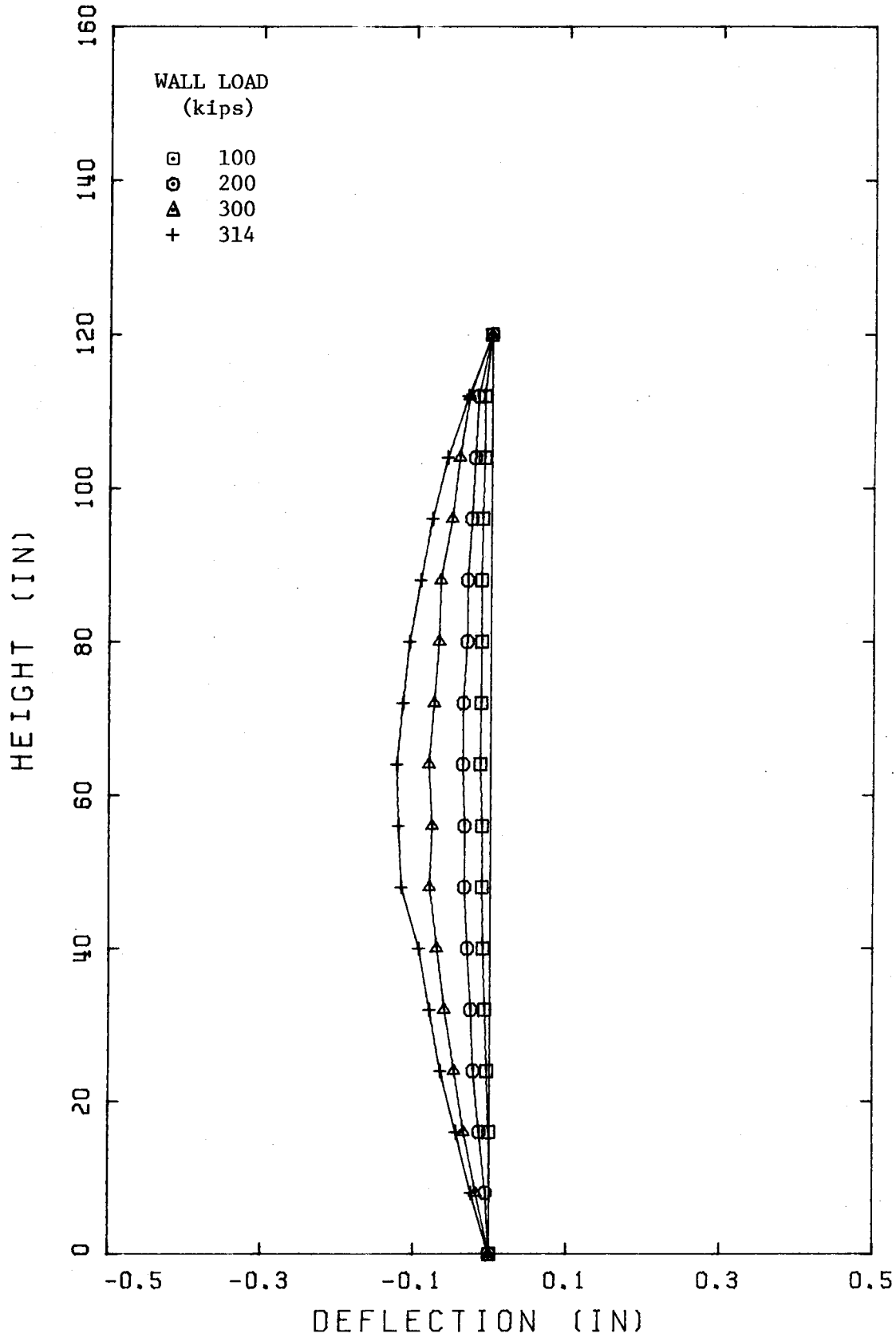

Fig. 4.24 Deflected Shape of Wall F1

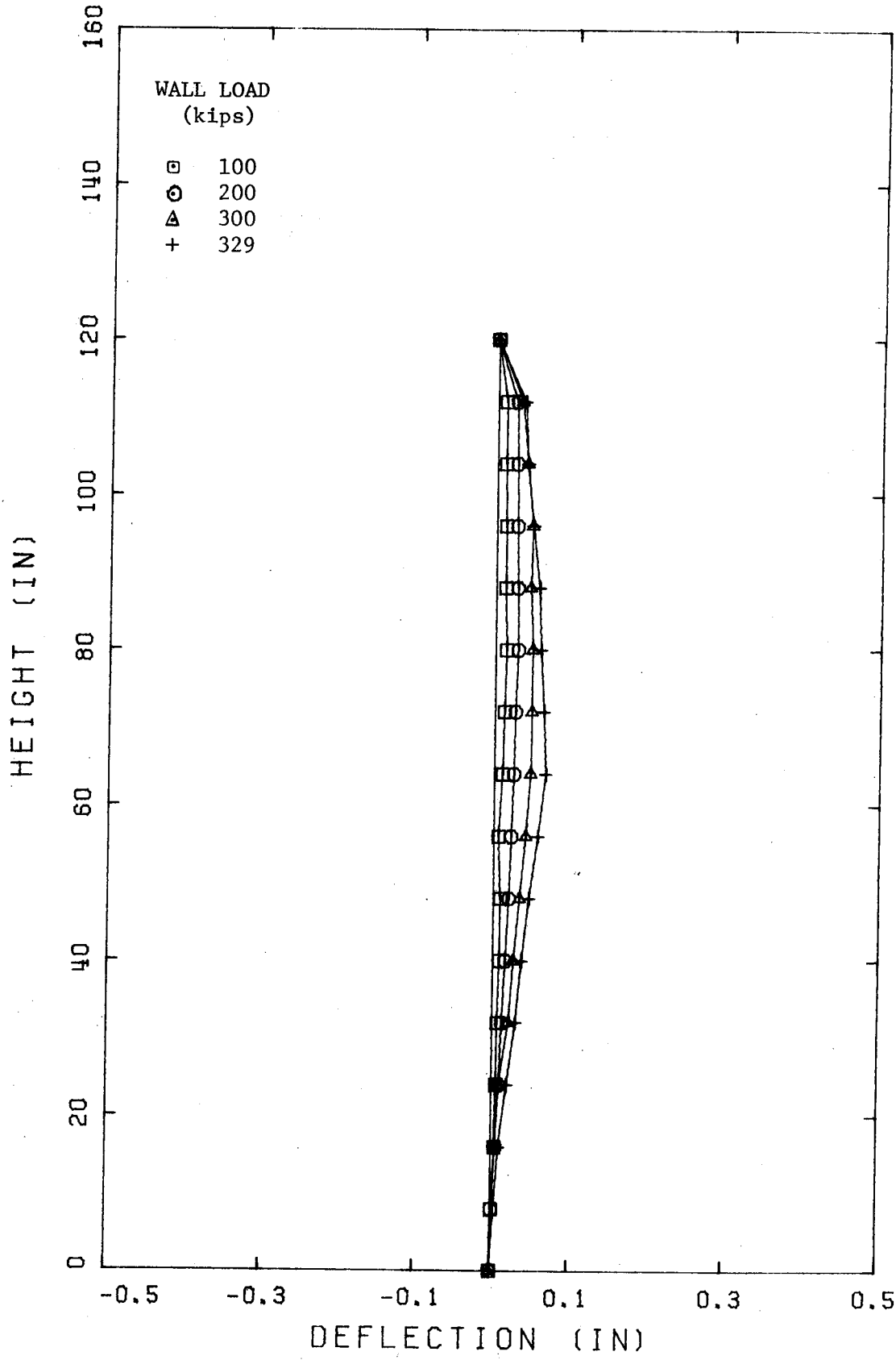

Fig. 4.25 Deflected Shape of Wall F2

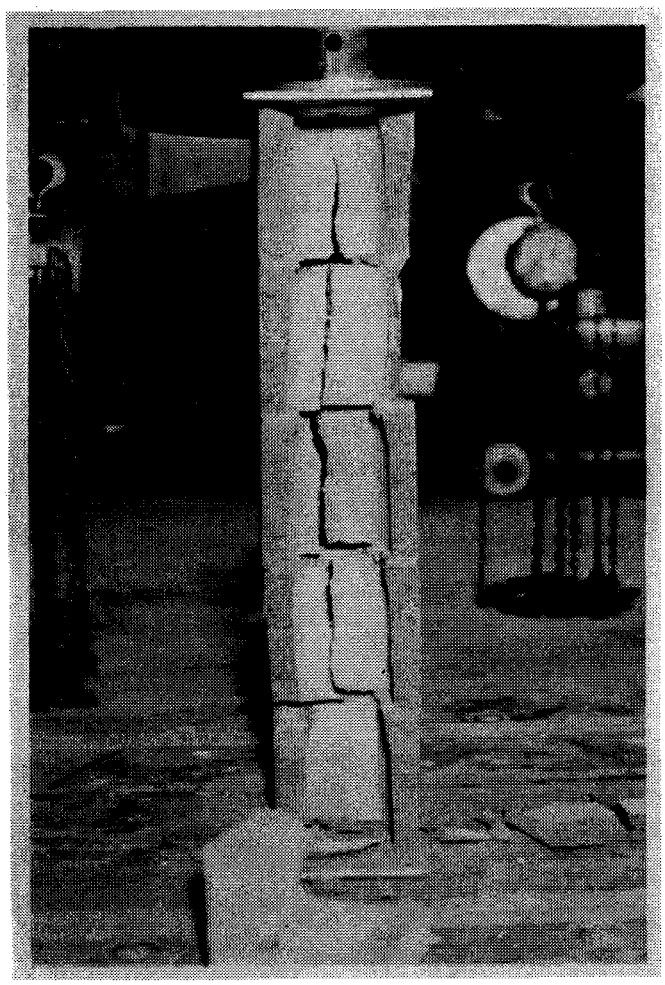

Plate 4.1 Typical Prism Failure

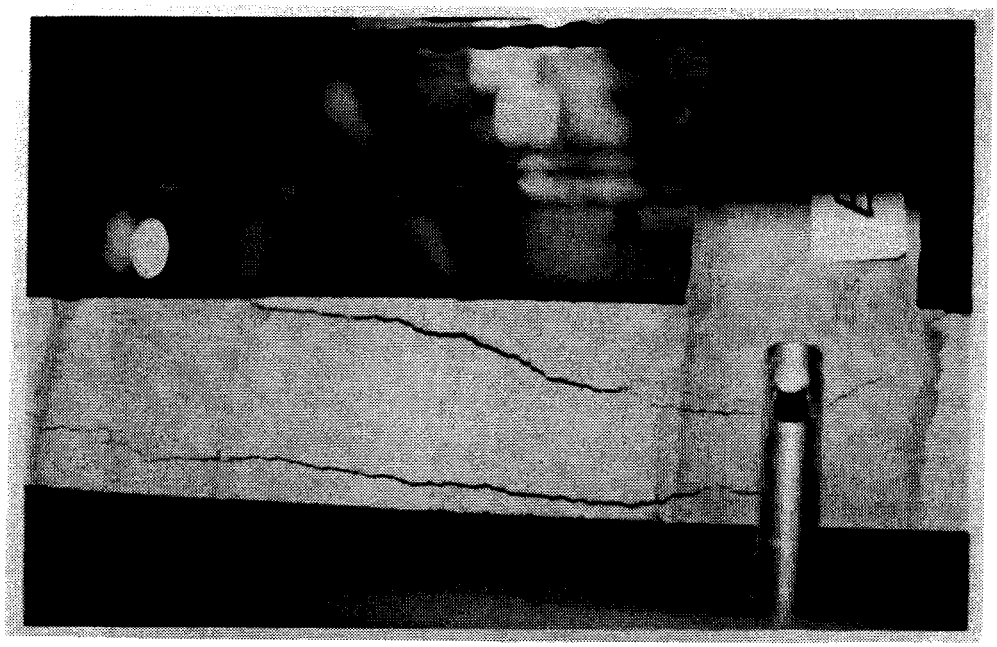

Plate 4.3 Wall E100 at Failure

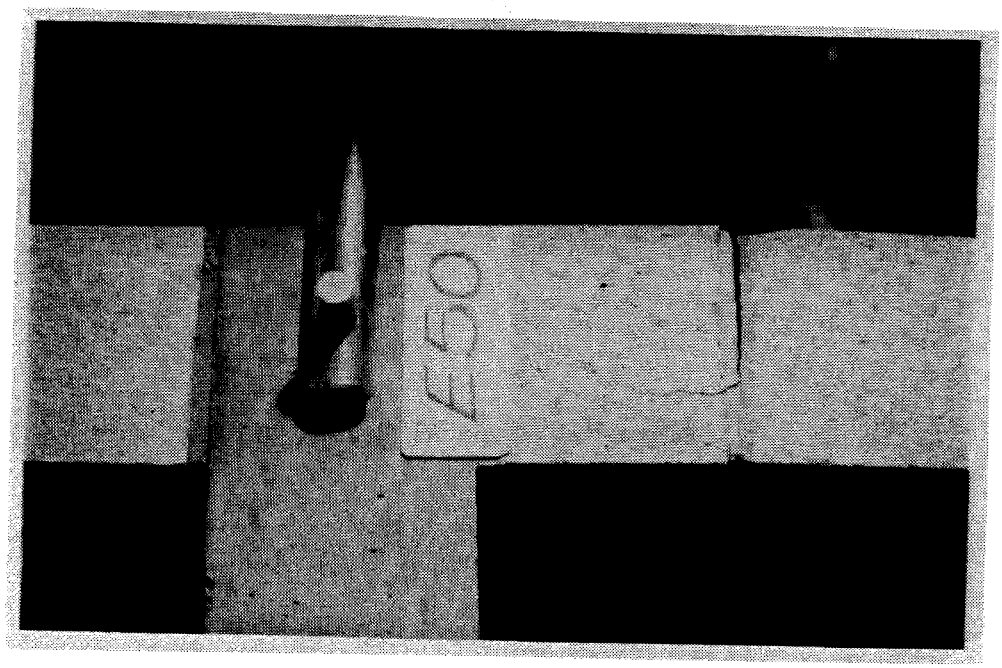

Plate 4.2 Wall E50 at Failure

Plate 4.4 Wall B50 at Failure

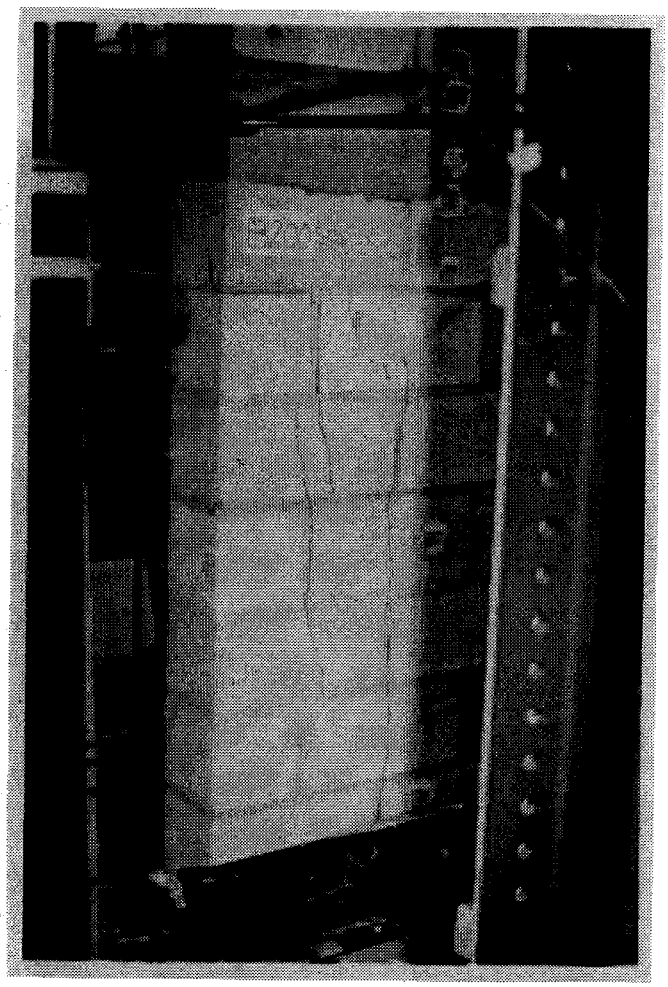

Plate 4.5 Wall B200 at Failure

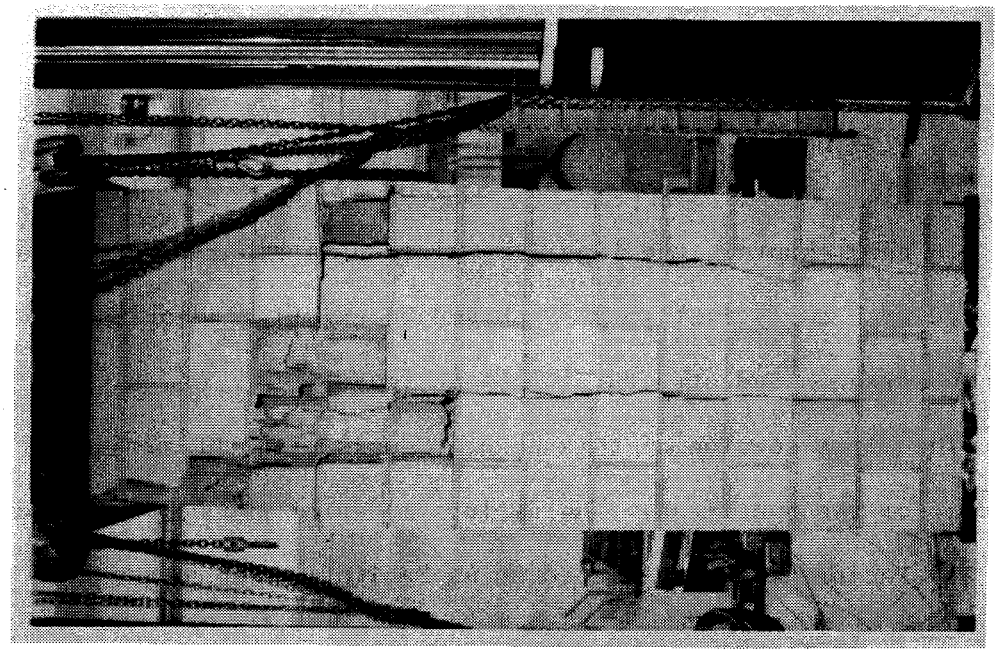

Plate 4.7 Tension Face of Wall F1 at Failure

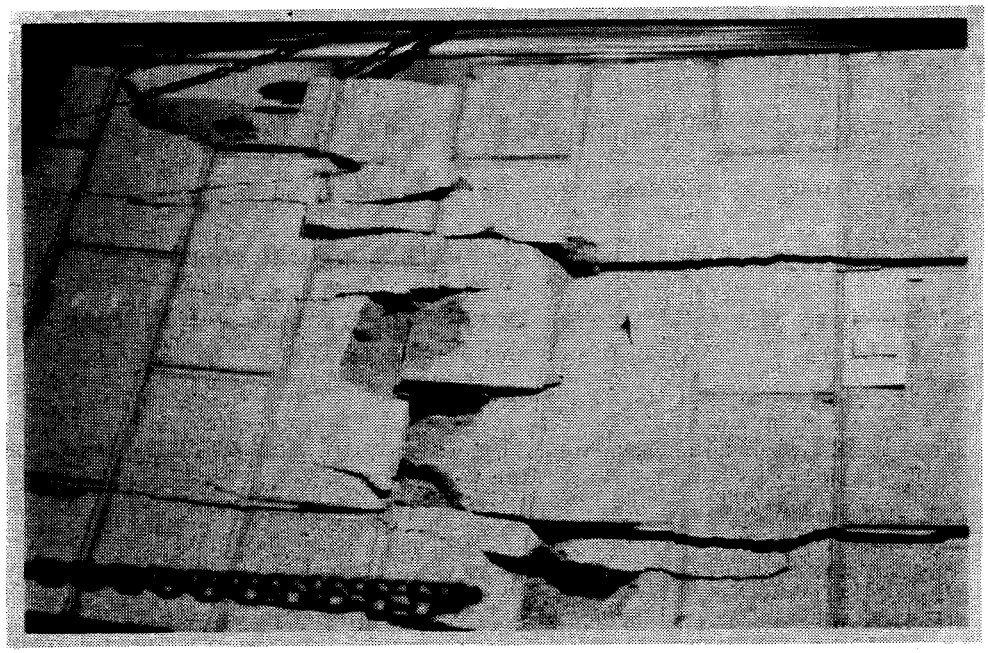

Plate 4.6 Compression Face of Wall F1 at Failure

CHAPTER V

DISCUSSION OF TEST RESULTS

5.1 Introduction

In this chapter, the experimental results are interpreted and compared with analytical results based on existing theories of concrete masonry strength and structural interaction.

The first section of this chapter deals with the moment-rotation behavior of the specimens. The failure modes of the walls are compared with the failure modes predicted using Sahlin's[2] and Ferguson's[12] joint performance theories.

The second section compares the ultimate strength of the wall specimens to the ultimate strengths predicted by a computer program written by Dr. J. Warwaruk. This computer program had not been published prior to or during the writing of this thesis.

The third section discusses the effect of mortar strength on the load-moment capacity and behavior of unreinforced 8 inch wall specimens.

The fourth section studies the effect of the degree of slab penetration into the wall cross-section for reinforced 10 inch wall specimens.

The fifth section examines the effect of the wall tie back on wall strength and behavior.

The sixth, and final section of this chapter compares the actual moment-rotation performance of the specimens to the predicted performance given by current rigid frame analysis theories and procedures.

5.2 Test Results Compared With Sahlin's and Ferguson's Theories

In Chapter 2, a theory of wall-slab interaction by Sahlin was described. Sahlin developed his theory upon examining the rotational behavior of the wall-slab joint. He monitored the joint rotation, θ, throughout the entire wall loading sequence and concluded that for any wall, the joint rotated rigidly ($\theta = 0$) until the maximum wall moment, M_{max}, was achieved. Once M_{max} was obtained the wall failed in one of three possible modes as described below:

1. $\theta = 0.$ $(\phi_v = \phi_h)$ $0 \leq M \leq M_{pl}$ $\sigma_{edge} = \sigma_{ult}$ axial

   Failure occurs when the ultimate edge stress is reached before the limiting slab restraining moment is reached.

2. $0 < \theta < \theta_{ult}$ $M = M_{pl}$ $\sigma_{edge} = \sigma_{ult}$ axial

   Failure occurs when the ultimate edge stress is reached after the limiting slab restraining moment is attained.

3a. $0 < \theta = \theta_{ult}$ $M = M_{pl}$ $\sigma_{edge} < \sigma_{ult}$ axial

   Failure occurs when the limiting joint rotation is reached.

3b. $0 < \theta = \theta_{ult}$ $M = M_{pl}$

   For cases where there is not a pronounced yield point, i.e. gradual yielding occurs at the joint.

Ferguson concluded that the three modes of failure described by Sahlin could be separated into two groups by considering the level of axial load on the wall in relationship to the balanced load, P_b. Specimens with axial wall loads higher than P_b had compression type failures and those with axial wall loads lower than P_b had tensile type failures. Ferguson found the balanced load to be the load at which zero strain occurs on the tensile face of the wall, as shown in Fig. 5.1.

The compressive failure mode category is identical to Sahlin's No. 1

failure mode category in which the wall fails immediately upon reaching M_{max} with $\theta = 0$. Fig. 5.2 shows the cross-sectional stresses for this type of failure. Ferguson's walls in this failure criterion category failed due to crushing of the concrete in the blocks immediately above the slab end.

The tensile failure mode incorporated Sahlin"s two failure modes, (No. 2 and No. 3), in which the joint becomes "plastified", i.e. $\theta > 0$, upon reaching M_{pl}. The internal cross-sectional stress distributions for the tensile failure mode are shown in Fig. 5.3. In these cases, Sahlin found the walls rotated plastically under a constant moment equal to M_{pl}. The cracked or unloaded part of the cross-section becomes so large that the internal stresses cannot balance the applied loads. The joint rotation increases until the compressive strength of the block is reached. The rotation at which this occurs is defined by Sahlin as θ_{ult}.

5.2.1 Unreinforced 8 Inch Walls

The balanced loads, P_b, for Series A and Series E specimens were 100 kips and 95 kips, respectively. Thus,specimens A50 and E50 fell into the tensile type failure category, specimens A150 and E150 fell into the compressive type failure category, and specimens A101 and E100 were borderline.

As predicted by Sahlin and Ferguson, specimens A50 and E50 exhibited only horizontal, i.e tensile cracks during testing, and underwent large joint rotations upon achieving M_{pl}. The joint rotation increased under M_{pl} until ultimate rotations, θ_{ult}, of 1.66 degrees and 1.74 degrees were achieved by specimen A50 and E50, respectively. At this point the walls failed due to localized crushing of the blocks adjacent to the slab.

The behavior of specimens A150 and E150 followed the predicted behavior given by Sahlin. Neither specimen experienced any significant joint rotation and both failed suddenly upon attainment of M_{max}, due to the compressive strength of the walls being reached on the compressive face of the walls. Since no joint rotation ever occurred, M_{pl} was not reached, i.e. $0 \leq M \leq M_{pl}$.

Specimens A101 and E100 were only slightly above P_b. Therefore, indications of both tensile and compressive failure were present. The tensile failure characteristics included the development of a horizontal tensile crack in the joint of specimen A101 near M_{max}. Also specimen E100 exhibited a small amount of joint rotation upon achieving M_{max}. The compressive failure characteristics included the development of several vertical cracks in both specimens at 90% of M_{max}, as well as the sudden failure of specimen A101 upon achieving M_{max}.

Horizontal cracks opened up in specimen A50 at 84% M_{max} and in specimen E50 at 76% M_{max}. This did not agree with Sahlin's statement that all joints rotate rigidly until M_{max} is reached. Fig. 5.4 graphically presents the relationship between slab rotation and wall moment for all Series A and Series E specimens. It appears that none of the walls behaved rigidly prior to achieving M_{max}. But when considering the difficulty that arose in measuring rotations, due to cracks occurring in the blocks and slab, and the magnitude of joint rotation, θ, in proportion to the magnitude of slab rotation, ϕ_h, it can be assumed that all the joints of walls with compressive type failures behaved rigidly until M_{max} was obtained, and all the joints of walls with tensile type failures behaved rigidly until 80% M_{max} was obtained.

5.2.2 Reinforced 8 Inch Walls

The balanced load for Series B was calculated to be 210 kips. Thus specimen B50 fell into the tensile type failure category, specimen B320 fell into the compressive type failure category, and specimens B150 and B200 were borderline.

The joint behavior of specimen B50 was identical to the behavior of the tensile type failure specimens A50 and E50. The joint behaved rigidly up to 81% of M_{max}, at which point the first horizontal crack opened up. No vertical compressive cracks were detected during the entire testing sequence. Once M_{pl} was achieved the specimen continued to resist M_{pl} until θ equaled 1.25 degrees. At this instant, the moment capacity of the specimen was drastically reduced, signifying failure of the wall.

The behavior of specimen B320 was typical of the behavior of a compressive type failure as described by Sahlin and Ferguson. The wall experienced only vertical compressive cracks, no joint rotation occurred, the maximum wall moment did not reach M_{pl}, and the specimen failed suddenly when the maximum load was applied.

The axial loads on specimens B150 and B200 were close to the balanced load. Therefore, characteristics of both tensile and compressive type failures were exhibited by both specimens. The tensile failure characteristics included the development of a horizontal tensile crack in specimen B150 just prior to attaining M_{max}, and crushing of the block immediately below the slab in both specimens as M_{max} was approached. The compressive failure characteristics included the development of several vertical compressive cracks in both specimens at 70% M_{max}, the sudden failure of both specimens upon achieving M_{max}, and $M_{max} < M_{pl}$ since no joint rotation occurred.

The relationship between slab rotation and wall moment for all Series B specimens is graphically presented in Fig. 5.5. The reason for the presence of joint rotation for specimens B150 and B200 as M_{max} was approached was due to the vertical cracking of the slab and the blocks adjacent to the slab, resulting in localized rotations. This phenomenon is illustrated in Plate 5.1. Therefore, the joint in the specimens categorized as compressive type failure rotated rigidly until M_{max} was obtained, and the joints in the specimens categorized as tensile type failures rotated rigidly until 81% M_{max} was obtained.

5.2.3 Reinforced 10 Inch Walls With Full Penetration Slabs

The balanced load for Series C specimens was calculated to be 300 kips. Specimens C200 and C300 failed similarly, in a combination of the tensile type and the compressive type failure mode. Fig. 5.6 presents the relationship between the joint rotation and the wall moment. The values for the joint rotation are inaccurate due to the localized rotations produced by the vertical cracking of the specimens as illustrated in Plate 5.2. This phenomenon made the measuring of block and slab end rotations impractical after large vertical cracks had appeared in the vicinity of the slab.

The tensile type failure mode characteristics included the capability of both specimens to withstand moment and undergo substantial joint rotation after M_{max} had been obtained. The crack types and patterns favored the compression failure mode. All cracks were vertical compressive splitting cracks.

Therefore, the two specimens C200 and C300, had axial loads near P_b, and could not be considered to lie completely in either of the two failure categories. The joints for these two specimens rotated rigidly up to M_{max}. After this point, the specimens could still resist

load, but the degree of cracking made any further use of the specimens impractical and dangerous.

5.2.4 Reinforced 10 Inch Walls With Partial Slab Penetration

The balanced load of 300 kips for Series D specimens was the same as the balanced load for Series C specimens since the masonry walls were constructed to be identical in both Series.

All four specimens from Series C and Series D behaved similarly, as shown by the comparison of the crack patterns of specimen C300 and D200 presented in Plate 5.2 and Plate 5.3, respectively. The only difference was that the ultimate moment capacity of the Series D specimens averaged only 87% of the ultimate moment capacity of the corresponding Series C specimen. This was due to the degree of slab penetration into the wall cross-section.

The mixed failure mode was indicated by the specimen resisting moment and undergoing joint rotation after the attainment of M_{max} and the occurence of vertical cracks. The ability of the specimen to resist moment and undergo joint rotation after M_{max} was attained is a characteristic of the tensile type failure mode. The occurrence of vertical cracks in the specimen is a characteristic of the compressive failure mode.

The joint rotation-moment relationship for the specimens of Series D is graphically illustrated in Fig. 5.6. As with the Series C specimens, the Series D specimens rotated rigidly until M_{max} was reached.

5.2.5 Summary of Joint Behavior

All specimens tested exhibited the characteristics of the failure mode type in which they were categorized. Therefore, the balanced wall load, P_b, described by Ferguson can be used as a standard to separate the wall-slab joint specimens into the failure modes described by Sahlin.

The characteristics of the compressive type failure mode are:

1. Sudden failure occurs upon achieving M_{max}, due to the ultimate compressive edge stress being obtained.
2. The wall-slab joint rotates rigidly throughout the loading sequence, i.e. $\theta = 0$.

The characteristics of the tensile type failure mode are:

1. Rigid joint rotation occurs up to 80% M_{max}.
2. Once the maximum moment, M_{pl}, is attained, the wall can still resist M_{pl} while the joint rotation increases significantly.
3. Failure occurs when the ultimate joint rotation, θ_{ult}, is reached, or when the ultimate edge stress, σ_{ult}, is achieved. Failure due to attainment of θ_{ult} occurs for low axial wall loads, while failure due to attainment of σ_{ult} occurs for higher axial loads.

Although the joints of the compression failure mode specimens rotated rigidly throughout the tests, substantial vertical cracking occurred in the walls above 80% M_{max} to indicate that the specimens reached their useful limit at this point.

Therefore, it can be concluded that all the wall-slab specimens can be analysed assuming rigid joint rotation, bearing in mind that the serviceability capacity of the wall is reached at 80% M_{max}.

5.3 Comparison of Load-Moment Relationships Obtained From Tests With Analytical Results

The theoretical load-moment interaction relationships were calculated by a computer program developed by Dr. J. Warwaruk . The program is capable of determining load-moment interaction curves for reinforced and unreinforced masonry block walls. It allows for the presence of

grouted and ungrouted voids of any desired size at any desired location. Interaction curves are produced on the basis of the strength of the cross-section, (h/t = 0). The assumptions used in the computer analysis were;

1. Cross-sections which are plane prior to loading remain plane after the load is applied. Test results obtained from the full scale wall tests support this statement.
   Fig. 5.7 to Fig. 5.11 graphically illustrate the linearity of the wall cross-sectional strain.
2. Sufficient bonding of the grout to the reinforcing bars is developed to prevent slipping between the two materials. This ensures that the strain in the embedded bar is the same as that of the surrounding grout.
3. The stress-strain relationship of the grout follows a second degree parabola proposed by Hognestad[20].
4. The stress-strain relationship of the masonry follows a second degree parabola proposed by Hognestad.
5. The tensile strength of the ungrouted masonry wall is assumed to be zero.
6. The stress-strain relationship for steel is linear until the yield strength of the steel is reached after which it is plastic. Test results on individual bars used in this study supported this assumption for strains up to and beyond the magnitude of those that occurred in the full scale wall tests.

There was good correlation between the results predicted by this computer program and the experimental results. The interaction diagram given by the computer program along with the ultimate load-moment results

from the tests are graphically presented for the unreinforced 8 inch walls in Fig. 5.12, for the reinforced 8 inch walls in Fig. 5.13, and for the reinforced 10 inch walls in Fig. 5.14.

The ultimate load-moment test results are presented as a plot of the axial wall load versus the maximum wall moment, M_{max}. A comparison of the computer program results with the experimental results indicates that for a given axial load, the value of M_{max} was the same as the ultimate moment capacity of the wall. For the walls failing in the compressive failure mode and the walls failing in a mixture of the compressive and tensile failure modes, the plastification moment defined by Sahlin, M_{pl}, corresponded to the ultimate moment capacity of the wall, M_{ult}. For the walls failing solely in the tensile failure mode the plastification moment, M_{pl}, corresponds to a fraction of the ultimate moment, αM_{ult}. For the test specimens that failed solely in the tensile failure mode (specimens A50, B50 and E50), it was found that $\alpha = 0.8$ i.e. $M_{pl} = 80\% M_{ult}$. The value of α for walls with axial loads bordering around the balanced load, P_b, was found to equal 1.0.

It can be assumed the value of α equals 1.0 for walls with axial loads higher than or equal to the balanced load and α is less than 1.0 for wall axial loads lower than the balanced load. The exact relationship between the value of the axial wall load and the value of α cannot be determined by this study due to an insufficient number of test results. Only one wall in each of Series A, B, and E failed in the tensile type failure mode.

In conclusion, the computer program accurately predicts the ultimate moment capacity of the wall specimen for a given axial wall load. The joints of the walls with axial loads greater than P_b or about equal to P_b rotate rigidly until M_{max} is achieved. M_{pl} is equal to M_{max} for these

specimens since failure occurs immediately upon attaining this ultimate moment. The joints of the walls with axial loads much lower than P_b rotated rigidly until the plastification moment was achieved. After M_{pl} was obtained the specimens supported an increase in moment, up until M_{ult}, while the joint rotation increased. For this type of failure $M_{pl} < M_{ult}$.

5.4 Effect of Mortar Strength

Mortar strength had no effect on the flexural strength of the walls. This is illustrated by the closeness of the results of Series A specimens (Mortar A) and Series E specimens (Mortar B) as shown in Fig. 5.12.

Mortar strength had no effect on the failure mode of the walls. Throughout the entire testing sequence, the joint and wall behavior of specimens A50 and E50 was identical. Similarly there was identical behavior for A101 and E100, and for A150 and E150.

5.5 Degree of Slab Penetration

The ultimate moment capacity for a wall was greatly reduced when the slab did not extend across the entire wall cross-section. Fig. 5.14 shows the test result moment capacity for the 10 inch reinforced walls. Series C specimens had full slab penetration while Series D had 84% wall cross-section penetration. The reduction in moment capacity of the Series D specimens compared to the appropriate Series C specimens is about 25%, i.e. M_{max} (Series D) = 75% M_{max} (Series C) for the corresponding axial wall load. Many more tests would have to be done before a definite correlation could be made between the moment capacity of a

wall and the degree of slab penetration.

The degree of slab penetration has no effect on the rotational behavior of the joint or on the failure mode of the specimen as pointed out by Fig. 5.6 and the description of the specimen behavior given in Section 4.7. All four specimens, C200, C300, D200 and D300, behaved identically, having the same types of cracks and the same joint rotation behavior.

5.6 Tie Back Effect

The tie back has no effect on the ultimate moment capacity of the walls as shown by Fig. 5.12 and Fig. 5.13, which give a comparison of this study's test results with the results of Ferguson's tests which had no tie back. The moment applied to the wall is equal to the applied slab moment plus the vertical wall load times its lever arm. For the pin ended walls in this study the lever arm is the eccentricity of the wall load which is equal to the horizontal deflection of the wall at the point where the moment is to be determined. The load-deflection portion of the total moment is called the P-Delta moment. The total moment at the ultimate loading condition is the same for walls with tie backs and walls without tie backs; the only difference is the proportion the P-Delta moment accounts for in the total moment. For the case where the wall has no tie back the P-Delta moment is a significant portion of the total moment since large horizontal deflections occur. For the case where the wall is tied back no horizontal deflection of the wall-slab joint is allowed and hence the P-Delta moment is equal to zero.

The wall and joint behavior is affected by the tie back. With the tie back the entire specimen is in double curvature, as compared to

the single curvature configuration of the walls with no tie back. The tie back holds the wall-slab joint from translating horizontally. This resulted in the ultimate joint rotation being achieved in the tensile type failure of the walls with tie backs. Without the tie back, the large horizontal deflections at the level of the slab caused large P-Delta moments which altered the distribution of moments in the walls. Failure of the specimens occurred when the walls became unstable and tipped over. The tie back did not affect the joint behavior of the walls with compressive type failures.

5.7 Moment-Rotation Analysis of Specimens With a Rigid Joint

5.7.1 Structural Analysis of a Rigid Frame

In the design of members in a structural frame the designer must first predict the loads and moments on the structure. Building codes give detailed guidelines on choosing the amount of snow, wind, occupancy and other loads.

Methods to determine the distribution of loads and moments on the members of a rigid frame have been developed and are widely used for structural materials such as steel and concrete. If concrete masonry walls are found to behave in a predictable manner then it can be assumed that their interaction with other members in a structural frame can be analyzed. The steps required to carry out this type of structural analysis are:

1. Determine all of the loading conditions on the structure.
2. Choose trial members and calculate their values of E_m and I_e.
3. Complete a rigid frame analysis of the structure using any of the accepted methods.

4. Check that the capacity of the trial members has not been exceeded and check the estimate of E_m and I_e.
5. If the trial members and the estimates of E_m and I_e are acceptable the design is complete. If not, the process must be repeated starting from step (2). If the load-moment capacity of the wall has been exceeded, the joint will no longer act rigidly. Therefore the trial section chosen for the wall is insufficient and a new section will have to be selected.

5.7.2 Test Specimens Modelled for a Rigid Frame Analysis

The joints in specimens that failed in the compressive failure mode or in a mixture of the compressive and tensile failure modes, i.e. $P \geq P_b$, rotated rigidly until M_{max} was achieved. The joints in the specimens that failed in the tensile type failure mode, i.e. $P < P_b$, rotated rigidly until 80% M_{max}, after which they rotated plastically. Therefore, a rigid frame analysis can be applied up to M_{max} for the specimens failing in the compressive or mixed mode and up to 80% M_{max} for specimens failing in the tensile type failure mode.

The percentage of the total joint moment resisted by a member connected to the joint is equal to the percentage of the member's stiffness in relationship to the sum of the stiffnesses of every member framing into the joint. The stiffer the member the larger the end moment it will receive from the joint. In the test specimens the moment applied to the wall-slab joint by the cantilevered slab is resisted by the top and bottom walls, with the amount of moment resisted by each wall determined by its stiffness.

The stiffness of a wall is a function of the elastic modulus, E_m, of the material in the wall and the effective moment of inertia,

I_e, of the cross-section of the wall. An increase in either of these two variables will increase the stiffness of the wall.

The modulus of elasticity of concrete masonry, E_m, has not been intensively researched. E_m decreases as the axial load on the wall increases. Also the value for E_m is not the same for unloading as it is for loading. CSA Standard S304-1977[1] recommends that E_m be assumed equal to 1000 f'_m. The results from this study as well as the results of the study by Hatzinikolas[13] indicate that a more correct value for E_m would be 750 f'_m.

At the present time there is no satisfactory method for predicting the value of I_e for cracked concrete masonry walls subjected to large moments. It is known that the value of I_e must be a fraction of the uncracked moment of inertia, I_o. The moment of inertia also varies along the wall height due to tensile cracking. An equivalent moment of inertia for the whole wall is required to estimate the stiffness of the wall.

Hatzinikolas developed an equation for the equivalent stiffness of an unreinforced or reinforced wall to be used for design calculations. The equation is:

$$I_e = 2(1/2 - e/t)I_o$$

This equation yields a straight line plot of I_e vs e/t with intercepts at $I_e = I_o$ (when e/t = 0) and $I_e = 0$ (when e/t = 1/2). For small values of e/t this relation was found to give satisfactory results for I_e when compared to results from both Hatzinikolas' tests and Ferguson's tests, but unsatisfactory results when compared to the

results from this test series. For larger values of e/t the equation greatly underestimated I_e for the results of all three experimental studies. This may be conservative for design calculations but the value of I_e must be more accurately determined when it is used for the analysis of a structure. The plot of I_e versus e/t presented by Hatzinikolas indicates that a higher order equation (such as a 2nd degree parabola) may more accurately describe the relationship. The results of this test in terms of predicting I_e are examined in more detail in Section 5.7.3.

A computer program, PFT, was used to try and predict the rotation and deflection behavior of the specimens. This program is a modified version of the "Plane Frame and Truss Program"[13] and is one of the programs currently used at the University of Alberta for the structural analysis of rigid frames. The assumptions of material behavior in the program are widely accepted and used in most structural analysis methods. The program computes end moments, end shears, and end axial forces for each member in the frame and computes horizontal deflection, vertical deflection, and rotations of each joint.

The specimens were modeled by placing hinged joints at the ends of the walls, rigid joints at the wall-slab connection and at the location of transducers B and I (see Fig. 3.11), and a "free" joint at the end of the cantilevered slab. The tie back force was applied at the wall-slab joint. The output included the rotation of the wall-slab joint and the horizontal deflection of all the joints along the wall height.

5.7.3 Comparison of Test Results with Results of a Rigid Frame Analysis

The purpose of this section is to determine if the test specimens behaved in a predictable manner and to determine if the wall-slab joint behaved rigidly.

The major variables of the analysis were the value of the modulus of elasticity, E_m, and the values of the effective moment of inertia of the wall above the slab, I_{eu}, and the wall below the slab, I_{eL}. A trial and error procedure was used to determine these values. Initial values for these variables were selected and used in the PFT program. The deflected shape given by the program was compared to the measured deflected shape of the specimen. If the deflected shapes were the same, the initial values chosen for E_m, I_{eu}, and I_{eL} were assumed to be those of the actual wall. If the deflected shapes differed, then the program was run with new values for E_m, I_{eu} and I_{eL}. This process was repeated until the deflected shape given by the program was similar to the deflected shape of the actual specimen.

Specimens A50, A100 and B50 were not modeled as their deflected shapes were not satisfactory. The wall-slab joint and the top roller-channel assembly of these specimens underwent large undesired horizontal translations.

Specimen B320 failed upon the application of the precompression load and did not undergo sufficient horizontal deflections in the walls to model the specimen as a rigid frame.

For the remaining specimens, it was found that the deflections of all the joints and the rotations of the wall-slab joint could be accurately predicted by PFT after a few iterations. Tables 5.1

through 5.11 compare the values predicted by PFT with those actually measured.

All wall-slab joints behaved rigidly up to M_{max} except for the wall-slab joint of specimen E50 which was the only tensile failure mode specimen modeled. Somewhere after 74% M_{max} the wall-slab joint began to rotate plastically until at M_{max} the predicted slab end rotation was 0.42 degrees while the measured slab rotation was 1.36 degrees. This plastic rotation began at 75% M_{max} as discussed in section 5.2.1.

Figures 5.15 through 5.19 graphically present the effective moment of inertia of the lower walls of Series A, B, C, D, and E, respectively, plotted against the vertical wall load and wall moment. The points plotted for each specimen are the effective moment of inertia given by PFT for various axial load-wall moment combinations which occurred during testing. In the tests, the axial wall load was applied first and then the slab moment was added in increments which increased the wall moment. For each specimen, the sequence of points from left to right represent the sequence of loading. The effective moment of inertia for specimens with small amounts of wall moment was close to I_o and as the wall moment increased the values of I_e decreased. This was due to increasing tensile cracking. The graphs indicate that for a given axial wall load the moment of inertia is equal to I_o when the moment is zero, and decreases as the moment increases until the moment reaches M_{max}. At this point the moment of inertia is minimum. Not enough information was obtained from this test series to accurately determine the value of I_{emin} for each specimen. Table 5.12 lists a rough approximation of I_{emin} for the lower walls for each series along with the ratio I_{emin}/I_o. This ratio is approximately equal for all the series tested with the average being 0.38, i.e. $I_{emin} = 0.38\ I_o$.

A net of curves similar in shape to the ultimate load-moment curve could be drawn in as contours to fit the plotted data in Figures 5.15 to 5.19 if more data was available. More tests at varying axial wall load must be carried out before this net can be drawn.

The relationship between the stiffness of the wall and the eccentricity of the wall load is given in Fig. 5.20, 5.21 and 5.22 for the 8 inch unreinforced walls, the 8 inch reinforced walls, and the 10 inch reinforced walls, respectively.

Fig. 5.20 presents the variation of flexural rigidity with eccentricity for the 8 inch unreinforced walls (Series A and E). The equation by Hatzinikolas presented earlier in this chapter underestimates the effective moment of inertia for all cases. A best fit curve is drawn yielding the following equation:

$$EI_e/EI_o = 1 - (21/8)(e/t)^2$$

Although this equation gives the curve that best fits the data, the scatter of data points is too large to place any great deal of certainty on the equation.

Fig. 5.21 shows the variation of flexural rigidity with eccentricity for the 8 inch reinforced walls. The number of data points is too small and the scatter of data points is too great to fit any curve to this graph. Hatzinikolas' equation appears to greatly underestimate the effective moment of inertia.

Fig. 5.22 presents the variation of flexural rigidity with eccentricity for the 10 inch reinforced walls. Hatzinikolas' equation splits the data points very well, but the large degree of scatter as

well as the lack of data points for larger eccentricities makes the confirmation of this equation difficult.

The statics of masonry wall-floor slab interaction have been solved using the computer program PFT. For each loading condition of a particular specimen, random values of the modulus of elasticity times the moment of inertia for the top and the bottom walls were inserted into the computer program and a deflected shape was outputted. When the deflected shape given by PFT corresponded to the deflected shape measured during testing, it was assumed that the selected E_m and I_e values used in the interation were equal to the real E_m and I_e values of the actual specimen. No means of theoretically calculating the actual E_m and I_e values for the specimens was available to verify the PFT results.

Once more research has been conducted, a reliable method of predicting E_m and I_e can be developed which will enable the structural analysis of statically indeterminate frames with concrete masonry bearing walls to be carried out similarly to the procedures that would be used for reinforced concrete and structural steel frames.

TABLE 5.1 COMPUTED AND MEASURED ROTATIONS AND DEFLECTIONS FOR WALL A101

M_{slab} Kip-In	Pu Kips	Mu Kip-In	I_{eu} in^4	P_L Kips	M_L Kip-In	I_{eL} in^4	ΔB in	ΔC_L in	ΔI in	ϕ_h Degrees	
206	101	83	1025	106	110	1300	.017	.002	-.014	.08	C
							.017	.004	-.003	-.06	M
412	101	178	1000	111	209	1300	.038	.011	-.024	.15	C
							.053	.017	-.008	.03	M
600	101	261	900	115	304	1300	.065	.026	-.031	.24	C
							.066	.037	-.016	.14	M
752	101	316	600	118	394	1000	.113	.056	-.042	.41	C
							.100	.068	-.041	.30	M

1. C = Computed Values

2. M = Measured Values

TABLE 5.2 COMPUTED AND MEASURED ROTATIONS AND DEFLECTIONS FOR WALL A150

M_{slab} Kip-In	Pu Kips	Mu Kip-In	I_{eu} in^4	P_L Kips	M_L Kip-In	I_{eL} in^4	ΔB in	$\Delta \mathcal{L}$ in	ΔI in	ϕ_h Degrees	
203	151	25	1000	156	158	1300	.010	-.008	-.021	.07	C
							.011	.009	-.021	.15	M
408	151	120	950	160	259	1300	.032	.022	-.031	.15	C
							.034	.001	-.029	.24	M
602	151	210	850	164	354	1150	.058	.012	-.045	.26	C
							.063	.011	-.040	.33	M
719	151	266	725	167	410	950	.079	.016	-.061	.36	C
							.080	.018	-.060	.42	M

1. C = Computed Values

2. M = Measured Values

TABLE 5.3 COMPUTED AND MEASURED ROTATIONS AND DEFLECTIONS FOR WALL B150

M_{slab}	Pu	Mu	I_{eu}	P_L	M_L	I_{eL}	ΔB	$\Delta \mathcal{L}$	ΔI	ϕ_h	
Kip-In	Kips	Kip-In	in^4	Kips	Kip-In	in^4	in	in	in	Degrees	
601	152	241	650	165	327	1450	.077	.044	-.024	.26	C
							.060	.044	-.014	.13	M
792	152	330	775	169	419	1450	.088	.041	-.039	.32	C
							.080	.056	-.027	.21	M
1008	152	433	700	173	520	1250	.127	.064	-.050	.45	C
							.108	.068	-.033	.39	M
1123	152	483	600	176	583	1000	.155	.067	-.074	.60	C
							.135	.077	-.050	.66	M

1. C = Computed Values
2. M = Measured Values

TABLE 5.4 COMPUTED AND MEASURED ROTATIONS AND DEFLECTIONS FOR WALL B200

M_{slab}	Pu	Mu	I_{eu}	P_L	M_L	I_{eL}	ΔB	$\Delta \mathbb{C}_L$	ΔI	ϕ_h	
Kip-In	Kips	Kip-In	in^4	Kips	Kip-In	in^4	in	in	in	Degrees	
601	202	201	600	215	369	1700	.050	.012	-.042	.23	C
							.045	.029	-.026	.17	M
797	202	293	750	219	462	1650	.063	.012	-.055	.29	C
							.061	.033	-.046	.25	M
1010	202	407	650	224	552	1100	.098	.012	-.089	.49	C
							.100	.027	-.092	.39	M
1128	202	494	675	226	581	825	.100	-.022	-.134	.62	C
							.095	-.004	-.120	.54	M

1. C = Computed Values
2. M = Measured Values

TABLE 5.5 COMPUTED AND MEASURED ROTATIONS AND DEFLECTIONS FOR WALL C200

M_{slab}	Pu	Mu	I_{eu}	P_L	M_L	I_{eL}	ΔB	ΔC_L	ΔI	ϕ_h	
Kip-In	Kips	Kip-In	in^4	Kips	Kip-In	in^4	in	in	in	Degrees	
295	203	95	1500	209	165	2600	.019	-.001	-.023	.08	C
							.024	-.003	-.023	.09	M
576	203	218	1400	216	334	2400	.048	.077	-.041	.17	C
							.052	.000	-.034	.13	M
891	203	242	1400	218	435	2400	.065	.003	-.067	.26	C
							.071	-.005	-.060	.17	M
1104	203	445	1150	227	612	1900	.117	.034	-.078	.39	C
							.121	.014	-.075	.31	M

1. C = Computed Values
2. M = Measured Values

TABLE 5.6 COMPUTER AND MEASURED ROTATIONS AND DEFLECTIONS FOR WALL C300

M_{slab} Kip-In	Pu Kips	Mu Kip-In	I_{eu} in^4	P_L Kips	M_L Kip-In	I_{eL} in^4	ΔB in	ΔC_L in	ΔI in	ϕ_h Degree	
289	303	187	1300	310	92	2700	.020	.001	-.022	.08	C
							.017	.006	-.012	.09	M
548	303	303	1250	315	182	2500	.046	.005	-.043	.18	C
							.046	.007	-.035	.15	M
908	303	533	1200	323	340	2400	.097	.043	-.046	.28	C
							.098	.030	-.045	.23	M
942	303	595	850	324	309	1950	.097	.019	-.081	.36	C
							.091	-.011	-.079	.24	M

1. C = Computed Values

2. M = Measured Values

TABLE 5.7 COMPUTED AND MEASURED ROTATIONS AND DEFLECTIONS FOR WALL D200

M_{slab}	Pu	Mu	I_{eu}	P_L	M_L	I_{eL}	ΔB	$\Delta \mathcal{L}$	ΔI	ϕ_h	
Kip-In	Kips	Kip-In	in^4	Kips	Kip-In	in^4	in	in	in	Degree	
412	203	195	2100	212	201	2400	.032	.009	-.020	.10	C
							.037	.006	-.020	.06	M
607	203	289	1900	216	293	2300	.054	.020	-.028	.16	C
							.056	.013	-.029	.10	M
819	203	391	1700	220	393	2400	.086	.048	-.025	.22	C
							.085	.023	-.029	.13	M
911	203	430	1400	222	443	1900	.109	.053	-.041	.30	C
							.105	.027	-.039	.16	M

1. C = Computer Values

2. M = Measured Values

TABLE 5.8 COMPUTED AND MEASURED ROTATIONS AND DEFLECTIONS FOR WALL D300

M_{slab} Kip-In	Pu Kips	Mu Kip-In	I_{eu} in^4	P_L Kips	M_L Kip-In	I_{eL} in^4	ΔB in	$\Delta_L^{\mathbb{C}}$ in	ΔI in	ϕ_h Degree	
390	303	180	1900	312	195	2000	.028	-.002	-.030	.11	C
							.027	-.015	-.025	.09	M
580	303	269	1600	316	287	1900	.054	.012	-.040	.19	C
							.053	-.010	-.032	.11	M
821	303	353	1300	320	385	1700	.092	.033	-.050	.29	C
							.089	-.008	-.045	.08	M
868	303	389	1150	322	439	1550	.111	.042	-.056	.34	C
							.120	-.023	-.050	.03	M

1. C = Computed Values

2. M = Measured Values

TABLE 5.9 COMPUTED AND MEASURED ROTATIONS AND DEFLECTIONS FOR WALL E50

M_{slab} Kip-In	Pu Kips	Mu Kip-In	I_{eu} in^4	P_L Kips	M_L Kip-In	I_{eL} in^4	ΔB in	$\Delta \ell$ in	ΔI in	ϕ_h Degree	
207	51	24	500	56	171	1300	-.017	-.047	-.049	.08	C
							.099	-.003	-.040	.12	M
396	51	160	600	60	215	525	.012	-.063	-.095	.27	C
							.008	-.056	-.098	.36	M
464	53	216	500	63	231	400	.039	-.056	-.112	.42	C
							.046	-.015	-.153	1.36	M

1. C = Computed Values
2. M = Measured Values

TABLE 5.10 COMPUTED AND MEASURED ROTATIONS AND DEFLECTIONS FOR WALL E100

M_{slab} Kip-In	Pu Kips	Mu Kip-In	I_{eu} in^4	P_L Kips	M_L Kip-In	I_{eL} in^4	ΔB in	$\Delta \ell$ in	ΔI in	ϕ_h Degree	
48	101	19	1300	103	27	700	.000	-.007	-.009	.02	C
							-.003	-.009	-.008	.06	M
203	101	75	1300	106	117	950	-.001	-.026	-.034	.08	C
							-.006	-.026	-.030	.07	M
388	101	162	1200	110	205	1100	.017	-.022	-.045	.15	C
							.010	-.021	-.042	.17	M
581	101	249	900	114	302	800	.030	-.042	-.086	.30	C
							.027	-.019	-.095	.31	M
741	101	320	700	117	383	750	.066	-.021	-.094	.42	C
							.080	-.015	-.110	.47	M

1. C = Computed Values

2. M = Measured Values

TABLE 5.11 COMPUTED AND MEASURED ROTATIONS AND DEFLECTIONS FOR WALL E150

M_{slab} Kip-In	Pu Kips	Mu Kip-In	I_{eu} in^4	P_L Kips	M_L Kip-In	I_{eL} in^4	ΔB in	$\Delta \mathcal{L}$ in	ΔI in	ϕ_h Degree	
49	132	-42	1300	133	95	1300	-.032	-.052	-.039	.02	C
							-.004	-.022	-.042	.00	M
201	151	29	800	156	166	1300	-.017	-.046	-.047	.07	C
							.004	-.020	-.052	.04	M
391	151	114	700	160	261	1200	.012	-.030	-.056	.17	C
							.023	-.013	-.068	.17	M
600	151	208	625	165	365	975	.040	-.027	-.080	.31	C
							.048	-.005	-.084	.27	M
619	151	227	650	165	365	900	.040	-.032	-.086	.33	C
							.045	-.009	-.098	.28	M

1. C = Computed Values

2. M = Measured Values

TABLE 5.12 EFFECTIVE MOMENT OF INERTIA

Series	Minimum Effective Moment of Inertia I_{emin},(in^4)	Uncracked Moment of Inertia I_o,(in^4)	$\frac{I_{emin}}{I_o}$
A	500	1300	0.38
B	600	1450	0.41
C	850	2600	0.33
D	1100	2600	0.42
E	500	1300	0.38

Average = 0.38

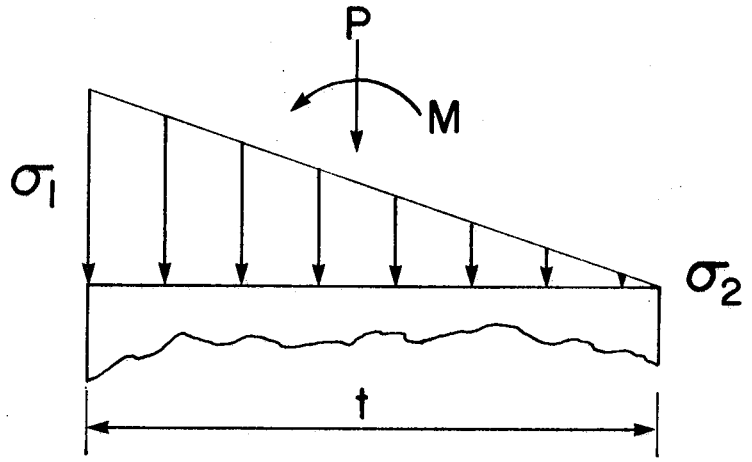

$P = Pb$ $\quad M = M_{max} = M_{PI}$

$\sigma_1 = f'm$ $\quad \sigma_2 = 0.$ $\quad (H) = 0.$

Fig. 5.1 Internal Stress Distribution on a Wall Cross-Section Having a Balanced Failure

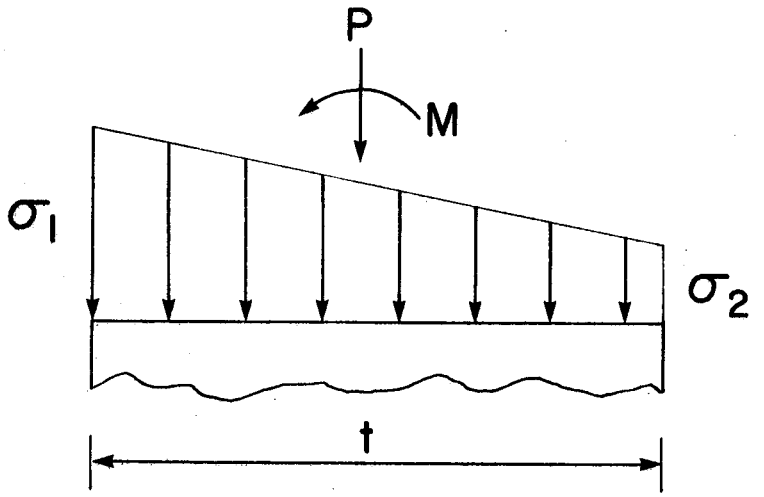

$P > Pb$ $\quad M = M_{max} = M_{PI}$

$\sigma_1 = f'm$ $\quad \sigma_2 > 0.$

Fig. 5.2 Internal Stress Distribution on a Wall Cross-Section Having a Compressive Failure

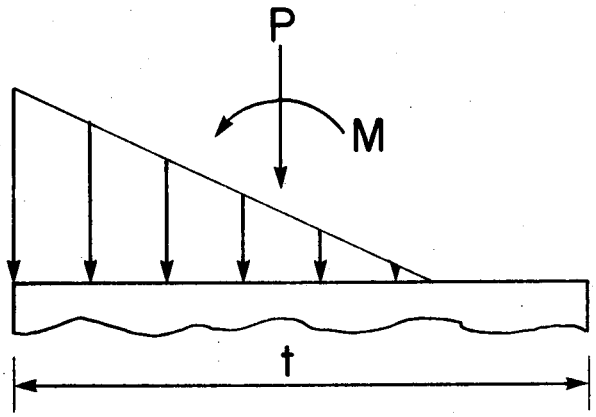

$P < Pb$ $\quad M = M_{max} = M_{PI}$

$\sigma_1 = f'm$ $\quad 0. < Ⓗ < Ⓗ_{ult}$

(a) Stresses when $Ⓗ < Ⓗ_{ult}$

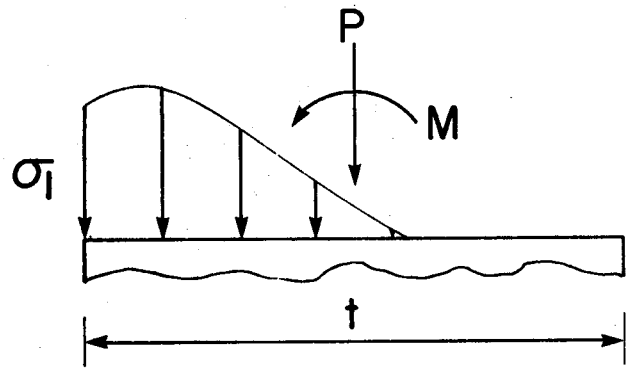

$P < Pb$ $\quad M = M_{max} = M_{PI}$

$\sigma_1 < f'm$ $\quad 0. < Ⓗ = Ⓗ_{ult}$

(b) Stresses when $Ⓗ = Ⓗ_{ult}$

Fig. 5.3 Internal Stress Distribution on a Wall Cross-Section Having a Tension Failure

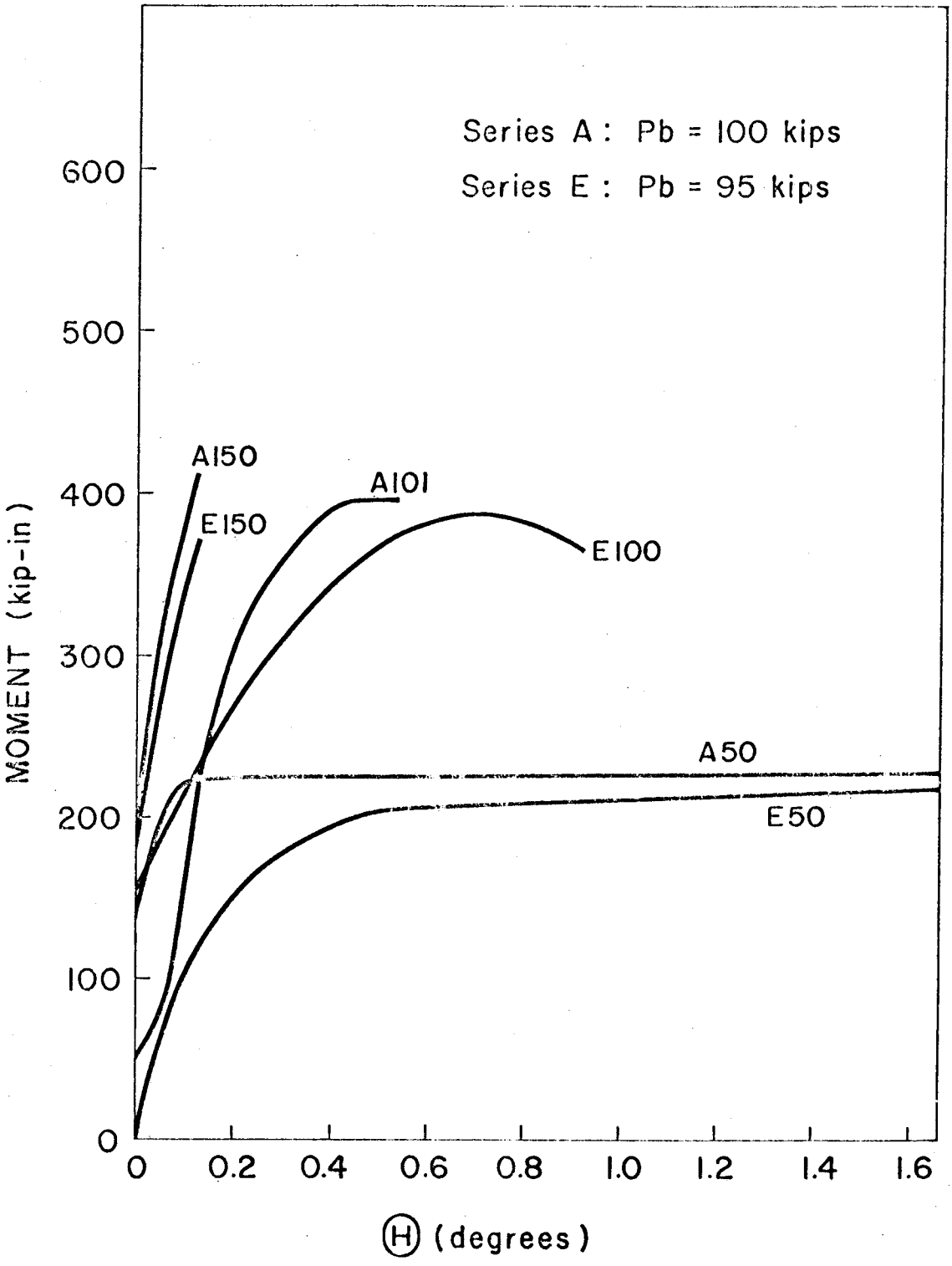

Fig. 5.4 Joint Rotation versus Moment for Unreinforced 8 Inch Walls

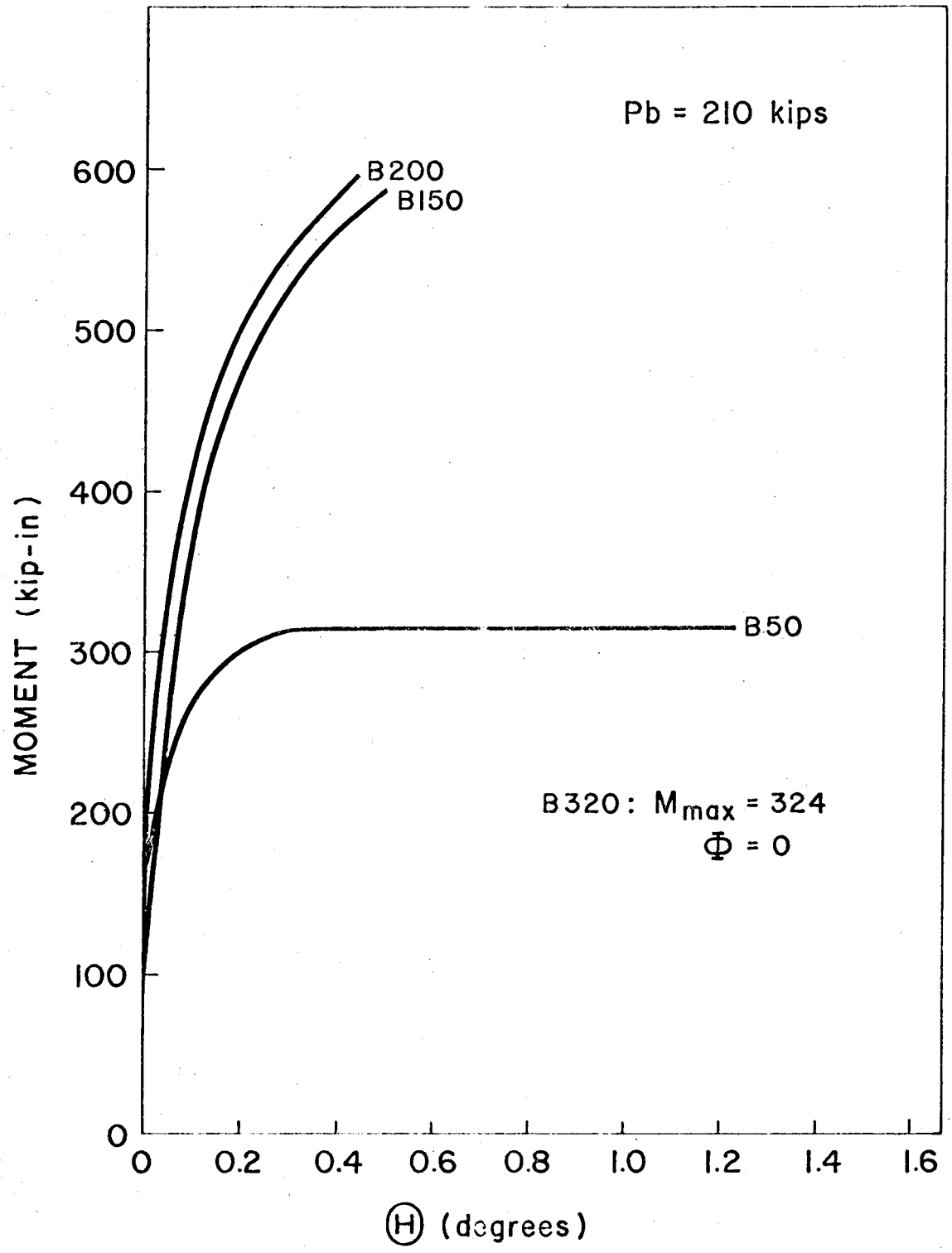

Fig. 5.5 Joint Rotation versus Moment for Reinforced 8 Inch Walls

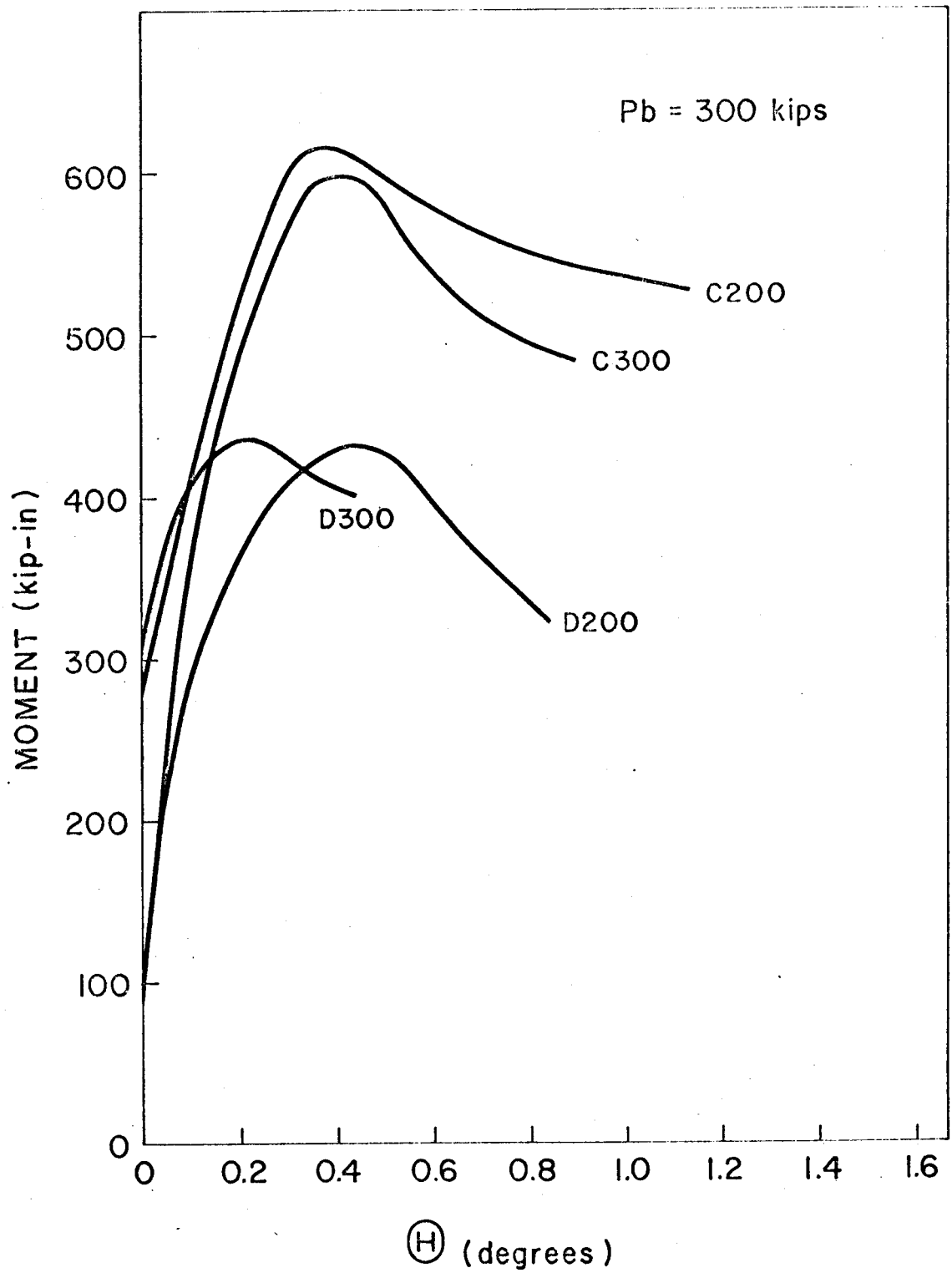

Fig. 5.6 Joint Rotation versus Moment for Reinforced 10 Inch Walls

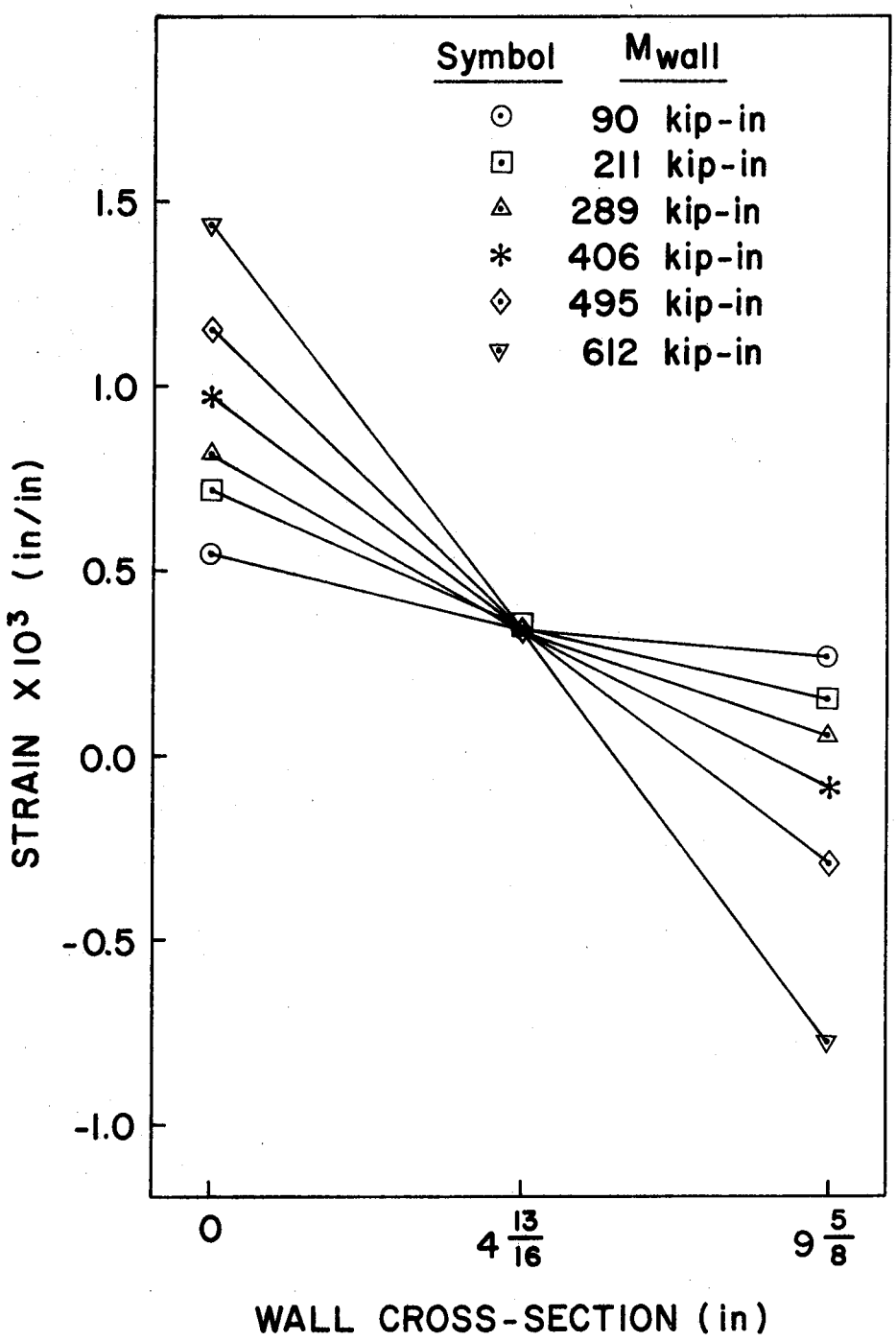

Fig. 5.7 Cross-Sectional Strains at First Block Under Slab for Wall C200

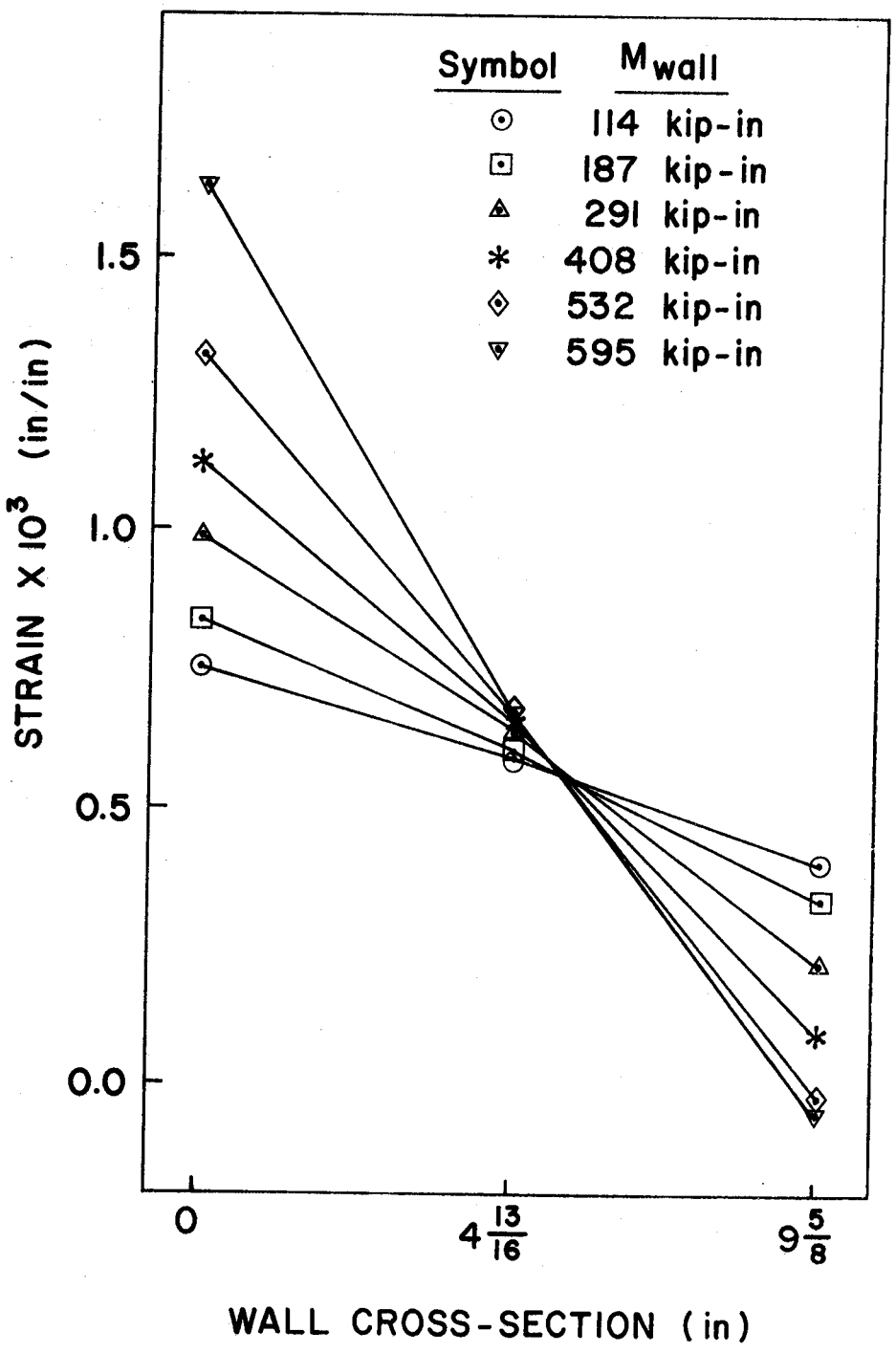

Fig. 5.8 Cross-Sectional Strains at First Block Under Slab for Wall C300

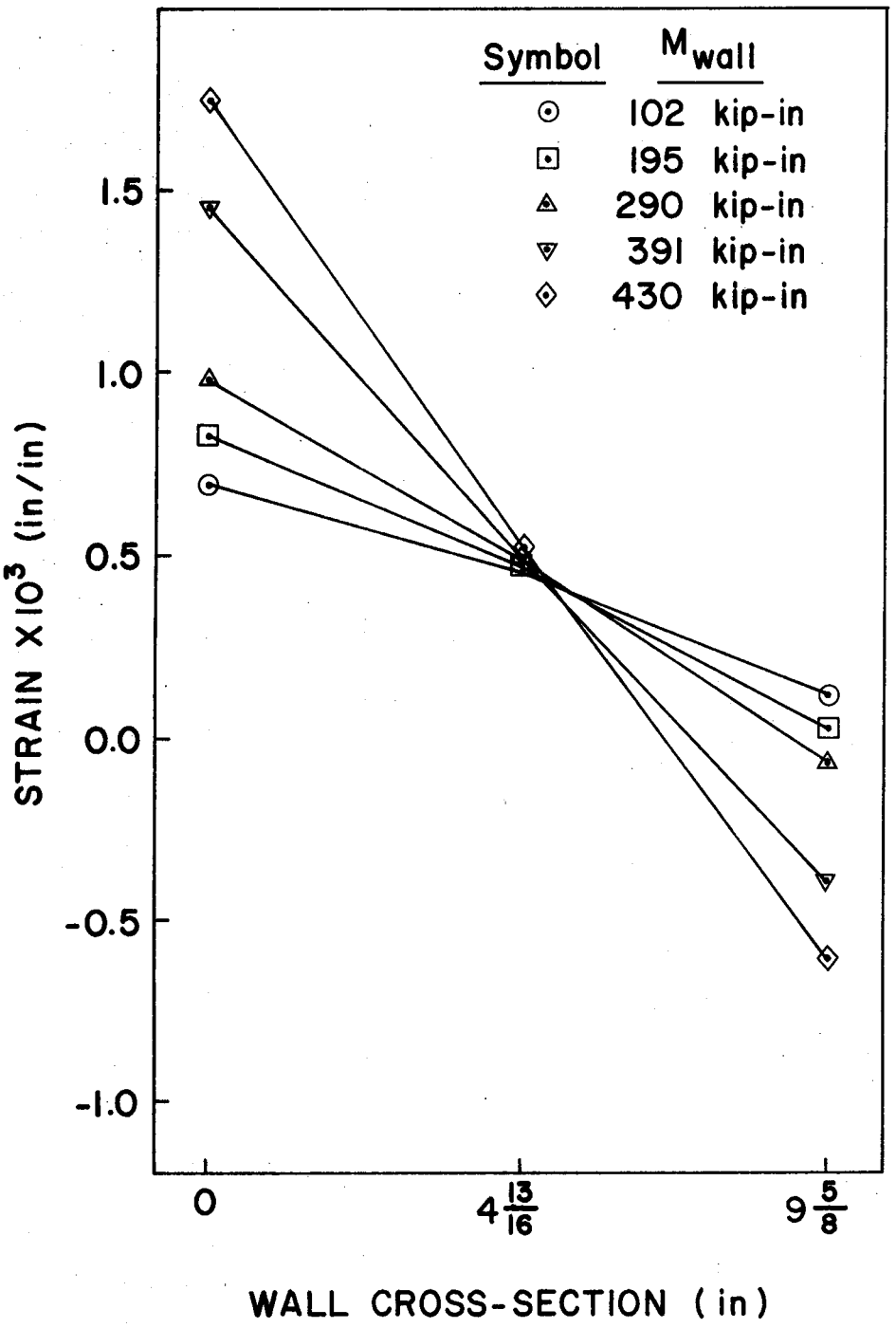

Fig. 5.9 Cross-Sectional Strains at First Block Under Slab for Wall D200

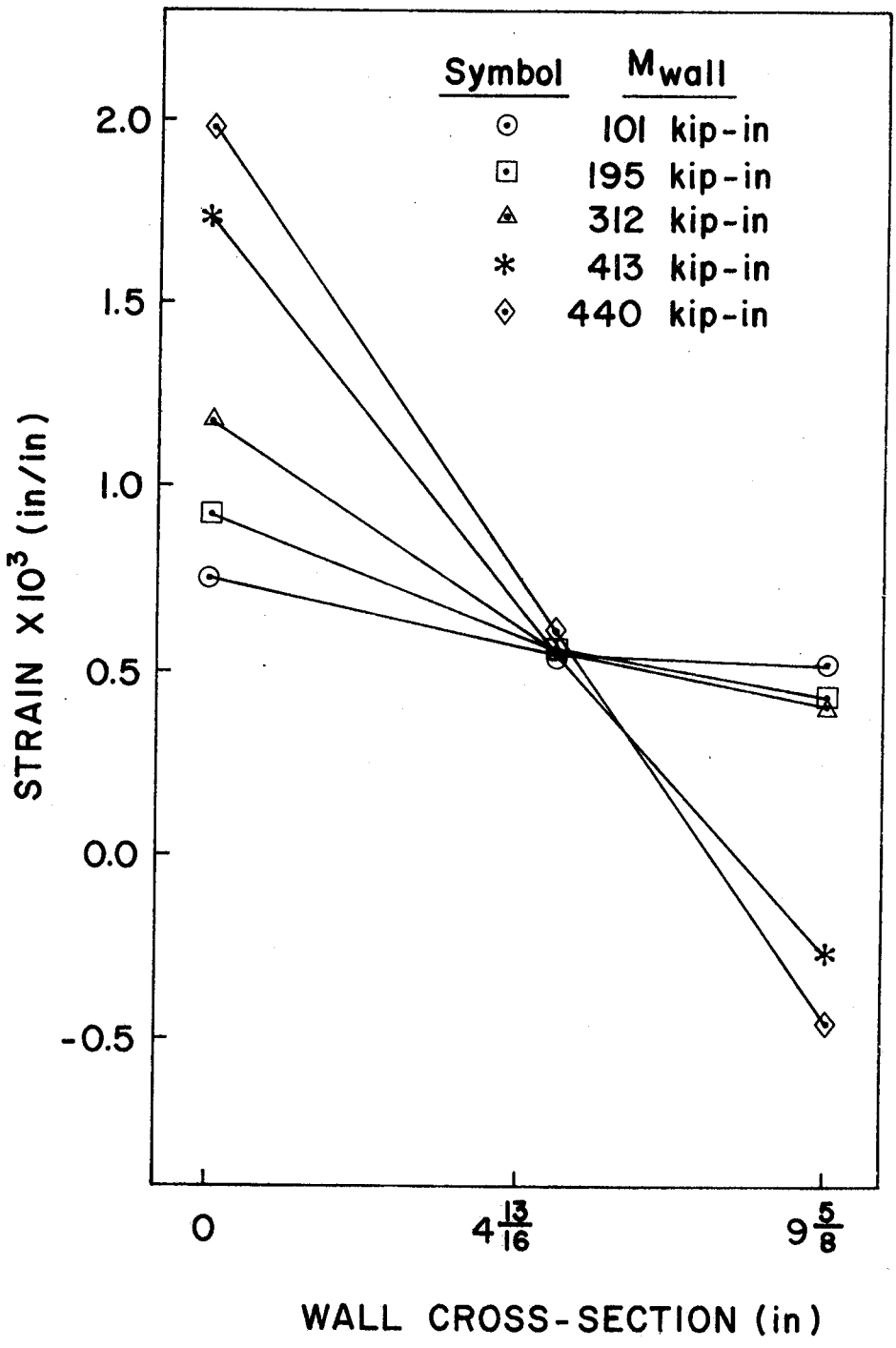

Fig. 5.10 Cross-Sectional Strains at First Block Under Slab for Wall D300

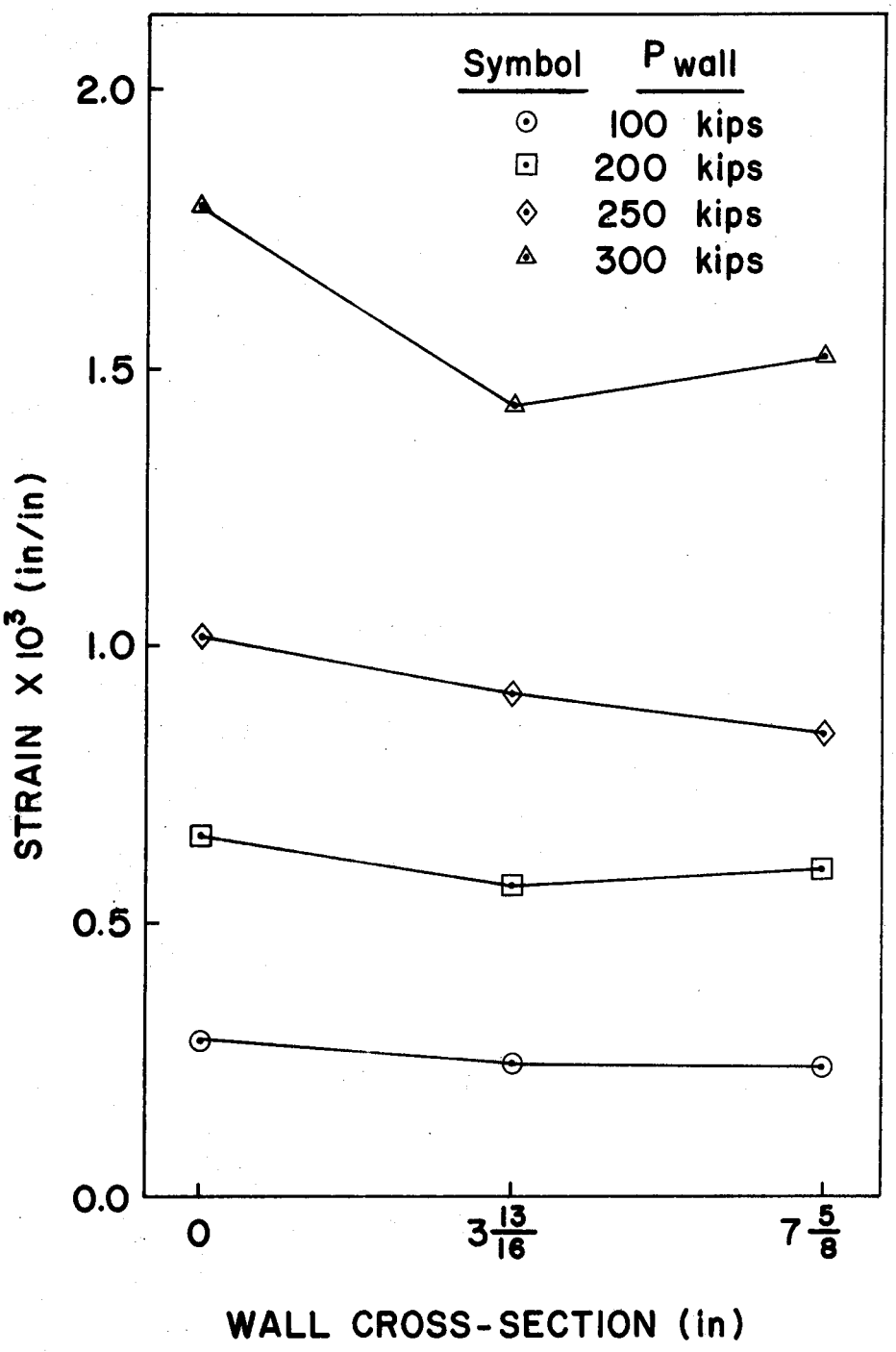

Fig. 5.11 Mid-Height Cross-Sectional Strains for Wall F1

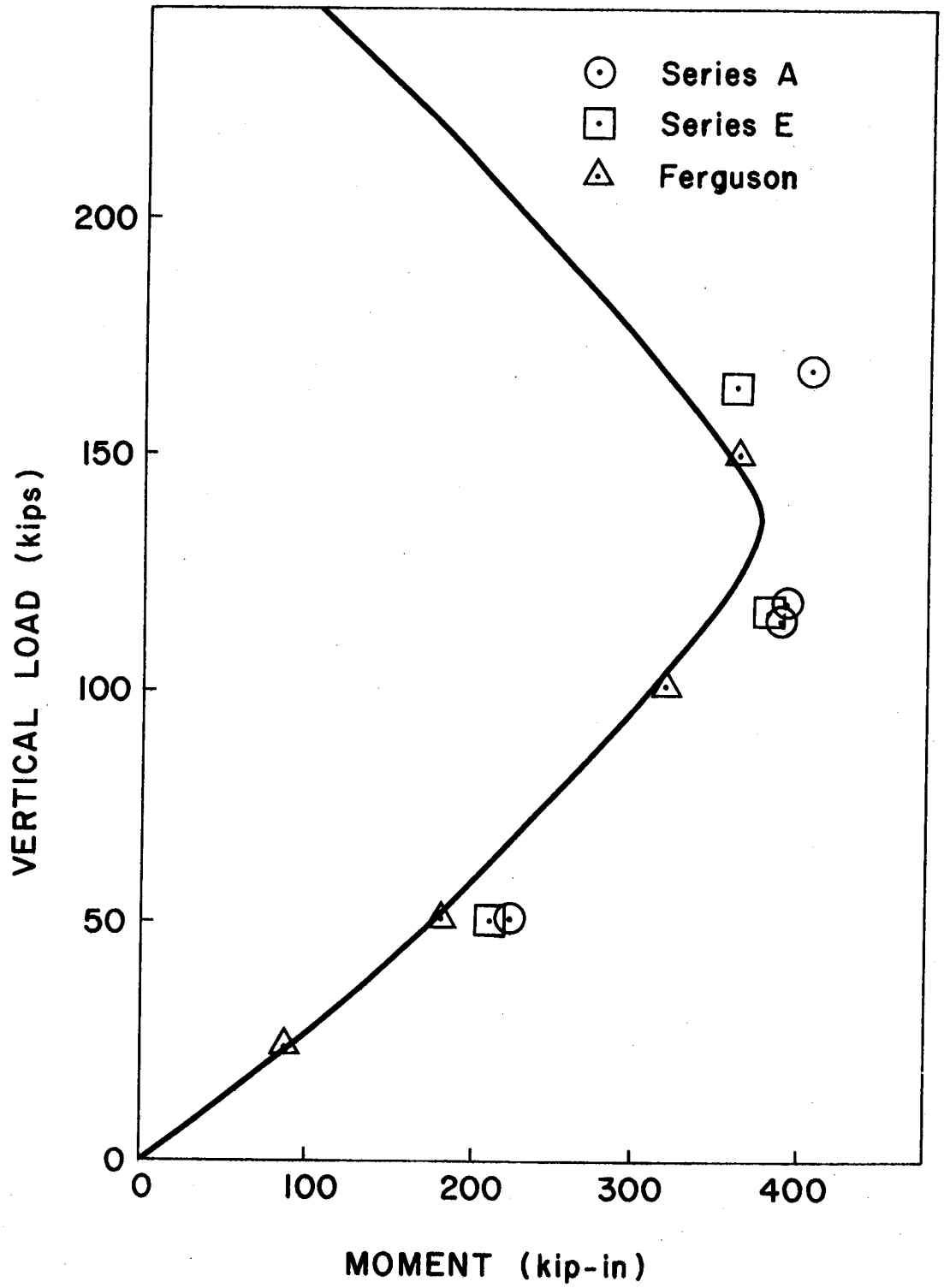

Fig. 5.12 Moment Interaction Diagram for Unreinforced 8 Inch Walls

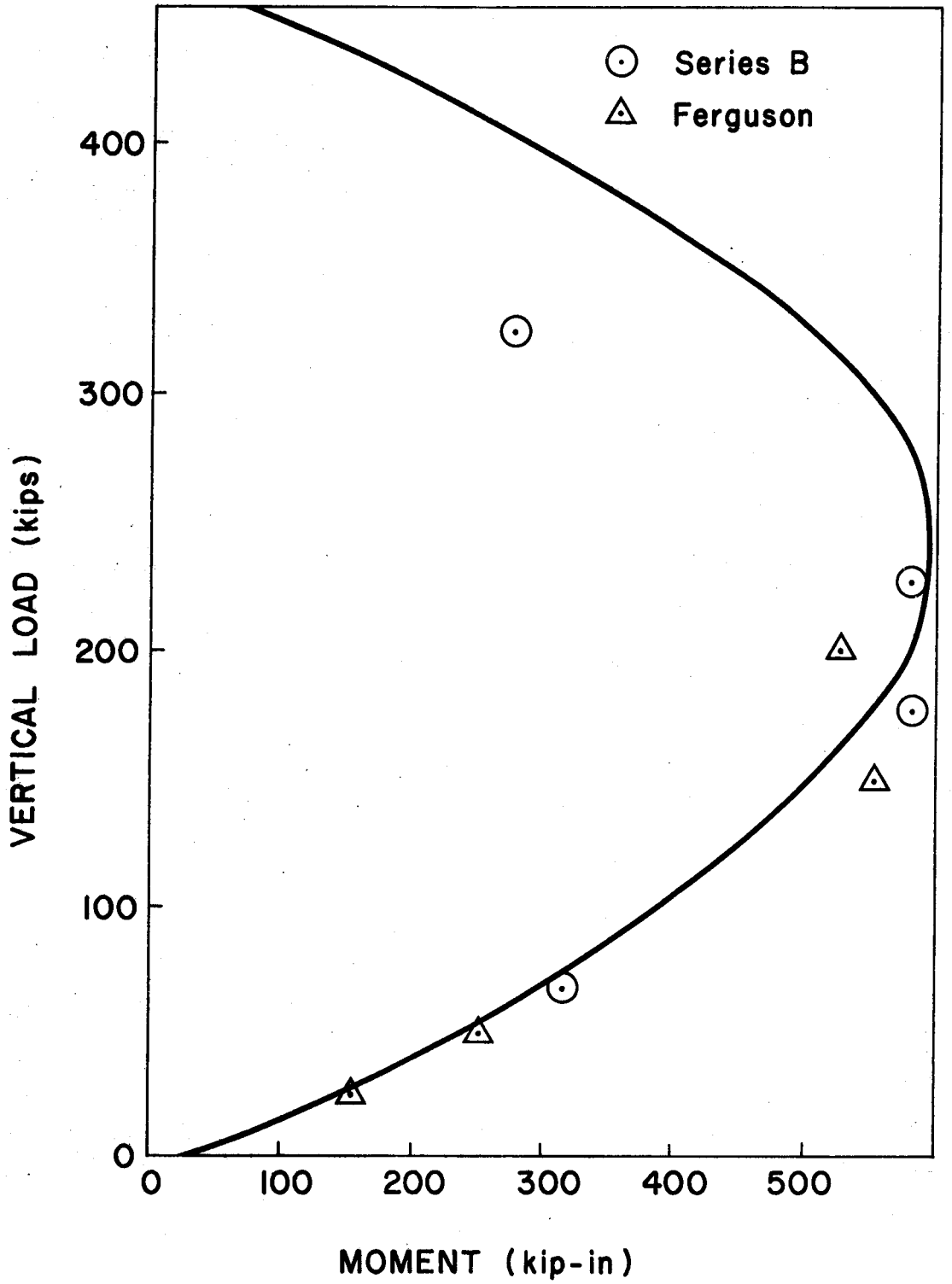

Fig. 5.13 Moment Interaction Diagram for Reinforced 8 Inch Walls

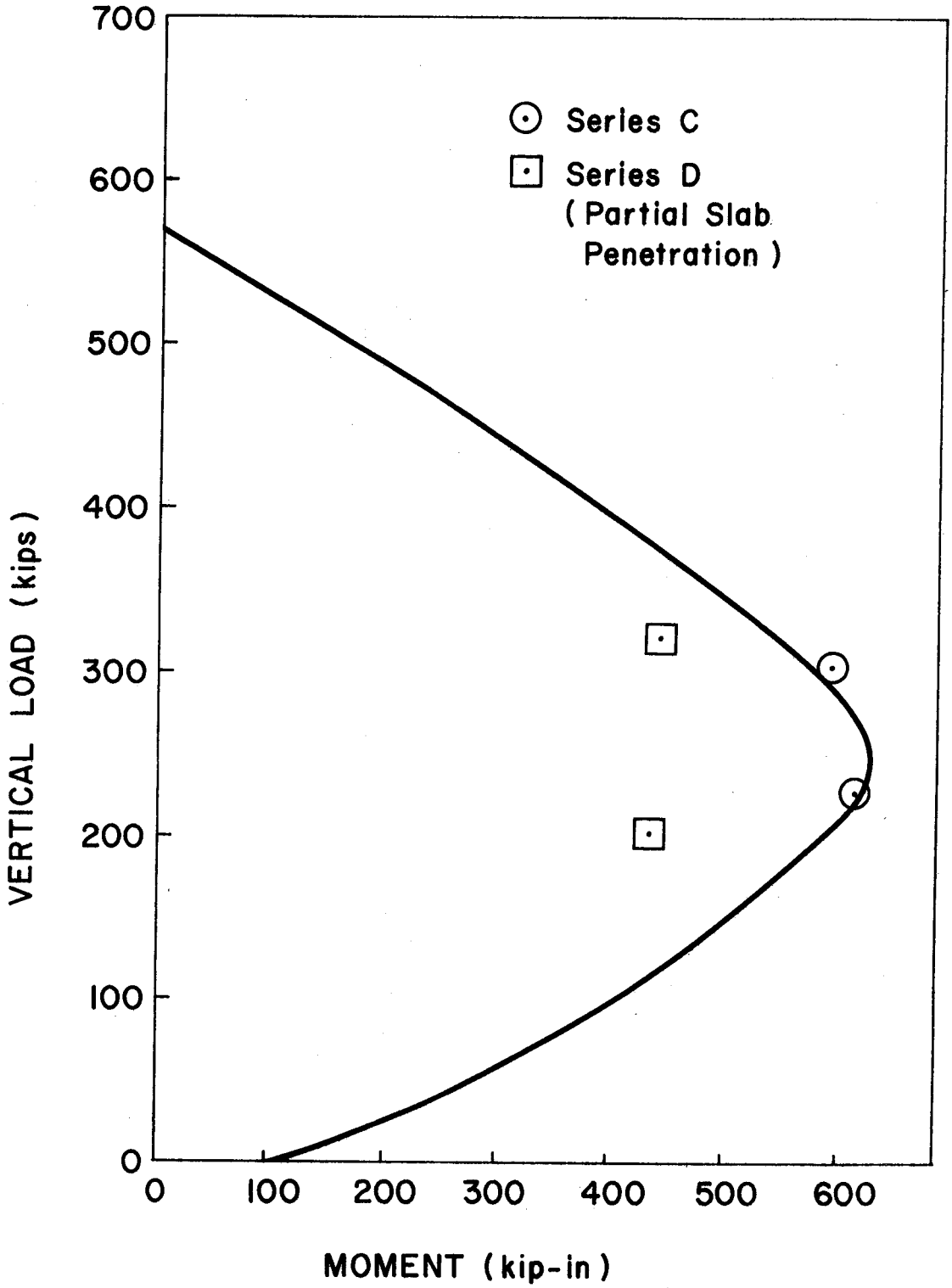

Fig. 5.14 Moment Interaction Diagram for Reinforced 10 Inch Walls

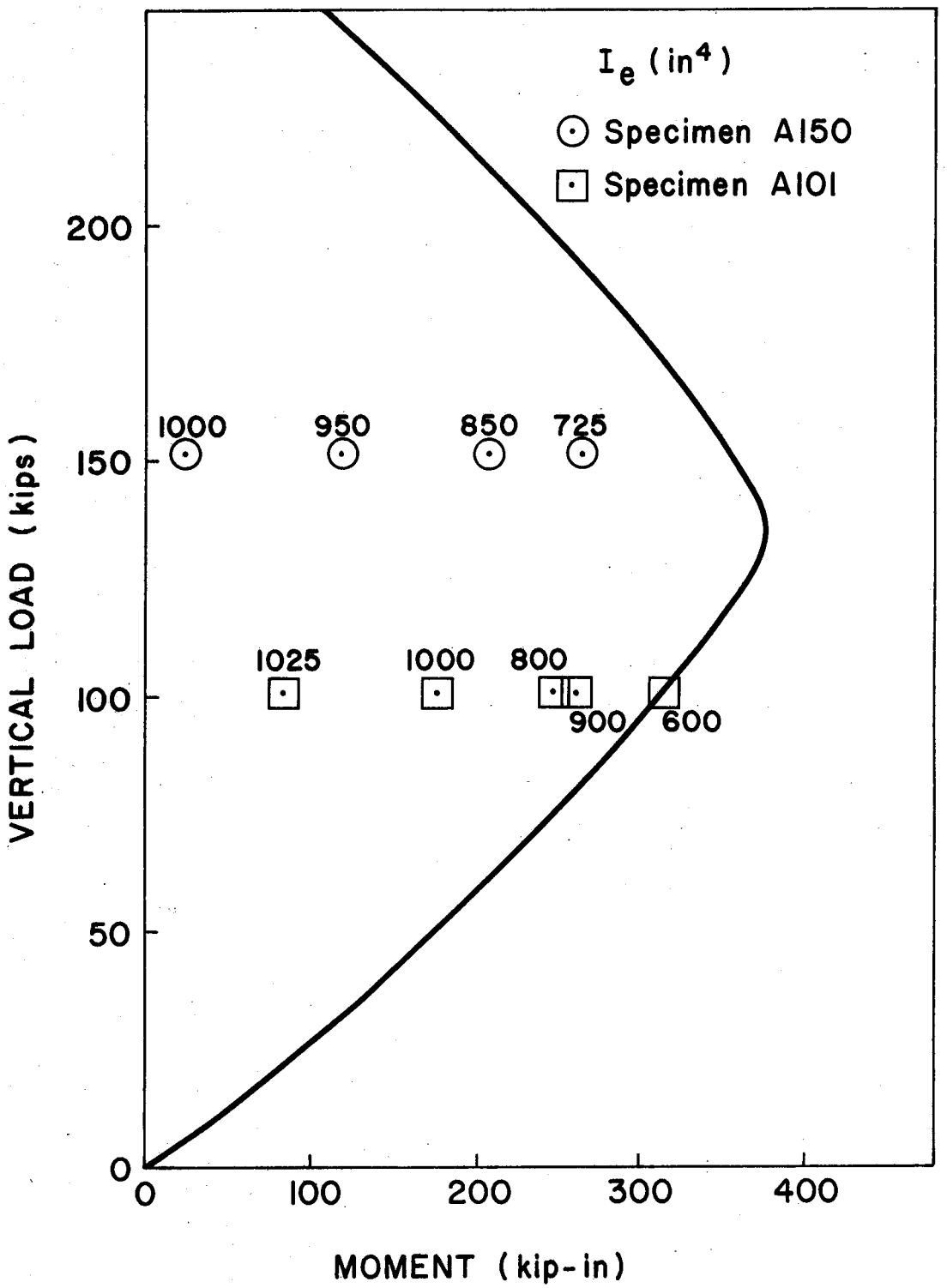

Fig. 5.15 Effective Moment of Inertia for the Lower Walls of Series A

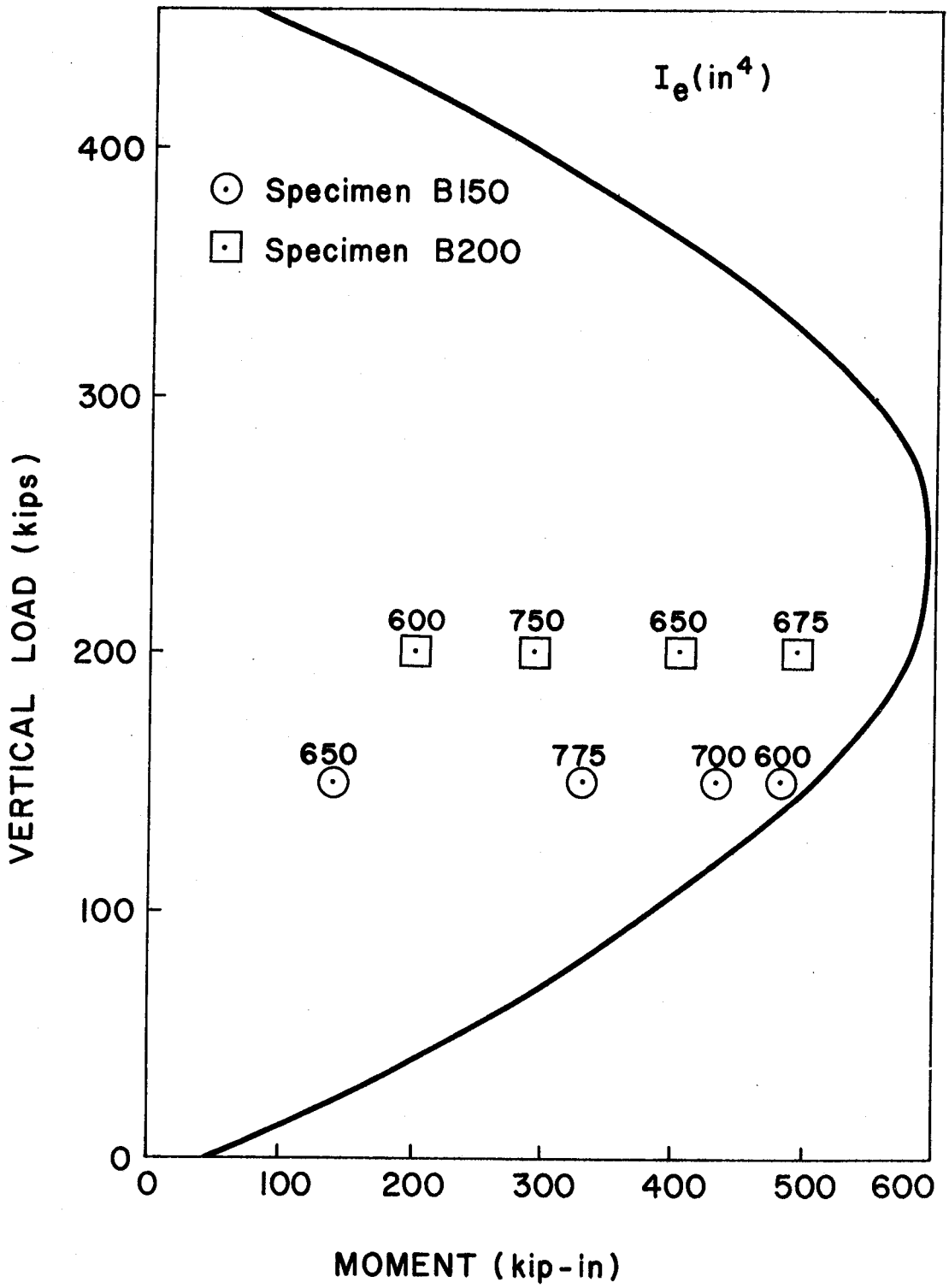

Fig. 5.16 Effective Moment of Inertia for the Lower Walls of Series B

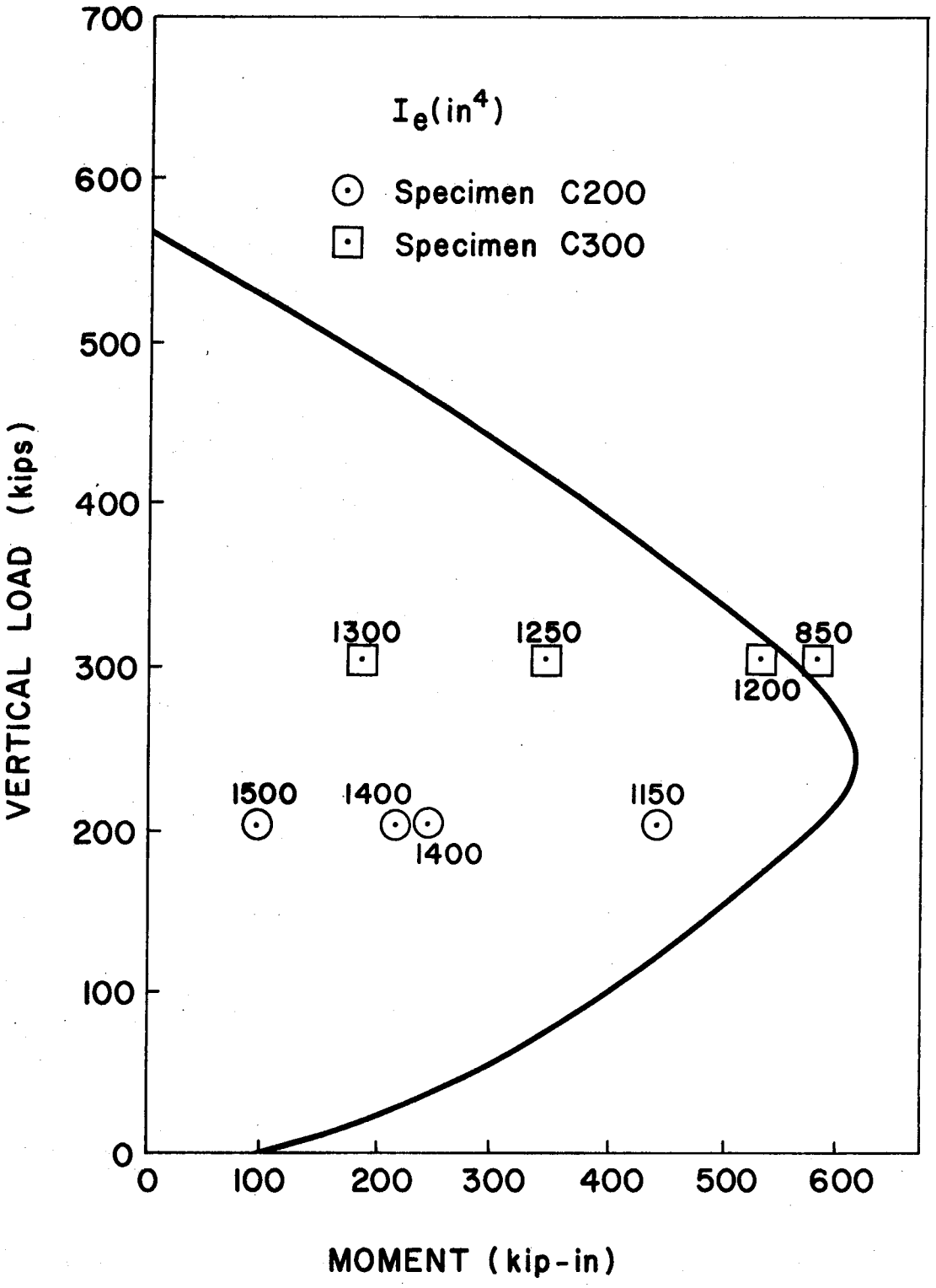

Fig. 5.17 Effective Moment of Inertia for the Lower Walls of Series C

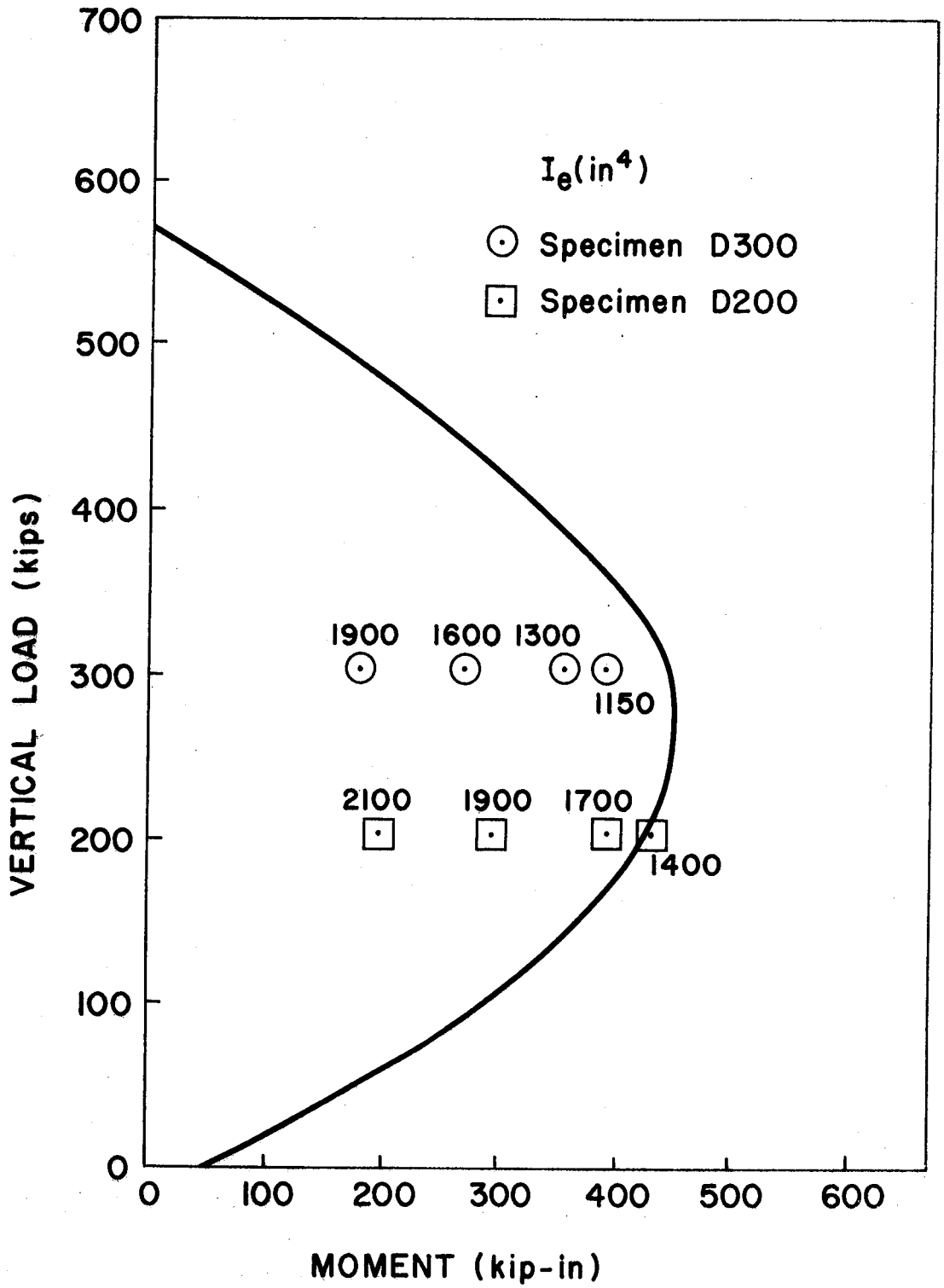

Fig. 5.18 Effective Moment of Inertia for the Lower Walls of Series D

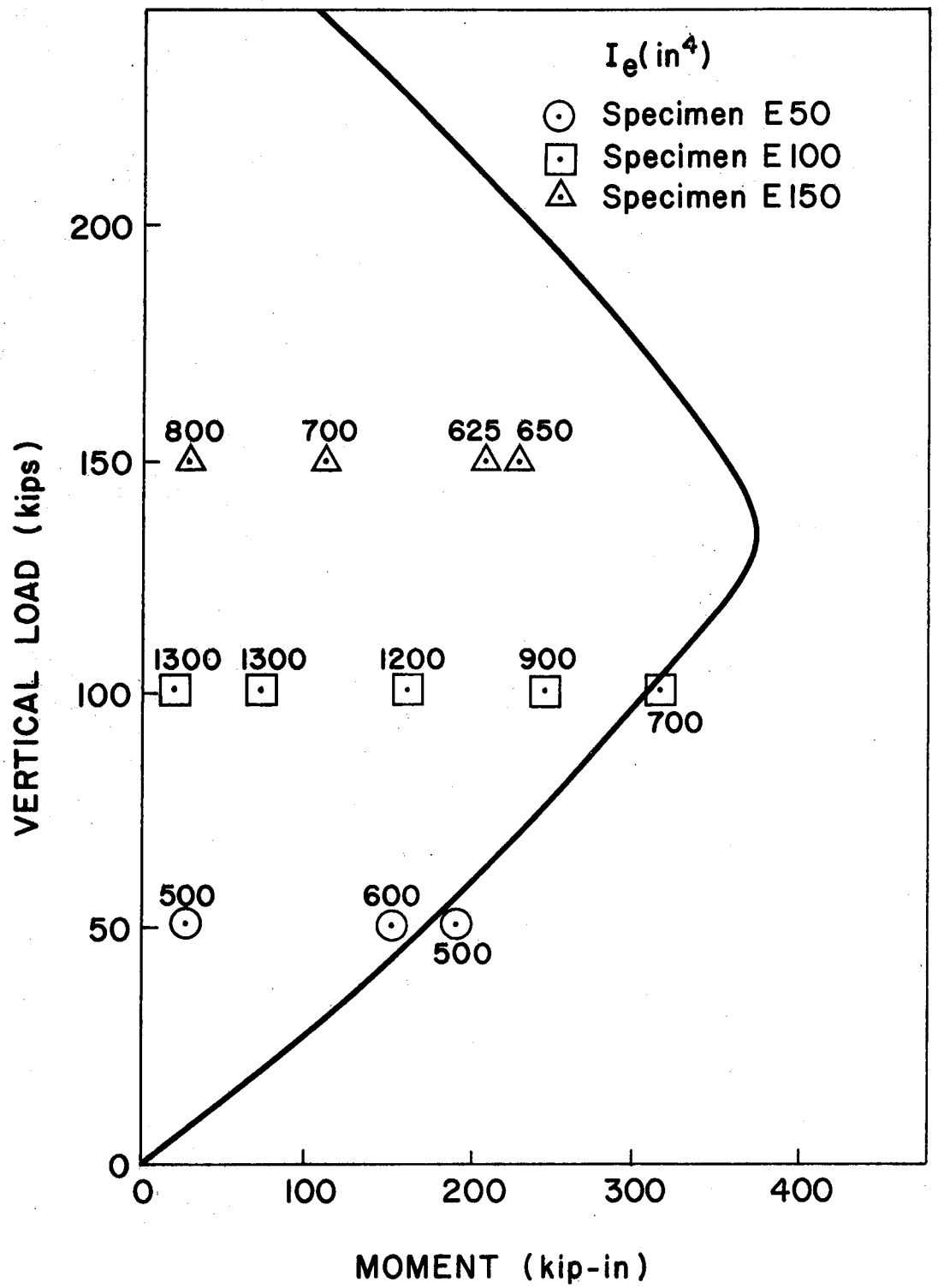

Fig. 5.19 Effective Moment of Inertia for the Lower Walls of Series E

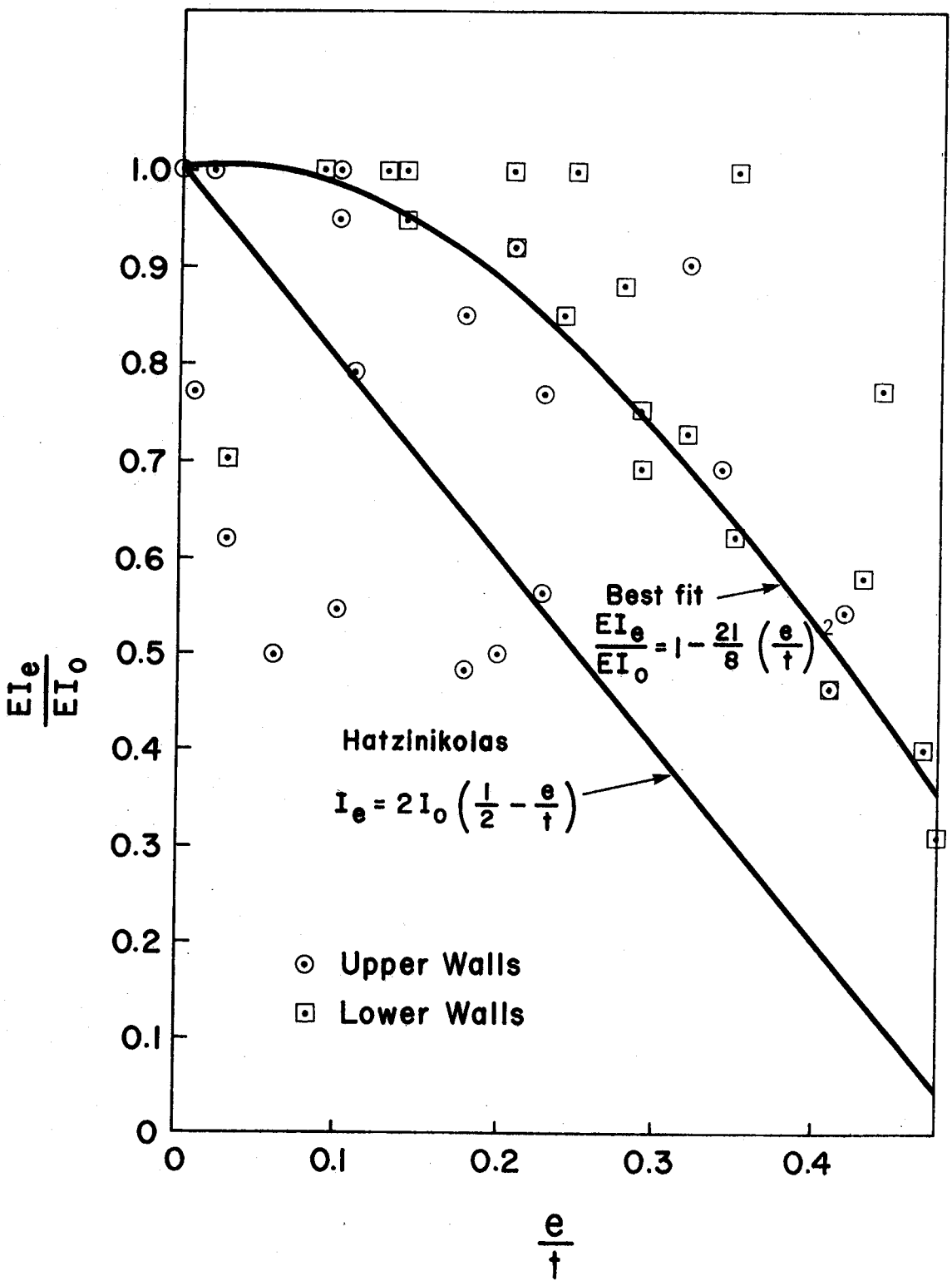

Fig. 5.20 Variation of Flexural Rigidity with Eccentricity for 8 Inch Unreinforced Walls

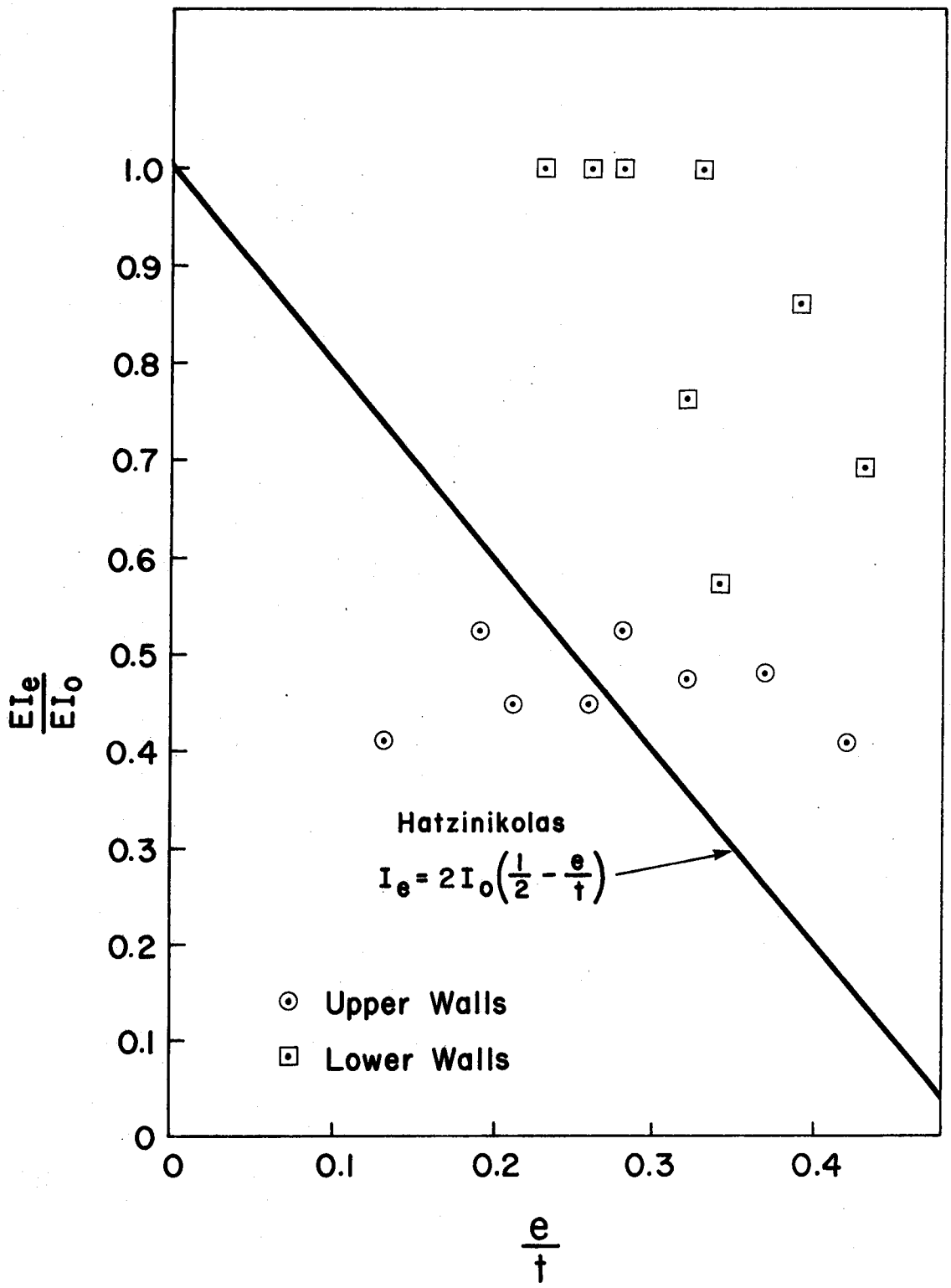

Fig. 5.21 Variation of Flexural Rigidity With Eccentricity for 8 Inch Reinforced Walls

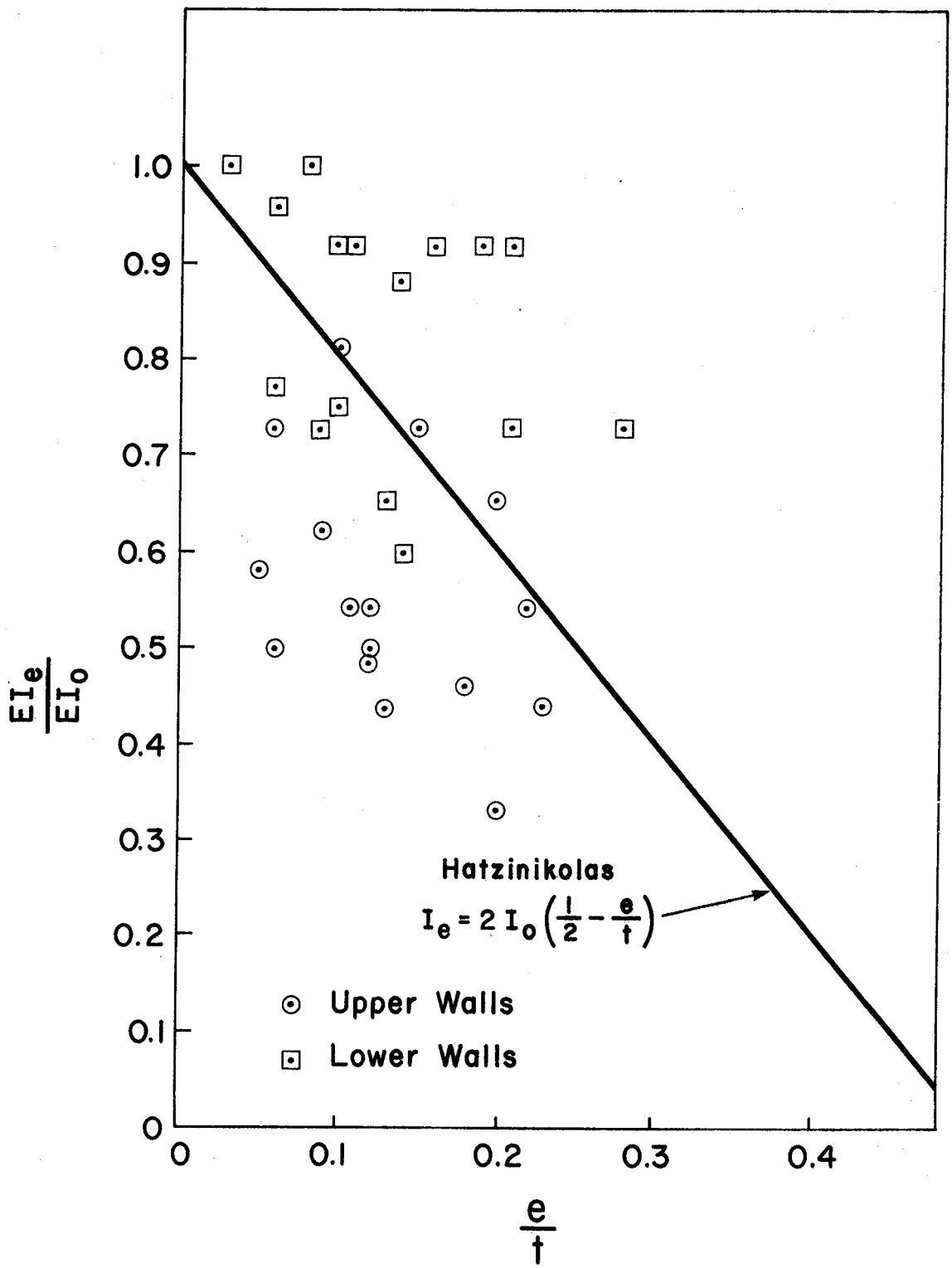

Fig. 5.22 Variation of Flexural Rigidity with Eccentricity for 10 Inch Reinforced Walls

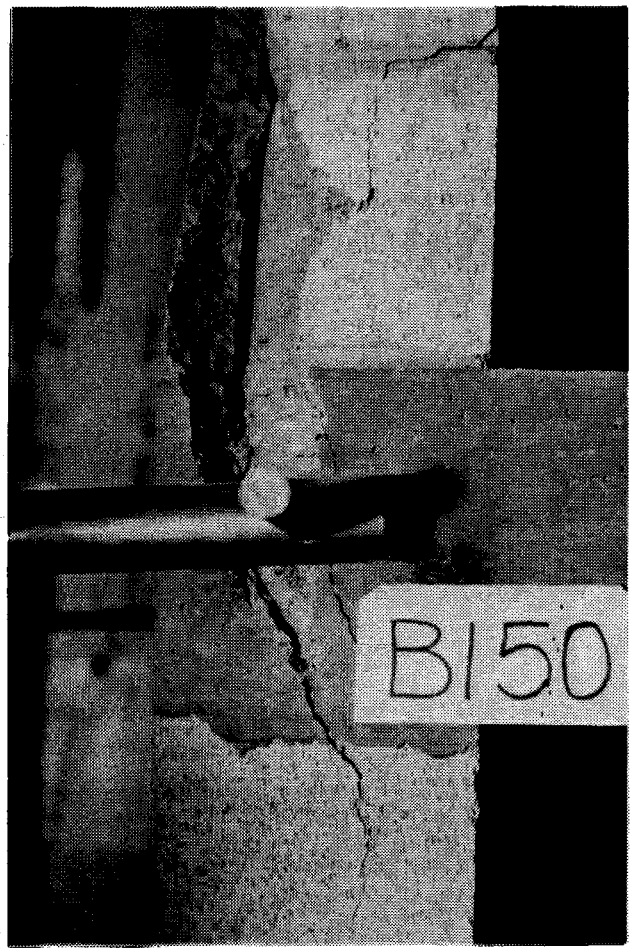

Plate 5.1 Wall B150 at Failure

3. The behavior of the specimens failing in a compressive mode was similar to the behavior described by Sahlin's compressive type failure mode.

4. Although some of the specimens could resist moment after M_{pl} was reached, sufficient cracking of the walls and slab occurred to conclude that the joint had reached its useful limit. Thus, the failure of the specimens with axial loads greater than or equal to P_b occurred when the ultimate moment capacity of the masonry walls was reached, and the failure of the specimens with axial loads less than P_b occurred when 80% of the ultimate moment capacity of the masonry walls was reached.

5. The wall-slab joint of the specimens can be considered as a rigid connection between the walls and the slab until the plastification moment is reached. For $P_{wall} \geq P_b$, $M_{pl} = M_{ult}$; and for $P < P_b$, $M_{pl} = 0.8\ M_{ult}$.

6. The degree of fixity of the rigid joint of the specimens is a function of the stiffness of the masonry walls; as the stiffness of the walls increased so did the resistance to rotation of the slab end. This stiffness, dependent on the equivalent moment of inertia and modulus of elasticity of the cracked wall, decreased as the eccentricity of the wall load increased and as the moment transferred to the wall increased due to cracking of the wall.

7. Stuctural analysis of a structure consisting of load bearing masonry walls and cast-in-place concrete slabs with joint details like those used in this study can be evaluated using existing rigid frame analysis methods.

8. The load-moment interaction strength of masonry bearing walls loaded in flexure can be predicted using the existing methods that are applicable to developing interaction diagrams for concrete and steel.
9. Mortar compressive strength has no effect on the flexural strength or on the behavior of the specimen.
10. The degree of slab penetration into the wall cross-section has no effect on the rotational behavior of the joint or on the failure mode of the specimen. The ultimate moment capacity of the wall is greatly decreased as the area of wall penetrated by the slab decreases.
11. The tie back has no effect on the ultimate moment capacity of the wall. It does, however, affect the behavior of the wall for tensile type failures. For this case, the restriction of the horizontal translation of the wall-slab joint allows the ultimate joint rotation to be achieved.
12. The modulus of elasticity of masonry determined in this investigation is equal to 750 f'_m.

6.3 Recommendations

1. Further tests on wall-slab interaction specimens should be undertaken to develop a theoretical relationship between the level of axial load and moment on the wall to the stiffness of the wall. In these tests, the top and bottom of the specimens as well as the wall-slab joint should be free to rotate but fixed against any horizontal translation, since even the slightest deflection at these points makes analysis of the

wall extremely difficult.

2. Further tests should be carried out to develop a theoretical relationship between the moment capacity of the wall and the degree of slab penetration into the wall.
3. Further tests should be carried out to determine a relationship between the value of M_{pl} with respect to M_{ult} as a function of the level of axial load on the wall.

REFERENCES

1. "Masonry Design and Construction for Buildings". CSA Standard S304-1977.

2. Sahlin, S. "Structural Interaction of Walls and Floor Slabs". National Swedish Council for Building Research, Report No. 35, 1959.

3. Sahlin, S. "Interaction of Brick Masonry Walls and Concrete Slabs". Designing, Engineering and Constructing with Masonry Products, Ed. F.B. Johnson. Houston, Gulf Publishing Co., 1969.

4. Sahlin, S. "Structural Masonry". Englewood Cliffs, N.J., Prentice Hall, 1971.

5. Maurenbrecher, A.H.P., and Hendry, A.W. "Aspects of the Strength and Fixity of the Joint Between a Brick Wall and a Floor Slab". Proceedings of the 2nd International Brick Masonry Conference, Stoke-on-Trent, England, April, 1970.

6. Colville, J., and Hendry, A.W. "Aspects of a Load Bearing Masonry Structure". 6th International Symposium on Load Bearing Brickwork, London, 1977.

7. Carlsen, B.E. "On the Bearing Capacity of Joints Between Precast Slabs and Brick Walls". CIB International Symposium on Bearing Walls, Warsaw, 1969.

8. Risager, S. "Structural Behavior of Linear Elastic Walls Having No Tensile Strength". Designing, Engineering and Constructing With Masonry Products. Ed. F.B. Johnston. Houston, Gulf Publishing Co., 1969.

9. Sinha, B.P., and Hendry, A.W. "An Investigation into the Behavior of a Brick Cross-Wall Structure". 6th International Symposium on Load Bearing Brickwork, London 1977.

10. Germanio G., and Macchi, G. "Experimental Research of a Frame-Idealization for a Bearing Wall Multistorey Structure". 6th International Symposium on Load Bearing Brickwork, London, 1977.

11. Furler, R., and Thurliman, B. "Strength of Brick Walls Under Enforced End Rotations". 6th International Symposium on Load Bearing Brickwork, London, 1977.

12. Ferguson, S.N. "Interaction of Concrete Masonry Bearing Walls and Concrete Floor Slabs". M.Sc. Thesis, University of Alberta, Edmonton, Spring, 1979.

13. Hatzinikolas, M. "Concrete Masonry Walls". Ph.D. Thesis, University of Alberta, Edmonton, Fall, 1978.

14. Gross, J.G., Dikkers, R.D. and Grogan, J.C. "Recommended Practice for Engineered Brick Masonry". Structural Clay Products Institute, McLean, Virginia, November, 1969.

15. "Mortar and Grout for Unit Masonry". CSA Standard A179M-1976.

16. "Standard Specification for Aggregate of Masonry Mortar". ASIM C144-76.

17. "Methods for Test For Concrete". CSA Standard CAN3-A23.2-M77.

18. "A Design Guide to the Engineered Clay Masonry Bearing Wall System". Clay Brick Association of Canada, BCI 5.4 Division 4, Willowdale, Ontario, 1975.

19. Beaufait, F.W., Rowan, W.L., Hoadly, P.G. and Hackett, R.N. "Computer Methods of Structural Analysis". Englewood Cliffs, N.J., Prentice Hall, 1970.

20. Hogestad, E. "A Study of Combined Bending and Axial Load in Reinforced Concrete Members". University of Illinois, Engineering Experimental Station, Bulletin Series No. 399, November, 1951, 128 pp.

21. Maurenbrecher, A.H.P. "Wall-Floor Slab Joint Behavior in Brickwork". Ph.D. Thesis, Edinburgh University, Scotland, 1972.

22. Colville, J. "Analysis and Design of Brick Masonry Walls". Research Fellowship, Edinburgh University, Scotland, June, 1977.

23. Sutherland, R.J.M. "Structural Design of Masonry Buildings". Proceedings of the International Conference on 'Planning and Design of Tall Buildings'. Bethlehem, Pennsylvania, August, 1972.

24. Mallet, R.J. "Structural Behavior of Masonry Elements". Proceedings of the International Conference on 'Planning and Design of Tall Buildings'. Bethlehem, Pennsylvania, August, 1972.

25. Smith, B.S., and Carter, C. "Distribution of Stresses in Masonry Walls Subjected to Vertical Loading". Proceedings of the 2nd International Brick Masonry Conference, Stoke-on-Trent, England, April 1970.

26. Awni, A., and Hendry, A.W. "A Simplified Method for Eccentricity Calculations". Proceedings of the 5th International Brick Masonry Conference, Washington, D.C., October 1979.

27. Hamid, A.A., Drysdale, R.G., and Heidebrecht, A.C. "Effect of Grouting on the Strength Characteristics of Concrete Block Masonry", North American Masonry Conference, University of Colorado, August, 1978.

RECENT STRUCTURAL ENGINEERING REPORTS

Department of Civil Engineering

University of Alberta

63. *A Classical Flexibility Analysis for Gentilly Type Containment Structures* by D.W. Murray, A.M. Rohardt, and S.H. Simmonds, June 1977.

64. *Substructure Analysis of Plane Frames* by A.A. Elwi and D.W. Murray, June 1977.

65. *Strength and Behavior of Cold-Formed HSS Columns* by Reidar Bjorhovde, December 1977.

66. *Some Elementary Mechanics of Explosive and Brittle Failure Modes in Prestressed Containments* by D.W. Murray, June 1978.

67. *Inelastic Analysis of Prestressed Concrete Secondary Containments* by D.W. Murray, L. Chitnuyanondh, C. Wong and K.Y. Rijub-Agha, July 1978.

68. *Strength of Variability of Bonded Prestressed Concrete Beams* by D.K. Kikuchi, S.A. Mirza and J.G. MacGregor, August 1978.

69. *Numerical Analysis of General Shells of Revolution Subjected to Arbitrary Loading* by A.M. Shazly, S.H. Simmonds and D.W. Murray, September 1978.

70. *Concrete Masonry Walls* by M. Hatzinikolas, J. Longworth and J. Warwaruk, September 1978.

71. *Experimental Data for Concrete Masonry Walls* by M. Hatzinikolas, J. Longworth and J. Warwaruk, September 1978.

72. *Fatigue Behaviour of Steel Beams with Welded Details* by G.R. Bardell and G.L. Kulak, September 1978.

73. *Double Angle Beam-Column Connections* by R.M. Lasby and Reidar Bjorhovde, April 1979.

74. *An Effective Uniaxial Tensile Stress-Strain Relationship for Prestressed Concrete* by L. Chitnuyanondh, S. Rizkalla, D.W. Murray and J.G. MacGregor, February 1979.

75. *Interaction Diagrams for Reinforced Masonry* by C. Feeg and J. Warwaruk, April 1979.

76. *Effects of Reinforcement Detailing for Concrete Masonry Columns* by C. Feeg, J. Longworth, and J. Warwaruk, May 1979.

77. *Interaction of Concrete Masonry Bearing Walls and Concrete Floor Slabs* by N. Ferguson, J. Longworth and J. Warwaruk, May 1979.

78. *Analysis of Prestressed Concrete Wall Segments* by B.D.P. Koziak and D.W. Murray, June 1979.

79. *Fatigue Strength of Welded Steel Elements* by M.P. Comeau and G.L. Kulak, October 1979.

80. *Leakage Tests of Wall Segments of Reactor Containments* by S.K. Rizkalla, S.H. Simmonds and J.G. MacGregor, October 1979.

81. *Tests of Wall Segments from Reactor Containments* by S.H. Simmonds, S.H. Rizkalla and J.G. MacGregor, October 1979.

82. *Cracking of Reinforced and Prestressed Concrete Wall Segments* by J.G. MacGregor, S.H. Rizkalla and S.H. Simmonds, October 1979.

83. *Inelastic Behavior of Multistory Steel Frames* by M. EL Zanaty, D.W. Murray and R. Bjorhovde, April 1980.

84. *Finite Element Programs for Frame Analysis* by M. EL Zanaty and D.W. Murray, April 1980.

85. *Test of a Prestressed Concrete Secondary Containment Structure* by J.G. MacGregor, S.H. Simmonds and S.H. Rizkalla, April 1980.

86. *An Inelastic Analysis of the Gentilly-2 Secondary Containment Structure* by D.W. Murray, C. Wong, S.H. Simmonds and J.G. MacGregor, April 1980.

87. *Nonlinear Analysis of Axisymmetric Reinforced Concrete Structures* by A.A. Elwi and D.W. Murray, May 1980

88. *Behavior of Prestressed Concrete Containment Structures - A Summary of Findings* by J.G. MacGregor, D.W. Murray, S.H. Simmonds, April 1980.

89. *Deflection of Composite Beams at Service Load* by L. Samantaraya and J. Longworth, June 1980.

90. *Analysis and Design of Stub-Girders* by T.J.E. Zimmerman and R. Bjorhovde, August 1980.

91. *An Investigation of Reinforced Concrete Block Masonry Columns* by G.R. Sturgeon, J. Longworth and J. Warwaruk, September 1980.

92. *An Investigation of Concrete Masonry Wall and Concrete Slab Interaction* by R.M. Pacholok, J. Warwaruk, and J. Longworth, October 1980.